Summer 2015

Dissolution mechanisms: theoretical and experimental investigations

Yang Qiu
University of Iowa

DISSOLUTION MECHANISMS: THEORETICAL AND EXPERIMENTAL INVESTIGATIONS

by

Yang Qiu

A thesis submitted in partial fulfillment
of the requirements for the Doctor of
Philosophy degree in Pharmacy (Pharmaceutics)
in the Graduate College of
The University of Iowa

August 2015

Thesis Supervisor: Professor Emeritus Douglas R. Flanagan

Graduate College
The University of Iowa
Iowa City, Iowa

Graduate College
The University of Iowa
Iowa City, Iowa

CERTIFICATE OF APPROVAL

_____

PH.D. THESIS

_____

This is to certify that the Ph.D. thesis of

Yang Qiu

has been approved by the Examining Committee
for the thesis requirement for the Doctor of Philosophy
degree in Pharmacy (Pharmaceutics) at the August 2015 graduation.

Thesis Committee: _____
Douglas R. Flanagan, Thesis Supervisor

_____
Dale E. Wurster

_____
Maureen D. Donovan

_____
Lewis L. Stevens

_____
Eric E. Nuxoll

ABSTRACT

Dissolution rate is an important indicator of drug bioavailability. In this work, a mixed-kinetic-controlled dissolution model was developed which encompasses transport control and interface control as limiting cases. This model is mathematically equivalent to two existing mixed-kinetic-control models, but provides physicochemical significance to the semi-empirical quantities in these models by treating a dissolving solid surface as a distribution of various types of detachment and re-deposition sites that interact with the solution according to chemical kinetic theory. The degree of interface control is determined by the ratio of the collective re-deposition rate constant to the transport rate constant.

In the first experimental investigation, the intrinsic dissolution behavior of benzoic acid, salicylic acid and *trans*-cinnamic acid was investigated under different temperature (37 ℃, 10 ℃ and 3 ℃) and agitation (50-800 rpm) conditions. These compounds dissolved by transport control at 37 ℃, but exhibited up to 27% interface control at lower temperatures, calculated from the plots of $1/J$ vs. $\omega^{-0.5}$ (J = dissolution rate, ω = rotational speed), and alternatively from the plots of $\ln J$ vs. $\ln \omega$. It was concluded that as the temperature decreases, the collective re-deposition rate constant decreases faster than the transport rate constant, thus shifting the dissolution mechanism towards interface control at low temperatures.

In the second investigation, the intrinsic dissolution rate of benzoic acid as a function of agitation intensity was studied in water and various NaDS concentrations above the CMC at 25°C. The plots of J vs. $\omega^{0.5}$, fitted with the functional form of the derived mixed-kinetic-control model, indicate significant interface control. An extended dissolution model which features a micelle-interface interaction mechanism was proposed to give meaning to the fitting parameters

and offer a possible explanation for their variation with the micelle concentration. The manner in which the parameter varies with C_{mic} in the present study also suggests possible micellar activity effects.

In the third investigation, the effects of FD&C Blue #1, a water-soluble dye on sulfathiazole dissolution were studied. It was shown that low concentrations (10-100 μg/mL) of the dye reduced the intrinsic dissolution rate of sulfathiazole by up to 34% in 0.1 N HCl, while the same levels of FD&C Blue #1 only slightly inhibited sulfathiazole dissolution in 0.01 N HCl and exhibited no effect in water. An adsorption mechanism was suggested in which the protonation of sulfathiazole solid surface makes detachment sites preferred adsorption sites for the anionic dye, thus causing the dissolution rate reductions in in HCl solutions.

PUBLIC ABSTRACT

The dissolution behavior of a drug substance is an important part of its bioavailability. Three solid dissolution mechanisms are recognized: transport control, interface control and mixed-kinetic control. The mixed-kinetic control mechanism is not well studied as the majority of dissolution phenomena in pharmaceutical research are assumed to be transport-controlled. A phenomenological model for mixed-kinetic control was developed in which the interfacial step comprises molecular detachment and re-deposition and is described by chemical kinetic theory. This model encompasses interface control and transport control as limiting cases.

Experimental studies on three organic compounds showed that they dissolved by transport control at 37 ℃, but exhibited certain degrees of interface control at lower temperatures (10 ℃ and 3 ℃), which, according to the model, indicates that reducing the dissolution temperature slowed down re-deposition more than transport. Using mathematical approaches derived from the model, up to 27% interface control was calculated from the experimental results.

The second experimental investigation showed significant degrees of interface control in benzoic acid dissolution in sodium dodecyl sulfate (NaDS) solutions at 25 ℃. The dissolution behavior was well described by the mixed-kinetic control model and up to 73% interface control was calculated. An extension of the model was proposed to describe a potential micelle-interface interaction mechanism indicated by the model-fitted parameters.

The third investigation showed that FD&C Blue #1, a water-soluble dye, inhibited sulfathiazole dissolution in acidic media but not in water. The inhibition was attributed to the blocking of dissolution sites by dye adsorption. A potential pH-dependent adsorption mechanism was proposed in which protonation at sulfathiazole solid surface gives rise to preferential dye adsorption on detachment rates and thus reduced dissolution rates.

TABLE OF CONTENTS

LIST OF TABLES

LIST OF FIGURES

CHAPTER 1 INTRODUCTION

Dissolution and Bioavailability

Drug bioavailability has long been a subject of prime importance in pharmaceutical research and formulation development. This issue is directly related to the release of a drug from its formulation. The release rate of a drug is affected by a variety of factors, among which its diffusion and intrinsic dissolution properties play important roles. Sperandio et al. pointed out that dissolution indeed plays a key role in the overall efficiency of compressed tablets.[1] Parrott et al. later indicated the importance of dissolution kinetics in evaluating drug availability to the body.[2] This view was further consolidated by Nelson and others, who found the accumulation of certain drugs in the blood stream was controlled by dissolution rate.[3-5] The importance of dissolution in the absorption process was demonstrated schematically by Wagner (Figure 1-1).[6] Therefore, it is well recognized that the dissolution of solid drugs can often be the rate-limiting step in the absorption process.[7]

In vitro dissolution testing is an important tool in oral dosage form development because it can provide valuable information that aids in the prediction of drug bioavailability.[8] Various test methods are available such as the USP basket and paddle methods and intrinsic dissolution methods.[9] The basket and paddle methods are widely used for the dissolution testing of particles, capsules and compressed tablets. The intrinsic method, on the other hand, is designed to maintain a constant apparent surface area during a dissolution test. The experimental setups for this method are such that dissolution occurs only from a flat face of a solid tablet (usually prepared by powder compression or compaction). The term “intrinsic” is used because, with the

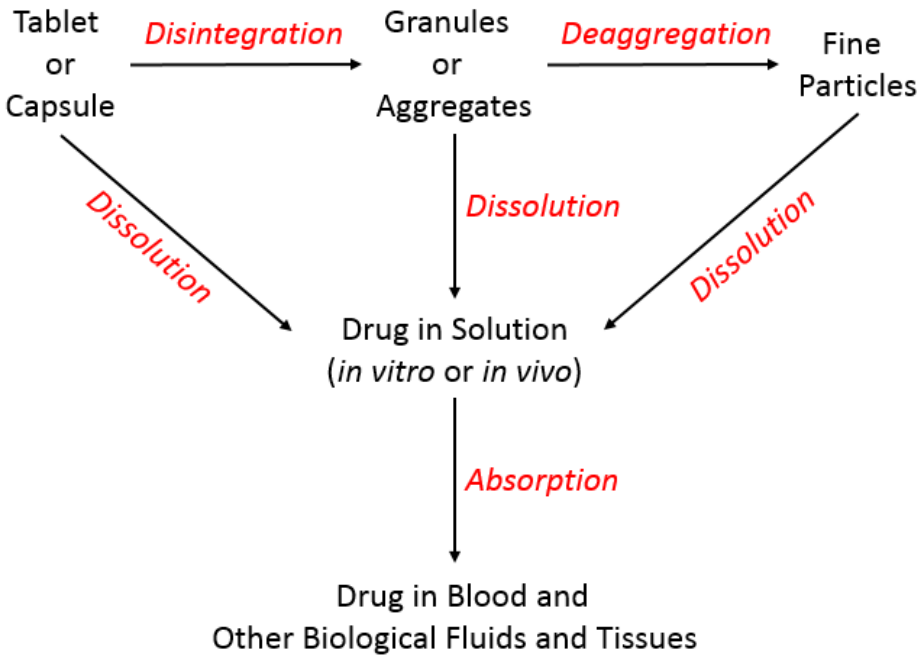

Figure 1-1. Schematic illustration of the role of dissolution in the absorption of drugs from solid dosage forms (diagram reproduced from Ref.6).

apparent surface area being constant, a steady dissolution rate is usually obtained under sink conditions which is function of solid-solvent interactions (i.e., solubility) and solute transport properties (such as diffusion coefficient and convection). This method has been widely used by pharmaceutical scientists who study dissolution phenomena from a fundamental, mechanistic point of view, because it eliminates varying surface area and particle aggregation issues with powder dissolution. Common intrinsic dissolution systems include those described by Nelson and the rotating disk dissolution system,[10,11] which will be discussed in more detail later.

Dissolution Mechanisms

It is well-established that the dissolution of a solid is a two-step process: (A) the interfacial step in which solid-state molecules become solvated, followed by (B) transport of these dissolved molecules into the bulk solution. At least three scenarios exist for controlling the dissolution process:

1) Step (A) is much faster than Step (B). In this case equilibrium solubility is rapidly established at the surface and transport becomes the rate-determining step;
2) Step (A) is much slower than Step (B). In this case the drug concentration near the surface is less than its solubility and the surface detachment step is rate-limiting.
3) Steps (A) and (B) are comparable in rate and neither the interfacial step nor transport are rate limiting.

Scenario (1) (transport-controlled dissolution) is the most widely adopted mechanism by pharmaceutical scientists. The first transport-controlled dissolution model was developed by Noyes and Whitney, who proposed that dissolution rate is directly proportional to the difference between solubility and bulk concentration:[12]

$$\frac{dM}{dt} = k(C_S - C_b) \tag{1-1}$$

where, M is the amount dissolved as a function of time, C_S is solubility, C_b is bulk concentration and k is a constant known as the "dissolution rate constant." This theory was seminal and simple but failed to elucidate the physical meaning of the constant k in terms of its dependence on the transport properties of the solute. Nernst and Brunner improved upon this theory by introducing the concept of a stagnant diffusion layer across which the solute diffuses from the solid surface

to bulk solution and forms a linear concentration profile (Figure 1-2).[13,14] This gives the dissolution rate constant (k) a simple and distinct meaning:

$$k = A\frac{D}{h} \tag{1-2}$$

where, A is the solid surface area, D is diffusion coefficient and "h" is diffusion layer thickness. This treatment effectively incorporates hydrodynamic complexities into the diffusion layer

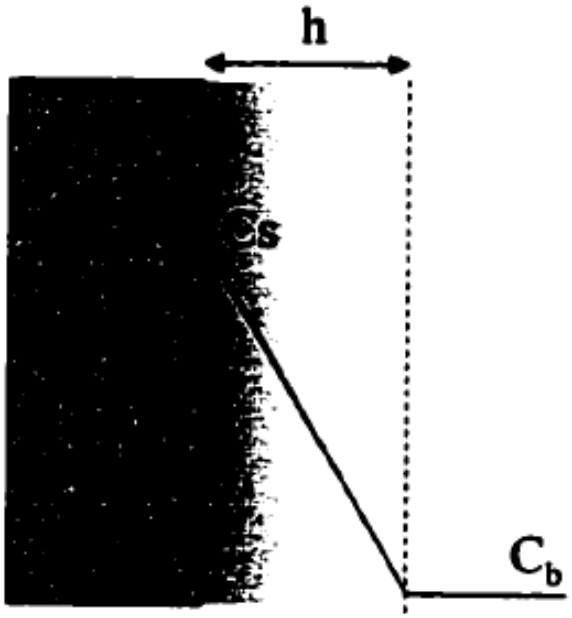

Figure 1-2. Nernst's diffusion layer model for dissolution form a planar surface, C_S = solubility, C_b = bulk solution concentration, h = diffusion layer thickness.[15]

thickness, "*h*". Therefore, it is not surprising that usually "*h*" cannot be determined *a priori* and has to be back-calculated from dissolution rate data. Such calculations can be problematic at times without first ascertaining if the dissolution is indeed transport-controlled. It also does not allow easy prediction of how system hydrodynamics affect the dissolution process.

Scenario (2) represents interface-controlled dissolution. This type of dissolution has little to no dependence on agitation type or intensity, since fluid flow has no effect on the interfacial step. Such phenomena have been investigated experimentally and theoretically by some investigators[16-19] but are rarely observed for compounds of pharmaceutical interest. This is often due to the fact that the agitation intensity required to attain interface control is too large (well beyond the laminar flow regime) to be of practical relevance. Dokoumetzidis et al. developed an interface-controlled dissolution model in which the interfacial step was regarded as a reversible reaction:[19]

$$\mathrm{s} + n\mathrm{w} \underset{k_{-1}}{\overset{k_1}{\rightleftharpoons}} \mathrm{c}$$

where, "s" is the undissolved solid, "*n*w" represents *n* free solvent molecules and "c" is the dissolved solid. The overall reaction rate was given by:

$$R = k_1[\mathrm{s}]^a[\mathrm{w}]^b - k_{-1}[\mathrm{c}] \tag{1-3}$$

Using Eqn.(1-3) and regarding $[\mathrm{w}]$ as a constant, the rate of change in solute concentration was calculated as:

$$\frac{d[c]}{dt} = k_1[\mathrm{w}]^b\left(\frac{M_0}{V} - [\mathrm{c}]\right)^a - k_{-1}[\mathrm{c}] \tag{1-4}$$

The numerical solution of Eqn.(1-4) was shown to describe the experimental dissolution results for commercial Naprosyn® and Furolin® tablets to a high degree of accuracy. However, this model is highly empirical in that [s] is defined as the amount of undissolved solid per unit volume of dissolution medium, which, although easily measurable, is not a real "concentration" in the physicochemical sense. This makes it difficult to interpret the "order", *a*, beyond just a variable (and empirical) fitting parameter. Also, the authors did not demonstrate the failure of the diffusion-layer model to describe their experimental results. In their experiments, the dissolving surface area decreased with time as a tablet dissolved, which means the diffusion-layer model could have also described the downward curving of their concentration-time profiles.

Scenario (3) may be called mixed-kinetic-controlled dissolution in that it is controlled by both the interfacial step and transport to comparable degrees. Theoretically, the rate of dissolution will be a function of not only the aforementioned mass transport properties, but also physicochemical parameters related to the kinetic processes of surface detachment and deposition. Berthoud viewed the interfacial step as an equivalent permeation process through an interfacial barrier and proposed a generalized version of the Nernst-Brunner equation:[20]

$$\frac{1}{A}\frac{dM}{dt} = \frac{(C_S - C_b)}{h/D + 1/p} \tag{1-5}$$

where, p is the effective interfacial permeability coefficient. The degree of control is thus determined by the relative magnitude of h/D versus $1/p$. However, since all surface processes are lumped together into an effective permeability coefficient, it does not provide a clear physical picture of the events occurring at the solid surface. Another widely adopted model for mixed-kinetic-controlled dissolution was proposed by Rickard et al., who assumed that the interfacial reaction rate, normalized with respect to the dissolving surface area, could be expressed as:[21]

$$J_{\mathrm{C}} = k_{\mathrm{C}}(C_{\mathrm{S}} - c_0)^n \tag{1-6}$$

where, c_0 is the concentration adjacent to the solid surface and k_{C} was termed a "chemical rate constant". The transport rate was expressed as:

$$J_{\mathrm{T}} = k_{\mathrm{T}}(c_0 - C_{\mathrm{b}}) \tag{1-7}$$

where, k_{T} was termed a "transport rate constant". At steady-state, J_{C} and J_{T} must be equal. For n = 1, the dissolution rate can be solved to give:

$$J = J_{\mathrm{C}} = J_{\mathrm{T}} = \frac{k_{\mathrm{T}}k_{\mathrm{C}}}{k_{\mathrm{T}} + k_{\mathrm{C}}}(C_{\mathrm{S}} - C_{\mathrm{b}}) \tag{1-8}$$

This is mathematically equivalent to Berthoud's model if the chemical rate constant and transport rate constant are identified with Berthoud's permeability coefficient (p) and Nernst and Brunner's D/h, respectively.

Experimental investigations of dissolution mechanisms have centered on the effects of experimental conditions such as temperature, agitation intensity and solution additives. Using a rotating disk apparatus, Rickard et al. showed that the dissolution of two types of calcite, Carrara marble and Iceland spar, in 0.7 M KCl solutions at pH 8.4 and 25 ℃ followed a mixed-kinetic-controlled mechanism with n = 1 (Eqn.(1-6)), as indicated by the non-zero intercept values for the plots of $1/J$ vs. $\omega^{-0.5}$ (ω: rotational speed) or equivalently by the curvature of the plots of J vs. $\omega^{0.5}$.[21] (how these plots relate to the dissolution mechanism will be discussed further in Chapters 3 and 4.) In a later investigation, they studied the rotating disk dissolution of these calcite minerals at various temperatures and determined "empirical apparent activation energies" (EAAE) for their chemical rate constants from Arrhenius plots.[22] This study will be discussed in

more detail in Chapter 3.

Investigations of the dissolution mechanisms of sparingly soluble, small-molecule organic compounds have been scarce, partially because their dissolution is usually assumed to be transport-controlled under normal experimental conditions (e.g., physiological temperature, low agitation intensity). Touitou et al. investigated the rotating disk dissolution rate of benzoic acid as a function of rotational speed at various temperatures.[23] They found that at 37 ℃, the dependency of dissolution rate on rotational speed (up to 730 rpm) adhered well to transport control. As the temperature decreased, deviations from transport control occurred. This study will be discussed in detail in Chapter 3.

Convective Diffusion Equation

The mass transport of a solute in a flowing fluid is described by the convective diffusion equation, given in vector calculus form by:

$$\frac{\partial c}{\partial t} = D \cdot \nabla^2 c - (\mathbf{v} \cdot \nabla) c \tag{1-9}$$

where, $c = c(\mathbf{r}, t)$ is concentration distribution, $\mathbf{v} = \mathbf{v}(\mathbf{r}, t)$ is fluid velocity distribution and ∇ is the Del operator. In Cartesian coordinates, Eqn.(1-9) becomes:

$$\frac{\partial c}{\partial t} = D\left(\frac{\partial^2 c}{\partial x^2} + \frac{\partial^2 c}{\partial y^2} + \frac{\partial^2 c}{\partial z^2}\right) - v_x \frac{\partial c}{\partial x} - v_y \frac{\partial c}{\partial y} - v_z \frac{\partial c}{\partial z} \tag{1-10}$$

In most dissolution cases, we are interested in the concentration distribution after the system has reached a steady-state, when both the velocity distribution and concentration distribution cease to vary with time. With a steady-state assumption, Eqn.(1-9) simplifies to:

$$0 = D \cdot \nabla^2 c - (\mathbf{v} \cdot \nabla) c \tag{1-11}$$

where, $\mathbf{v} = \mathbf{v}(\mathbf{r})$ is the steady-state velocity distribution. If this distribution is known, Eqn.(1-11) combined with appropriate boundary conditions can be solved analytically or numerically to give steady-state concentration profiles.

Rotating Disk Dissolution Systems (RDDS)

The rotating disk dissolution system is a frequently used for intrinsic dissolution studies. It is similar in concept to the rotating disk electrode (RDE) system. In this method, a solid material (usually powdered) is compressed into a disk in a die. The die is then mounted to a shaft that connects it to a rotor. During a dissolution test, the die is immersed in a dissolution medium and rotated at a designated speed, as shown in Figure 1-3.[24] The fluid flow profiles of the system, which can be obtained by numerically solving the Navier-Stokes equations, are shown in Figure 1-4, where the distance (z) measured perpendicularly from the disk surface and velocity components are non-dimensionlized according to:[25]

$$\begin{aligned} z_1 &= \left(\frac{\omega}{\nu}\right)^{1/2} z, \\ v_r &= r\omega F(z_1), \\ v_\phi &= r\omega G(z_1), \\ v_z &= -(\omega\nu)^{1/2} H(z_1). \end{aligned} \tag{1-12}$$

(v_r: radial; v_ϕ: azimuthal; v_z: axial; ν = kinematic viscosity; ω = rotational speed). Figure 1-5 gives a streamline representation of the flow pattern.[26]

In cylindrical coordinates, Eqn.(1-11) becomes:

$$0 = D(\frac{\partial^2 c}{\partial r^2} + \frac{1}{r}\frac{\partial c}{\partial r} + \frac{1}{r^2}\frac{\partial^2 c}{\partial \phi^2} + \frac{\partial^2 c}{\partial z^2}) - v_r \frac{\partial c}{\partial r} - \frac{v_\phi}{r}\frac{\partial c}{\partial \phi} - v_z \frac{\partial c}{\partial z} \tag{1-13}$$

The axial symmetry of the rotating disk system dictates that *c* cannot depend explicitly on ϕ. Levich further assumed that *c* was independent of *r*, which means the concentration is homogeneous in each lamina parallel to the disk.[27] These assumptions simplify Eqn.(1-13) to the case of one-dimensional transport normal to the disk:

$$0 = D\frac{\partial^2 c}{\partial z^2} - v_z \frac{\partial c}{\partial z} \tag{1-14}$$

Under sink conditions, the boundary conditions are:

$$\begin{aligned} c &\to 0 \text{ as } z \to \infty; \\ c &\to c_0 \text{ as } z \to 0. \end{aligned} \tag{1-15}$$

Using an asymptotic expression for the axial velocity component:[28]

$$H(z_1) = 0.510 z_1^2 - \frac{1}{3} z_1^3 + 0.103 z_1^4 - ... \tag{1-16}$$

Eqn.(1-14) can be solved to give

$$c_\rho = c_0 \left[1 - \frac{I(\rho)}{I(\infty)} \right] \tag{1-17}$$

where,

$$\rho = \frac{z}{\delta_M},\ \delta_M = 1.805 \left(\frac{D}{\nu} \right)^{1/3} \left(\frac{\nu}{\omega} \right)^{1/2} \tag{1-18}$$

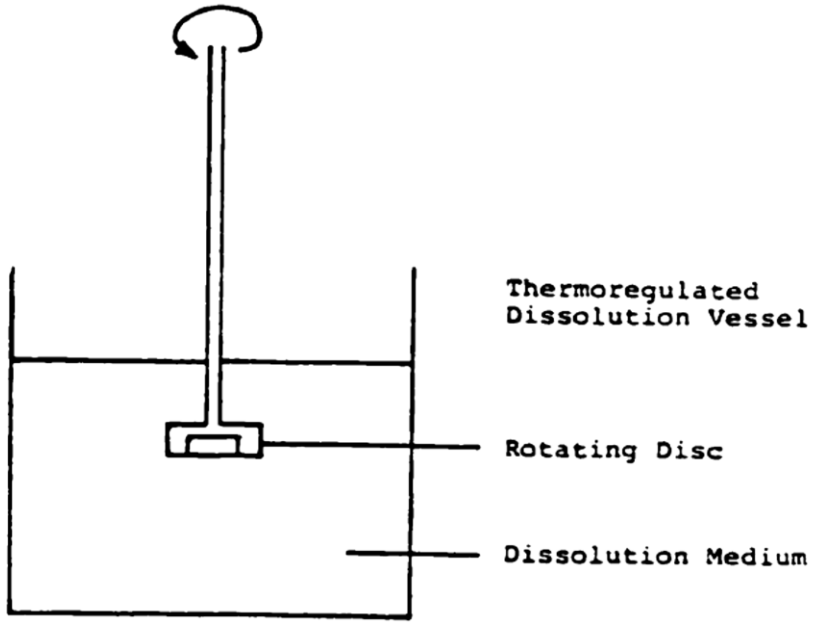

Figure 1-3. Rotating disk dissolution system.[24]

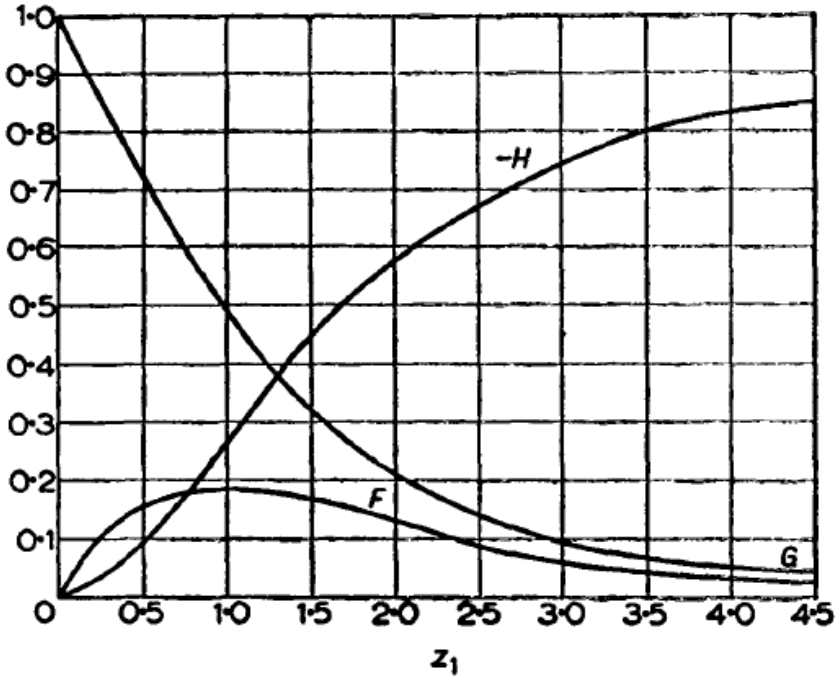

Figure 1-4. Normalized radial (*F*), axial (*G*), azimuthal (*H*) velocity profiles near a rotating disk.[25]

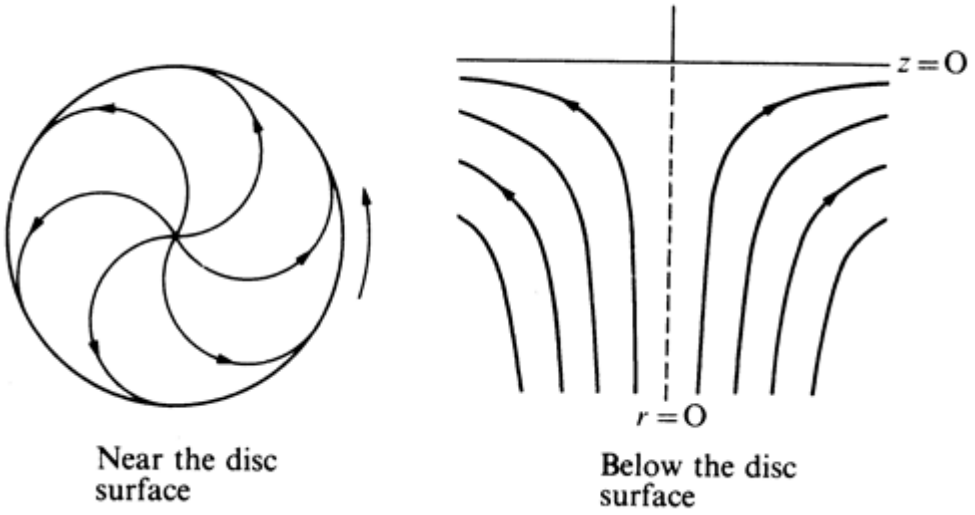

Figure 1-5. Schematic streamlines for the rotating disk system.[26]

and

$$I(\rho) = \int_0^{\rho} \exp\left\{-\rho^3 + 0.885\left(\frac{D}{\nu}\right)^{1/3}\rho^4 - 0.394\left(\frac{D}{\nu}\right)^{2/3}\rho^5 + \ldots\right\} \tag{1-19}$$

It can be seen that all concentration profiles are similar, described by the common factor $1 - I(\rho)/I(\infty)$. Figure 1-6 shows a typical concentration profile in a rotating disk system. It should be noted that the integral $I(\infty)$ contains a caveat, since the asymptotic expression (1-16) for v_ρ is only valid for small distances. Levich justified this by noting that since $D/\nu \sim 10^{-3}$ for most solutions at normal temperatures, the integral I converges rapidly beyond $z > \delta_M$, $\rho > 1$.[27] This means the concentration approaches the limiting value c_∞ at $\sim 0.18(\nu/\omega)^{1/2}$, well before

Eqn.(1-16) becomes inapplicable. It is for this reason that Levich regarded δ_M as the thickness of the transport boundary layer, i.e., the distance measured normal to the disk surface over which there is an appreciable concentration gradient. He further assumed that the convergence of the power series (Eqn.(1-19)) is so rapid that only the term in ρ^3 needs to be considered, so that:

$$I(\infty) = 0.8934 \tag{1-20}$$

Gregory and Riddiford calculated the contributions from terms proportional to ρ^4 and ρ^5 in $I(\infty)$ and found that for values of D/ν in the range $0 - 4\times10^{-3}$, $I(\infty)$ could be estimated more accurately by the empirical expression:[29]

$$I(\infty) = 0.8934 + 0.316\left(\frac{D}{\nu}\right)^{0.36} \tag{1-21}$$

For $D/\nu = 10^{-3}$, Eqn.(1-21) is ~3% higher than Eqn.(1-20). A difference of this magnitude is immaterial in all cases except those in which extreme precision is required. Figure 1-6 shows the true concentration profile as compared to Nernst's "equivalent linear concentration profile". The thickness of the Nernst layer is given by:

$$\delta_{\mathrm{N}} = 1.805 \cdot I(\infty)\left(\frac{D}{\nu}\right)^{1/3}\left(\frac{\nu}{\omega}\right)^{1/2} \tag{1-22}$$

Thus, the whole fluid body may be divided into two regions: $0 < y < \delta_{\mathrm{N}}$ and $y > \delta_{\mathrm{N}}$. For $y > \delta_{\mathrm{N}}$, mass transport is predominantly convective, whereas for $0 < y < \delta_{\mathrm{N}}$, it is both diffusive and convective. Near the disk surface, convection is minimal due to the viscous nature of the fluid and diffusion becomes the predominant means of transport. Thus, the mass transport flux from

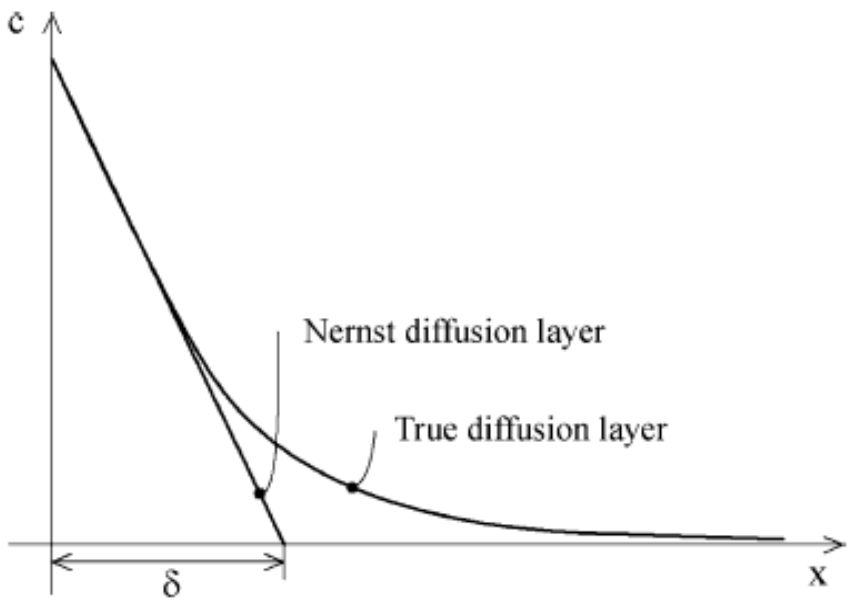

Figure 1-6. True diffusion layer versus Nernst diffusion layer.[30]

the disk surface is given by Fick's 1st law:

$$J_{\mathrm{T}} = -D\left(\frac{\partial c}{\partial z}\right)_0 = \frac{1}{1.805 \cdot I(\infty)} c_0 D^{2/3} \nu^{-1/6} \omega^{1/2} \approx 0.62 c_0 D^{2/3} \nu^{-1/6} \omega^{1/2} \qquad (1\text{-}23)$$

where, Eqns.(1-17)-(1-19) are used. It is clear from simple mass balance considerations that Eqn.(1-23) is also the dissolution flux (i.e., the amount of solid dissolved per unit disk area per unit time). This will be discussed further in Chapter 2.

If the dissolution is transport-controlled, $c_0 = C_{\mathrm{S}}$ and Eqn.(1-23) becomes:

$$J = 0.62 C_{\mathrm{S}} D^{2/3} \omega^{1/2} \nu^{-1/6} \qquad (1\text{-}24)$$

This is the well-known Levich equation. What distinguishes Eqn.(1-24) from the Nernst-Brunner model is that it contains only measurable quantities and no adjustable parameter such as the film thickness (*h*) and, therefore, allows for direct experimental verification. An important feature of Eqn.(1-24) is that for transport-controlled dissolution, the dissolution rate is proportional to the square-root of rotational speed (ω). This offers a straightforward way of ascertaining if dissolution is indeed transport-controlled. The relation between dissolution rate and agitation intensity for different dissolution mechanisms will discussed in more detail in Chapter 2.

Experimental Aspects of Rotating Disk Systems

Previously, it was shown that the convective transport theory for rotating disk systems was developed under a set of ideal assumptions, such as infinite disk span and infinite fluid volume, the absence of natural convection, etc. In practice, there are various deviations from these ideal situations, which are mainly hydrodynamic and related to the shapes of experimental rotating disks. According to Riddiford, a rudimentary requirement for a practical disk to be regarded as infinitely large is that the disk radius must be much greater than the thickness of the momentum boundary layer,[28] i.e.,

$$\frac{2.8}{r_0}\left(\frac{\nu}{\omega}\right)^{1/2} << 1 \tag{1-25}$$

where, r_0 is the disk radius and $\delta_p = 2.8(\nu/\omega)^{1/2}$ is, as discussed earlier, the momentum boundary layer thickness. Eqn.(1-25) is equivalent to:

$$2.8^2 \frac{\nu}{\omega r_0^2} = \frac{7.84}{\mathrm{Re}_0} << 1 \tag{1-26}$$

where, Re_0 denotes the overall Reynolds number, defined as the ratio of inertial forces (represented by ωr_0^2) to viscous forces (represented by ν) for a given flow condition. The appearance of the Reynolds number leads to additional requirements: a) Re_0 must be less than the critical value for the onset of turbulence, and b) the average Reynolds number must be much greater than the value which leads to a significant contribution from natural convection.[28] The critical Reynolds number for the onset of turbulence in a rotating disk system has been reported to be between 2×10^5 and 3×10^5.[31,32] Therefore, it is prudent to ensure that that the Re_0 does not exceed 2×10^5.

It is not difficult to check whether an experimental rotating disk apparatus meets the above requirements. However, deviations stemming from the geometry of practical disks are usually so complicated in nature that the understanding of them is at an empirical level. Such practical issues will not be dealt with in the present work, but will be cited where necessary.

Objectives

Owing to the fact that transport control is such a predominantly adopted assumption in pharmaceutical research, the mixed-kinetic-control mechanism for solid dissolution is not particularly well studied among pharmaceutical scientists. This research seeks to investigate the mixed-kinetic-control mechanism both theoretically and experimentally. Due to its generality in terms of encompassing transport control and interface control as limiting cases, understanding this mechanism may further our understanding of solid-state dissolution phenomena in general, which, in turn, may assist in understanding *in vitro* or *in vivo* performance and designing solid dosage forms tailored to a drug's intrinsic dissolution properties.

The specific objectives of this work include:

1. Describing the interfacial step of dissolution in terms of the distributions and energetic characteristics of various solid surface sites using chemical kinetic theory (Chapter 2);
2. Using the results from Objective 1 to derive a model for mixed-kinetic-controlled dissolution for rotating disk and general forced-flow systems and to compare with existing models (Chapter 2);
3. Experimentally investigating the effects of agitation intensity and temperature on dissolution behavior and analyze the results with the derived model (Chapter 3);
4. Experimentally investigating the effects of agitation intensity and surfactant concentration on dissolution behavior and modify the derived model so that it may be applied to dissolution behavior in micellar solutions (Chapter 4);
5. Investigate the effects of dye adsorption on intrinsic dissolution rates and show how the derived model qualitatively accounts for the data (Chapter 5).

CHAPTER 2 MIXED-KINETIC-CONTROLLED DISSOLUTION MODEL

A mixed-kinetic-control model for solid dissolution will be developed. This model will emphasize the kinetics of the interactions taking place at the solid-solution interface during dissolution. The model is concerned with steady-state dissolution processes that occur within a sufficiently short period of time after a solid is brought into contact with a solvent, so that the solid surface does not undergo significant morphological changes. The dissolution rate during this time is usually referred to as "initial dissolution rate."

Interfacial Kinetics

From a dynamic perspective, the interfacial step of dissolution involves molecular detachment of molecules from the solid surface and the re-deposition of solute molecules on the solid surface. The former is effected through reactions between the solvent and solid molecules, and the latter through reactions between solute molecules and certain sites on the solid surface. It is well recognized that molecules at the solid surface are in a different energetic environment than those in the interior.

Consider a crystalline solid with a simple cubic lattice. Figure 2-1 depicts typical microscopic structures found on its surface, with each molecule represented by a cube.[33] Molecules may be in the surface (0), on the surface (1), at a corner (2), at an edge (3), in a step (4), on a step (5), or at a kink in a step (k). Scenarios (-1) and (6) represent vacant sites created by removal of molecules from the surface or a step, respectively. A common feature of these molecules is fewer numbers

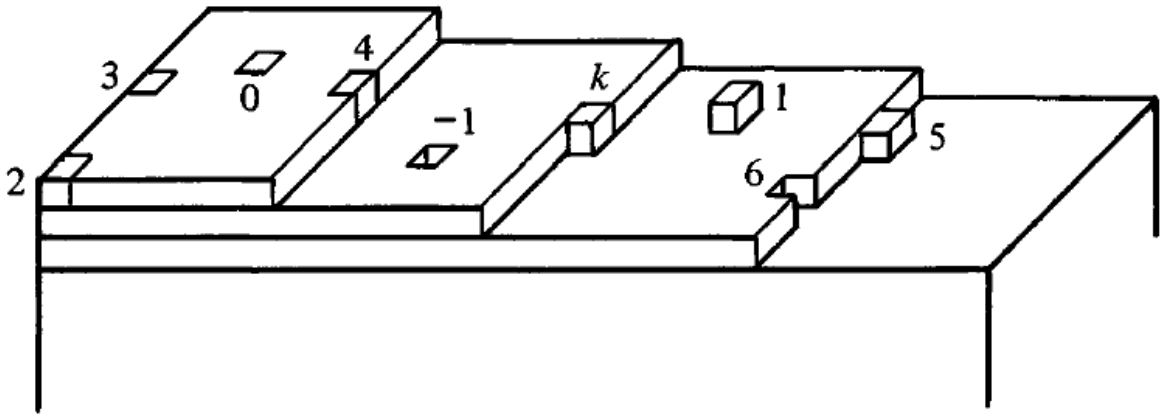

Figure 2-1. Schematic of the surface of a crystalline solid with a simple cubic lattice.[33]

of neighbors and consequently lower binding energies than their interior counterparts. These molecules are in direct contact with the liquid phase during dissolution.

Due to the strong interactions between molecules in the solid state, surface molecule detachment cannot be regarded as probabilistically independent. However, in so far as initial dissolution behavior is concerned, it is a reasonable approximation to assume that detachment occurs mainly for molecules with low binding energies at the solid surface, i.e., low coordination numbers. Examples of these molecules are "1" and "5" in Figure 2-1, which have 1 and 2 nearest neighbors (compared to 6 for a bulk molecule), respectively. These molecules, or "detachment sites", may be regarded as sufficiently far apart to be mutually independent. The reaction rate can be described by the number of molecules detached per unit time from unit surface area. If detachment sites are classified into various types according to their chemical environment, the detachment rate at each type of site may be written as:

$$R_{\mathrm{t},i} = k_{\mathrm{t},i}\sigma_{\mathrm{t},i} \tag{2-1}$$

where, $k_{\mathrm{t},i}$ is the reaction rate constant and $\sigma_{\mathrm{t},i}$ is the surface density of the *i*-th type of detachment site. According to the independence assumption, the total detachment rate can be obtained by summing Eqn.(2-1) over all types of detachment sites:

$$R_{\mathrm{t}} = \sum_i k_{\mathrm{t},i}\sigma_{\mathrm{t},i} \tag{2-2}$$

This treatment is analogous to that of heterogeneous surface kinetics by Constable.[34,35]

Re-deposition kinetics can be treated in a similar fashion. It has been recognized both theoretically and experimentally that kink sites ("k" in Figure 2-1) present the most probable position for solute re-deposition, followed by steps ("4"), while re-deposition on terraces ("0" and "1") is the least probable.[36] The high-probability sites may also be regarded as sufficiently far apart to be mutually independent. Since re-deposition is a reaction between re-deposition sites with the solute, the re-deposition rate at each type of site, classified according to the chemical environment, may be written as:

$$R_{\mathrm{p},i} = k_{\mathrm{p},i}\sigma_{\mathrm{p},i}c_0 \tag{2-3}$$

where, $k_{\mathrm{p},i}$ is the reaction rate constant, $\sigma_{\mathrm{p},i}$ is the surface density of the *i*-th type of re-deposition site and c_0 is the solute concentration at the boundary. The proportionality to c_0 is a result of dilute solution approximations which also ignores the possibility of re-deposition as self-associates (e.g., dimers). The independence assumption then allows the total re-deposition rate is given by

$$R_{\mathrm{p}} = \sum_i R_{\mathrm{p},i} = c_0 \kappa_{\mathrm{p}} \tag{2-4}$$

where, $\kappa_{\mathrm{p}} = \sum_i k_{\mathrm{p},i} \sigma_{\mathrm{p},i}$ may be regarded as a *collective re-deposition rate constant* for all types of re-deposition sites.

Finally, the total interfacial mass transfer flux is given by:

$$J_{\mathrm{I}} = R_{\mathrm{t}} - R_{\mathrm{p}} = R_{\mathrm{t}} - c_0 \kappa_{\mathrm{p}} \tag{2-5}$$

From Eqn.(2-6), it can be seen that $J_{\mathrm{I}} = 0$ if $c_0 = R_{\mathrm{t}} / \kappa_{\mathrm{p}}$. For this reason, the ratio $R_{\mathrm{t}} / \kappa_{\mathrm{p}}$ may be termed the "transient solubility":

$$\frac{R_{\mathrm{t}}}{\kappa_{\mathrm{p}}} \equiv C_{\mathrm{S,\,TRAN}} \tag{2-7}$$

Eqn.(2-5) may now be rewritten as:

$$J_{\mathrm{I}} = \kappa_{\mathrm{p}} (C_{\mathrm{S,\,TRAN}} - c_0) \tag{2-8}$$

which is similar to Eqn.(1-6) with n = 1. It should be noted, however, that the transient solubility is a function of the distribution of various detachment and re-deposition sites on a solid surface as well as their interaction properties with the solution. Therefore, it may not be the same as the equilibrium solubility (C_{S}), which is a thermodynamic quantity determined by a substance's chemical potentials in bulk solid and solution phases.

The importance of this section is that it describes the interfacial step of dissolution in terms of the distribution of various detachment and re-deposition sites on a solid surface and their reaction kinetics with the solution phase. In contrast, Berthoud[20] and Rickard et al.[21] both treated the

interfacial step in a semi-empirical manner by using an effective permeability coefficient (*p*) or chemical rate constant (k_C) without elucidating their physicochemical basis. Therefore, the present model attempts to further our phenomenological understanding of the interfacial processes during dissolution.

Mass Transport and Steady-state Dissolution Rate

In Chapter 1, it was shown that under the boundary condition $c(\infty) = 0$ (sink condition), the steady-state concentration profile for a rotating disk system is given by Eqn.(1-17):

$$c_\rho = c_0 \left[1 - \frac{I(\rho)}{I(\infty)} \right]$$

while the mass transport flux is given by Eqn.(1-23):

$$J_T = 0.62 c_0 D^{2/3} \nu^{-1/6} \omega^{1/2}$$

It can be shown that these results also apply to acids or bases which ionize in water (without other solutes such as buffer species). Consider a weak acid (HA) which ionizes according to:

$$HA \rightleftharpoons H^+ + A^-$$

In most cases, the quantity of interest is the total concentration of A, i.e., $c = c_{HA} + c_A$. According to Fick's 1st law, the total diffusive flux is given by:

$$J_T = J_{T,HA} + J_{T,A} = -D_{HA} c_{HA}' - D_A c_A' \tag{2-9}$$

where, the prime symbol is used to denote derivative with respect to the axial coordinate, *z*.

Define α as $\alpha \equiv c_A / c$, which is the fraction of A^-. Eqn.(2-9) can be rewritten as:

$$J_T = -[D_{HA}(1-\alpha) + D_A\alpha]c' + (D_{HA} - D_A)\alpha' c \tag{2-10}$$

Thus, the relationship between the total diffusive flux and the total concentration gradient, c', is not as simple as that for the individual species, because of the presence of the extra term, $(D_{HA} - D_A)\alpha' c$. However, since HA and A^- have almost identical diffusivities, i.e., $D_{HA} \approx D_A$, [37,38] this term may be neglected altogether in Eqn.(2-10), simplifying it to:

$$J_T \approx -[D_{HA}(1-\alpha) + D_A\alpha]c' \approx D_{HA}c' \approx D_A c' \tag{2-11}$$

Therefore, the convective diffusion equation may simply be established with respect to the total concentration:

$$D_{HA}c'' - v_z c' = 0 \tag{2-12}$$

which is the same as that for an unionizable solute.

Since c_0 is constant at steady-state, the interfacial mass transfer flux (J_I) must balance the transport flux (J_T):

$$R_t - \kappa_p c_0 = -D\left(\frac{\partial c}{\partial z}\right)_0 = 0.62 c_0 \omega^{1/2} \nu^{-1/6} D^{2/3} \tag{2-13}$$

which, upon the elimination of c_0, leads to the steady-state dissolution rate:

$$J = J_I = J_T = \frac{R_t}{1 + \dfrac{\kappa_p}{0.62\omega^{1/2}\nu^{-1/6}D^{2/3}}} \tag{2-14}$$

Eqn.(2-14) describes the mixed-kinetic-controlled dissolution rate from a rotating disk. It encompasses the limiting cases of transport-controlled and interface-controlled dissolution. The former is obtained when deposition occurs much faster than transport, i.e., $\kappa_p >> 0.62\omega^{1/2}\nu^{-1/6}D^{2/3}$, in which case Eqn (2-14) becomes:

$$J \approx 0.62\frac{R_t}{\kappa_p}\omega^{1/2}\nu^{-1/6}D^{2/3} \tag{2-15}$$

Interface-controlled dissolution is obtained when $\kappa_p << 0.62\omega^{1/2}\nu^{-1/6}D^{2/3}$. In this case, Eqn (2-14) becomes

$$J \approx R_t \tag{2-16}$$

i.e., the dissolution rate is practically equal to the detachment rate. The reason for this is obvious: the transport flux removes the solute away from the surface so fast that the boundary concentration, c_0, becomes very small and the re-deposition rate, which is proportional to c_0, becomes negligible compared to R_t.

Generalization to General Forced Flow Systems

The linearity of the transport equation makes it possible to deduce several important general features of mass transport in systems with simple flow characteristics. First, all steady-state concentration profiles are similar under sink conditions, i.e., given by a common distance function (such as $1-I(\rho)/I(\infty)$ in Eqn.(1-17)) multiplied by the boundary concentration c_0. If convection is generated by rotation around a fixed axis, the steady-state mass transport flux

under sink conditions may generally be expressed as:[39]

$$c_0 N(D,\nu)\omega^b \tag{2-17}$$

where, ω is rotational speed, $N(D,\nu)$ is some function of viscosity and diffusivity, and *b* is a hydrodynamic constant characterizing the system. The term $N(D,\nu)\omega^b$ may be conveniently called the transport rate constant. In the case of an ideal rotating disk system,

$$N(D,\nu) = 0.62 D^{2/3}\nu^{-1/6},\ b{=}0.5 \tag{2-18}$$

Eqn.(2-17) is usually valid for a wide range of ω , as long as flow is laminar and natural convection is neglected. Since R_t and κ_p are assumed to be unaffected by convection, we need only replace its right side with (2-17)

$$R_t - \kappa_p c_0 = c_0 N(\nu, D)\omega^b \tag{2-19}$$

This leads to:

$$J = \frac{R_t}{1 + \dfrac{\kappa_p}{N(D,\nu)\omega^b}} \tag{2-20}$$

Or, using the definition of transient solubility (Eqn.(2-7)),

$$J = C_{S,\,TRAN}\,\frac{\kappa_p N(D,\nu)\omega^b}{\kappa_p + N(D,\nu)\omega^b} \tag{2-21}$$

By comparing Eqn.(2-21) to Eqns.(1-5) and (1-8), it can be seen that this model is equivalent to the aforementioned models by Berthoud[20] and by Rickard et al.[21] under sink conditions ($C_b = 0$),

provided that Berthoud's permeability coefficient (*p*) or Rickard's chemical rate constant (k_C) is identified with the collective re-deposition rate constant (κ_p) and the transport rate constant, D/h or k_T, is expressed as $N(D,\nu)\omega^b$ (in the Nernst-Brunner theory, the film thickness, *h*, is usually some function of diffusivity and viscosity). To reiterate what has been stated before,

It can be readily seen that Eqn.(2-20) passes to transport control when $\kappa_p >> N(D,\nu)\omega^b$ and interface control when $\kappa_p << N(D,\nu)\omega^b$. This suggests a simple definition for the degree of interface control (P_I):

$$P_I = \frac{N(D,\nu)\omega^b}{\kappa_p + N(D,\nu)\omega^b} \tag{2-22}$$

The transport-controlled limit of Eqn.(2-20) is given by:

$$J \approx \frac{R_t}{\kappa_p} N(\nu,D)\omega^b \tag{2-23}$$

The power relation, $J \propto \omega^b$, is widely adopted among investigators of heterogeneous reactions.[14,39-41] Eqns.(2-20) and (2-23) suggest that one can determine the dissolution mechanism experimentally by investigating the *J* vs. ω^b dependency. Taking the logarithms of both sides of Eqn.(2-23) yields:

$$\ln J = b \ln \omega + C \tag{2-24}$$

Therefore, the hydrodynamic constant, *b*, can be determined by measuring the dissolution rates for a compound assumed to dissolve by transport control at various agitation intensities. The *b*-value is then obtained as the slope of ln*J* plotted against lnω.

CHAPTER 3 TEMPERATURE EFFECTS ON DISSOLUTION

Introduction

The mixed-kinetic-controlled dissolution model of Chapter 2 indicates that altering the temperature and agitation intensity (ω) can potentially increase the degree of interface control. According to the theory, the dissolution mechanism is determined by the relative magnitude of the collective re-deposition rate constant, $\kappa_p = \sum_i k_{p,i}\sigma_{p,i}$, versus the transport rate constant, $N(D,\nu)\omega^b$. The limiting case of transport control is obtained when the dimensionless quantity $\kappa_p / [N(D,\nu)\omega^b] >> 1$. In order to increase the degree of interface control, $\kappa_p / [N(D,\nu)\omega^b]$ must be reduced. The rate constants, κ_p and $N(D,\nu)\omega^b$, are both increasing functions of temperature. If κ_p decreases faster than $N(D,\nu)$ as the temperature decreases, the ratio $\kappa_p / N(D,\nu)$ will be reduced. In this case, lowering the dissolution temperature while increasing the agitation intensity will increase the degree of interface control.

Touitou et al. studied the dissolution of benzoic acid at low temperatures using a rotating disk apparatus. They found that at 37 ℃, the dissolution behavior conformed well to the Levich equation, indicating complete transport control of dissolution. At lower temperatures (10 ℃, 15 ℃ and 25 ℃), negative deviations from the Levich equation appeared, and the plots of *J* vs. $\omega^{1/2}$ became somewhat downwardly curved (Figure 3-1). They concluded that at high rotational speeds and low temperatures the interfacial reactions became the rate-limiting step in benzoic acid dissolution. This conclusion is questionable because the authors did not provide the sources

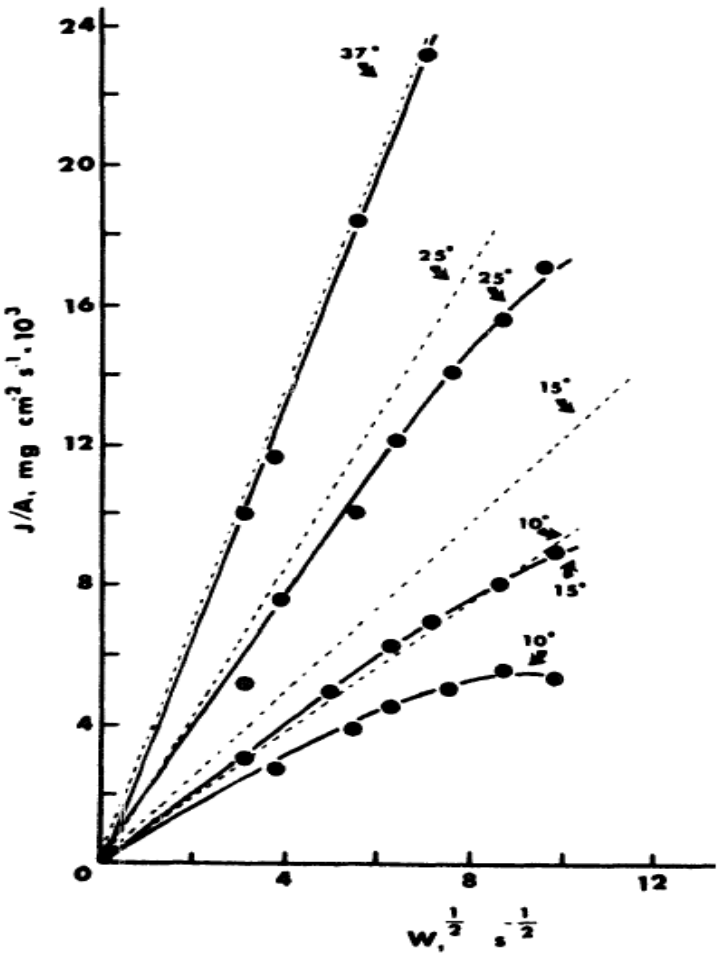

Figure 3-1. Plots of dissolution rate (J / A) against $\omega^{1/2}$ for benzoic acid dissolution at different temperatures from Touitou et al.; ---: calculated by the Levich equation.[22]

of solubility, diffusivity and viscosity values used in calculating the theoretical dissolution rates (dashed lines in Figure 3-1). Tables 3-1 - 3-3 list some of the literature values for benzoic acid solublity, diffusivity and water viscosity at 37 ℃. By taking the average value for each of these quantities and converting to cm-mg-min units, the theoretical dissolution rates can be obtained from the Levich equation (Table 3-4). It can be seen that the experimental rates are 20-26% lower than the calculated ones, contrary to the close agreement claimed by the authors. This most

Table 3-1. Literature values for benzoic acid solubility (C_S) in water at 37 ℃.

Source	C_S (37 ℃, mg/mL)
Banerjee et al.[42]	5.131
Humphreys et al.[43]	5.129 (0.01 N HCl)

Table 3-2. Literature diffusivity (D) values for benzoic acid in water at 37 ℃.

Source	D (x10^{-5} cm^2/s)
Delgado[44]	1.35
Kaunisto et al.[45]	1.30 (±0.07)

Table 3-3. Literature values for the kinematic viscosity of water (v) at 37 ℃.

Source	v (x10^{-2} cm^2/s)[1]
Korson et al.[46]	0.693
Kestin et al.[47]	0.697

1. Obtained by interpolation between values at 35 ℃ and 40 ℃; the average of the uncertainties for the 35 ℃ and 40 ℃ values by Kestin is 0.0053 mm^2/s.

Table 3-4. Comparison of calculated dissolution rates with those reported by Touitou et al. at 37°C (ω: rotational speed; C_S: solubility; D: diffusivity; v: kinematic viscosity; J_C: calculated dissolution rates using the Levich equation; J_{EXP}: dissolution rate reported by Touitou et al.) [22]

ω (RPM)	C_S (mg/mL)	D (x10^{-3} cm^2/min)	v (cm^2/min)	J_C (mg/min-cm^2)	J_{EXP}[4] (mg/min-cm^2)
98	5.130[1]	0.795 ($\pm$0.042)[2]	0.417 ($\pm$0.003)[3]	0.78 ($\pm$0.03)	0.60
140				0.94 ($\pm$0.03)	0.70
300				1.37 ($\pm$0.05)	1.10
500				1.77 ($\pm$0.06)	1.39

1. The average of the two values in Table 4-1.
2. Converted from the variability value (0.07x10^{-9} m^2/s) reported by Kaunisto et al.[45]
3. Converted from the variability value (0.005 mm^2/s) reported by Kestin et al.[47]
4. Data extracted from Touitou et al.[22] using Origin® 8.5.

likely indicates systematic deviations of their experimental apparatus from an ideal rotating disk system. In fact, their apparatus was similar in geometry to the Vankel® USP VI intrinsic dissolution apparatus described in Chapter 5 and the apparatus described later in this chapter. This geometry, along with several others, was found by Riddiford and others to exhibit the most marked deviations from the Levich theory.[28] For example, deviations up to 15% have been reported by Prakongpan et al. in a study of benzoic acid dissolution using this type of apparatus.[48] Due to such systematic deviations, one cannot draw definitive conclusions about dissolution mechanisms solely from a comparison of experimental dissolution data with the

Levich model.

Another notable investigation of temperature effects on dissolution behavior was conducted by Sjöberg et al. (briefly mentioned in Chapter 1).[22] Figure 3-2 shows the rotating disk dissolution rates for Carrara marble and Iceland spar (two types of calcite crystals, $CaCO_3$) at pH 8.4 in 0.7 M KCl plotted against $\omega^{1/2}$ (ω: rotational speed) at different temperatures. The

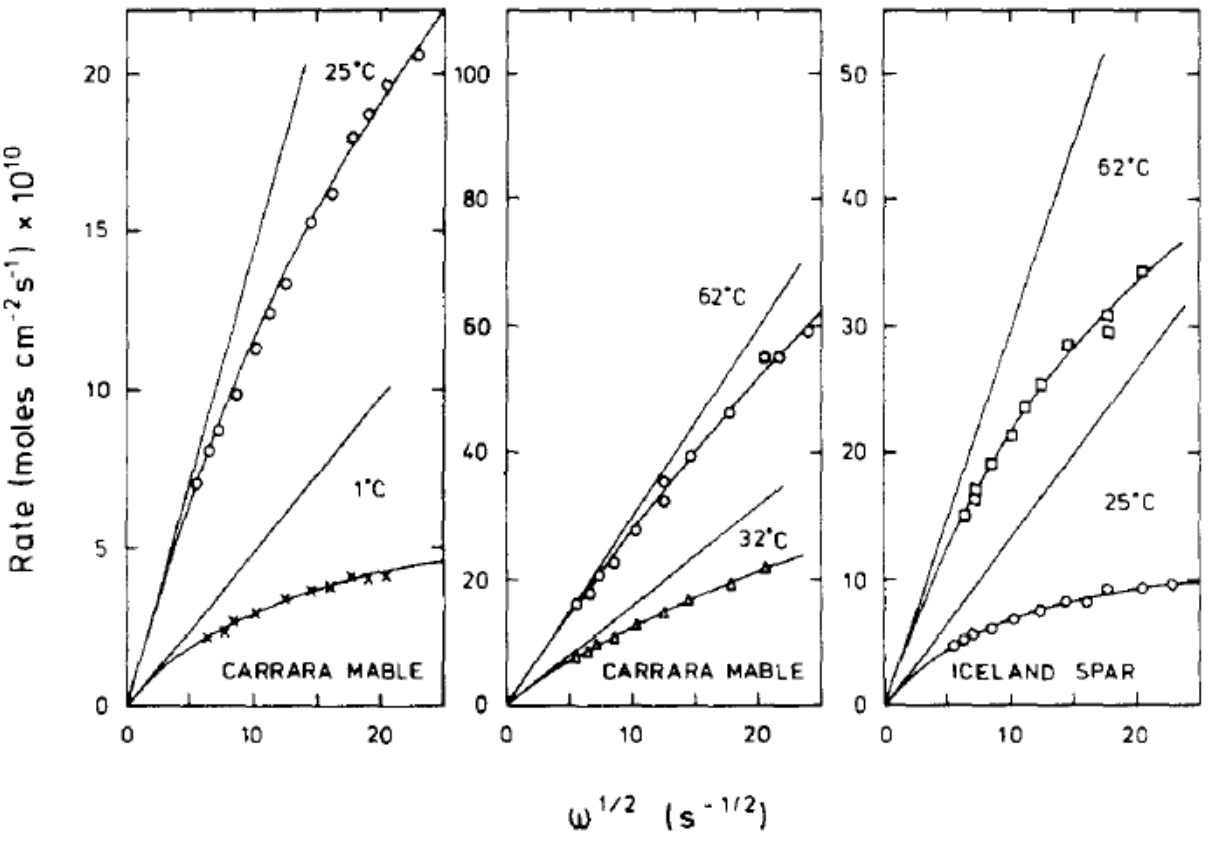

Figure 3-2. Plots of dissolution rate versus $\omega^{1/2}$ (ω: rotational speed) for Carrara marble and Iceland spar at pH 8.4 in 0.7 M KCl solutions at different temperatures (the straight lines represent purely transport controlled dissolution at each temperature).[22]

straight lines in these graphs represent purely transport controlled dissolution and are calculated using the Levich equation: $J \approx 0.62 C_S \omega^{1/2} \nu^{-1/6} D^{2/3}$. The experimental data were fitted with Eqn.(1-8), derived by themselves and discussed in Chapter 1:[21]

$$J = \frac{k_T k_C}{k_T + k_C} C_S$$

where, $k_T = 0.62 \omega^{1/2} \nu^{-1/6} D^{2/3}$ is the transport rate constant for a rotating disk system, k_C is the chemical rate constant describing the interfacial processes, and the bulk concentration, C_b, was dropped since sink conditions were maintained in their experiments. Under transport control, $k_T << k_C$ and Eqn.(1-8) reduces to $J = k_T C_S$. Since $k_T > \frac{k_T k_C}{k_T + k_C}$, dissolution controlled by mixed kinetics is always slower than if it were transport-controlled at the same temperature. Therefore, the negative deviations from the straight lines in Figure 3-2 indicate that Carrara marble and Iceland spar dissolved by mixed-kinetic control under the specified conditions. To obtain the chemical rate constants from these plots, Eqn.(1-8) was inverted to give:

$$\frac{1}{J} = \frac{1}{0.62 C_S \omega^{1/2} \nu^{-1/6} D^{2/3}} + \frac{1}{C_S k_C} \qquad (3\text{-}1)$$

Eqn.(3-1) indicates that the reciprocal dissolution rate, $1/J$, varies linearly with $\omega^{-1/2}$ with the slope and intercept being $(0.62 C_S \nu^{-1/6} D^{2/3})^{-1}$ and $(C_S k_C)^{-1}$, respectively. Figure 3-3 shows the linearly fitted plots of $1/J$ vs. $\omega^{-1/2}$ for these calcite crystals. The value of k_C at each temperature was determined from the corresponding intercept and solubility. Figure 3-4 shows the Arrhenius plots for k_C for these calcite crystals. The activation energies were determined by linear

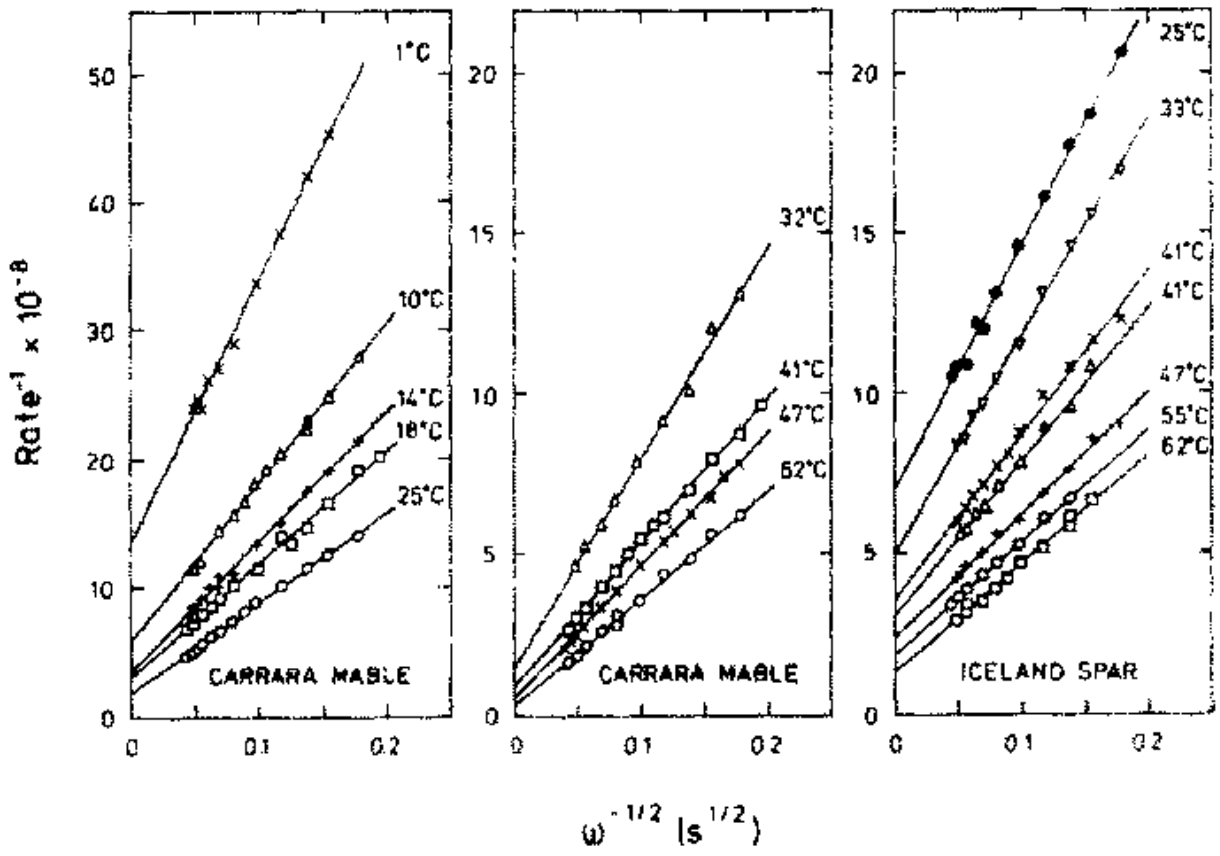

Figure 3-3. Plots of reciprocal dissolution rate versus $\omega^{-1/2}$ for Carrara marble and Iceland spar at pH 8.4 in 0.7 M KCl solutions at different temperatures.[22]

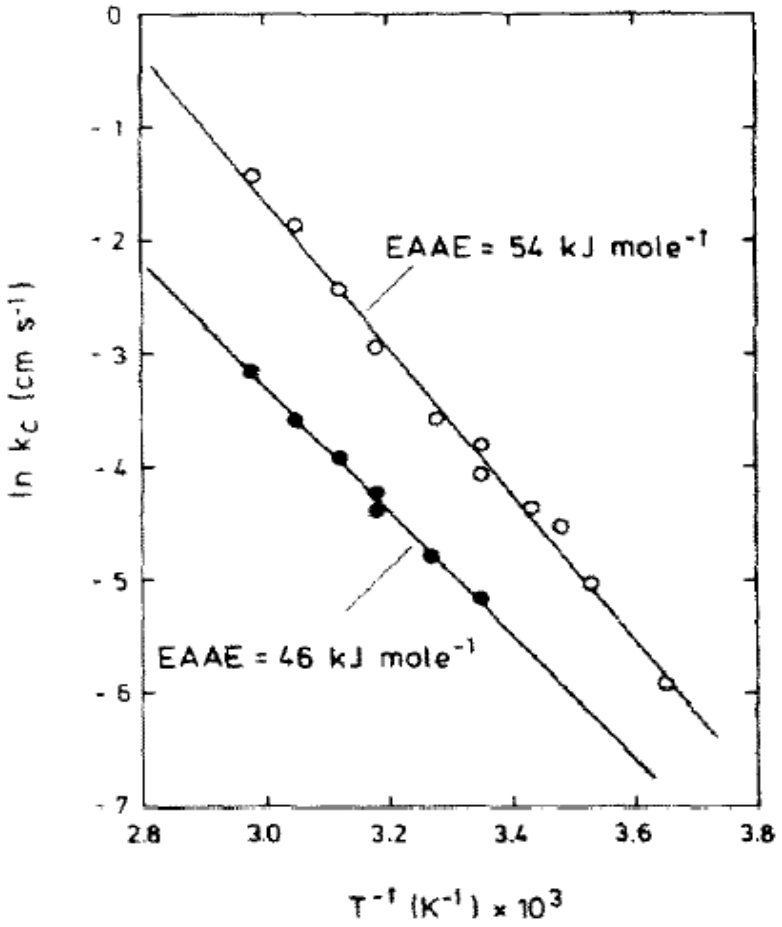

Figure 3-4. Arrhenius plots for the chemical rate constant, k_C, for Carrara marble (○) and Iceland spar (●).[22]

regression to be 54 kJ/mol and 46 kJ/mol for Carrara marble and Iceland spar, respectively.

An important result from Sjöberg's study is that calcite dissolution deviated most significantly from transport control at low temperatures and high agitation intensities (as indicated by the deviations from the straight lines in Figure 3-2). Therefore, it may be concluded that the combination of low temperature and high agitation intensity can increase the k_T / k_C ratio

and bring out the effects of interface control. This chapter presents experimental investigations of the effects of temperature and agitation intensity on dissolution mechanism for three organic compounds and analyses of the results using the mixed-kinetic-controlled dissolution model.

Materials and Methods

Materials

Benzoic acid, salicylic acid and *trans*-cinnamic acid (AR reagent grade, Sinopharm Chemical Reagent Co.) were used as received for this investigation. Some of their physicochemical properties are listed in Table 3-5. These compounds were chosen for the following reasons:

1) They each have relatively low aqueous solubilities, so that their dissolution would be slow enough not to cause significant surface roughening or rapid boundary recession. This is an essential requirement for intrinsic dissolution testing;

2) Other than solubilization and ionization, they don't interact with the dissolution medium (aqueous HCl solution or pure water) to complicate theoretical analysis;

3) They have good compression characteristics for preparing flat-faced tablets;

4) They are easy to assay by spectroscopic methods;

5) They are not known to change crystal form under compression.

The dissolution medium for benzoic acid was 0.011 N in HCl, prepared by diluting 0.9 mL, 37% HCl (Kaixin Chemical Reagent Co.) to 1000 mL with distilled water. This is sufficient to completely suppress benzoic acid ($pK_a = 4.20$) ionization so that it may be treated as an unionizable compound. For salicylic acid and cinnamic acid, pure water was used as the dissolution medium to demonstrate the applicability of the dissolution model of Chapter 2 for a weak acid under conditions where it is weakly ionized.

Table 3-5. Literature solubilities and pK_a's for the three model compounds used in this study.

	Molecular Weight	Solubility (mg/mL)	pK_a (25 ℃)[49]
Benzoic acid	122.12	5.13[43] (37 ℃)	4.2
Salicylic acid	138.12	2.62[50] (37 ℃)	2.98
trans-Cinnamic acid	148.16	0.51[51] (25 ℃)	4.44

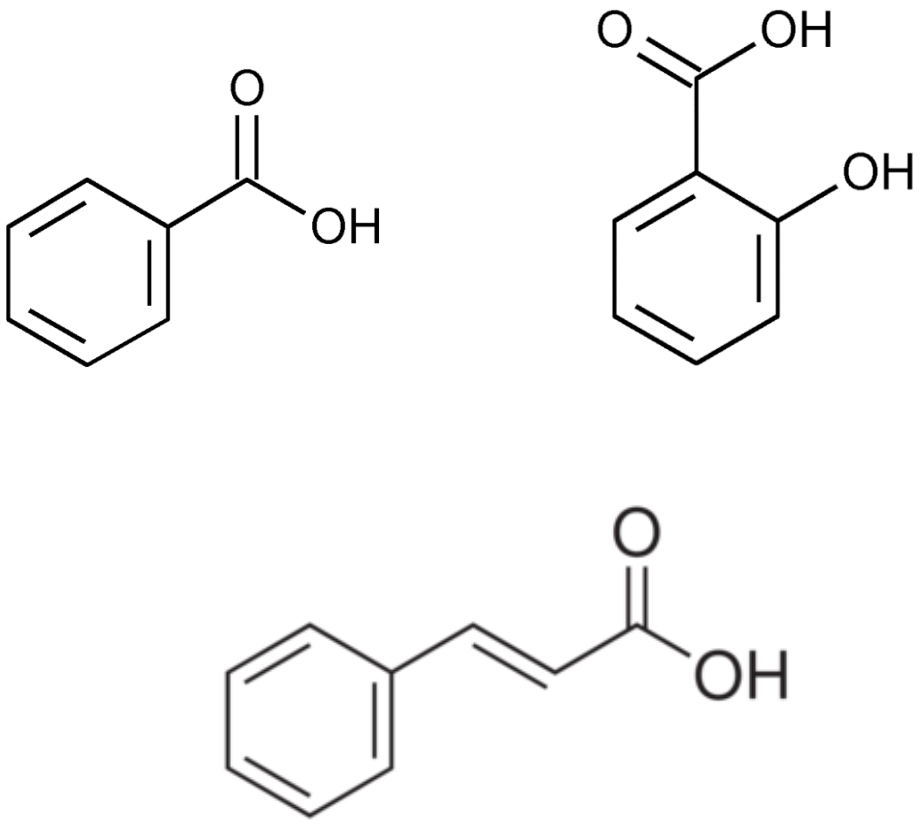

Figure 3-5. Molecular structures of benzoic acid (top left), salicylic acid (top right) and *trans*-cinnamic acid (bottom).

Apparatus and Tablet Preparation

The basic setup of the dissolution test system is similar to the Vankel® apparatus described in the previous chapter (Figure 3-6). A BOS-110-S stirrer (Shanghai Youyi Instrument Co., Ltd.) was used to provide fixed-axis rotation for all dissolution tests. Solid tablets were prepared by direct compression of drug powder using a custom-made holder-punch-die set which resembles the Varian® accessory (Figure 3-7). Compression was done on a Shimadzu SSP-10A hydraulic press with a force of 15 kN and a dwell time of 30 s. The diameters of the die and tablet were 2.77 cm and 0.971 cm, respectively. After compression, the holder, with the flat-surfaced solid disk, was attached to the threaded stirrer shaft (Figure 3-8).

Dissolution Test Procedure

All dissolution experiments were carried out in a HJ 22 Digital Display Bath (Jintan Jiangnan Instrument Co., Ltd.). The bath was connected to a DW-2003 chiller (Hangzhou David Science and Education Instrument Co., Ltd.) which controlled the temperature. The bath medium was 99.5% ethanol at low temperatures and water at 37 ℃. Prior to each dissolution test, the bath, dissolution medium and replacement medium (for medium replacement during dissolution runs) were equilibrated by the chiller until the temperatures reached the set point (± 0.1 ℃).

Dissolution testing was initiated by bringing the stirrer to the desired rotational speed and carefully lowering the holder into the dissolution medium (200 mL) to a depth of ~1.5 cm (measured from the top of the medium). Samples (5 mL) were withdrawn at 2.5- or 5-minute intervals and immediately replaced with an equal volume of fresh medium to maintain a constant total volume. For each compound, dissolution testing was performed at 50, 120, 230, 360, 530, and 800 rpm at three temperatures (37 ℃, 10 ℃ and 3 ℃). According to Chapter 1, the Reynold's

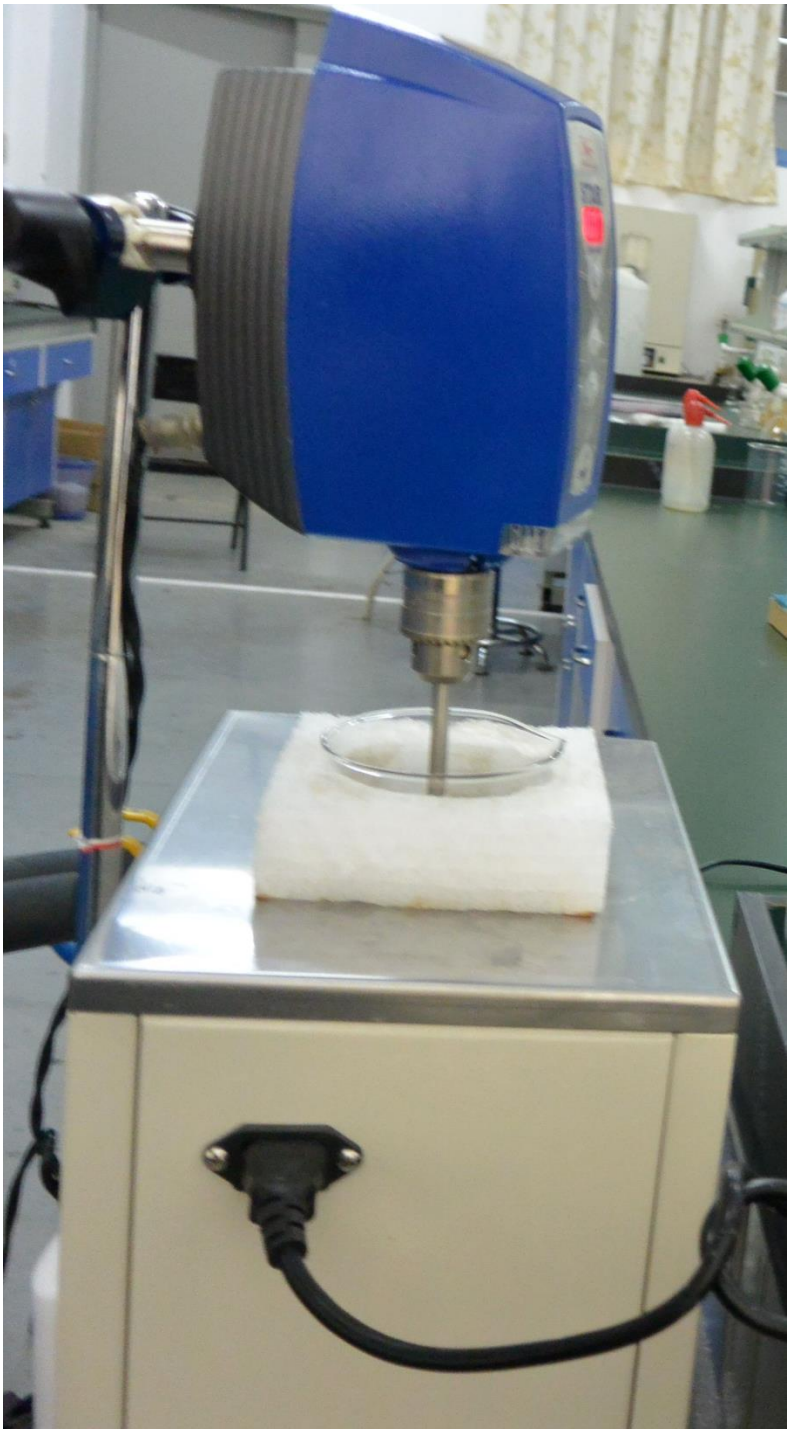

Figure 3-6. Experimental setup with rotor (top) and chiller bath (bottom); the rotating disk is in the beaker and not visible).

Figure 3-7. Flat-faced powder compact (white disk) in a custom-made die.

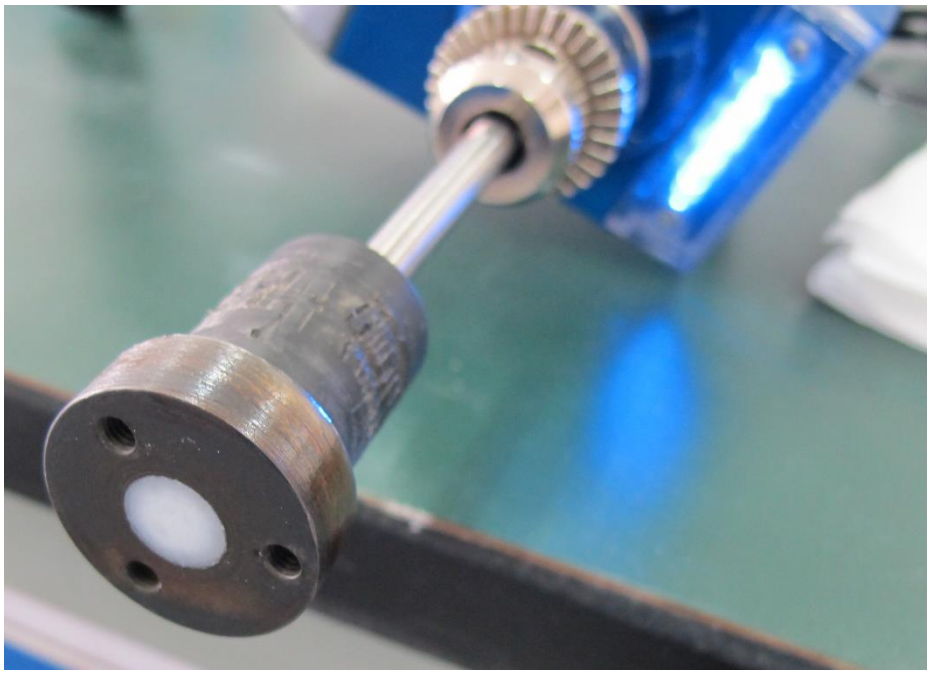

Figure 3-8. Die with tablet attached to stirrer shaft.

number for this type of apparatus may be estimated by:

$$\mathrm{Re} = \frac{d^2 \omega}{4\nu} \tag{3-2}$$

where, $d = 2.77$ cm is the diameter of the entire rotating disk, ω is rotational speed and ν is kinematic viscosity. The maximum Reynold's number in this study was achieved at the highest rotational speed (800 rpm) and lowest viscosity (~0.007 cm^2/s at 37 ℃[46]) and was ~2.3 x 10^4, which is well below the critical value for the onset of turbulence (Chapter 1). The duration of each dissolution run was 15-40 minutes depending on the temperature and rotational speed. All experiments were performed in duplicate.

After a completed dissolution run, the thermometer was immediately inserted into the dissolution medium to check the temperature. A small temperature increase (0.3-0.7 ℃) was observed after each test, which was likely a result of frictional heating caused by disk rotation. These temperature changes did not alter the overall linearity of dissolution profiles.

Sample Assay

All dissolution samples were assayed with a Shimadzu UV-2450 UV-Vis spectrophotometer. The spectra of benzoic acid, salicylic acid and cinnamic acid can be found in the Appendix B. The wavelength of maximum absorption was chosen for the quantitation of each compound. Samples whose concentrations were out of calibration range were diluted with corresponding dissolution media. The standard plots for these compounds can be found in Appendix A.

Results and Discussion

Figure 3-9 shows the concentration vs. time profiles for benzoic acid at 10 ℃. The other profiles obtained in this study can be found in Appendix A. Linear regression was performed on duplicate data sets (Figure 3-9), and the slopes were divided by the dissolution surface area of the tablet (0.741 cm^2) to obtain dissolution rates. These rates have the units of [mass] / [time]•[length]^2 and can be interpreted as mass fluxes. They are given in Tables 3-6 - 3-8.

The main purpose of this analysis is to calculate the degree of interface control from the variation of dissolution rate (J) with rotational speed (ω). In Chapter 2, the degree of interface control is defined by Eqn.(2-22):

$$P_{\mathrm{I}} = \frac{N(D,\nu)\omega^{b}}{\kappa_{\mathrm{p}} + N(D,\nu)\omega^{b}}$$

where, κ_{p} is the collective re-deposition rate constant, $N(D,\nu)$ is a general function describing the dependence of the steady-state transport flux on diffusivity and viscosity and ω is rotational speed. To simplify, $N(D,\nu)$ will be abbreviated as N in what follows. It is clear from Eqn.(2-22) that the degree of interface control is a function of rotational speed, which is to be expected since the transport rate itself is a function of rotational speed. As discussed in Chapter 2, the hydrodynamic constant, b, for a general forced flow system can be determined from the slope of ln$J$ plotted against lnω in the transport-controlled regime. It has been confirmed that the rotating disk dissolution of benzoic acid at 37 ℃ is transport-controlled at rotational speeds up to 600 rpm.[48] For the present system, the plot of ln$J$ vs. lnω for benzoic acid dissolution at 37 ℃ (Figure 3-10) indicates that the transport-controlled regime extends to at least 800 rpm, since the last point (corresponding to ω = 800 rpm) also falls on the straight line. Therefore, the b-value is

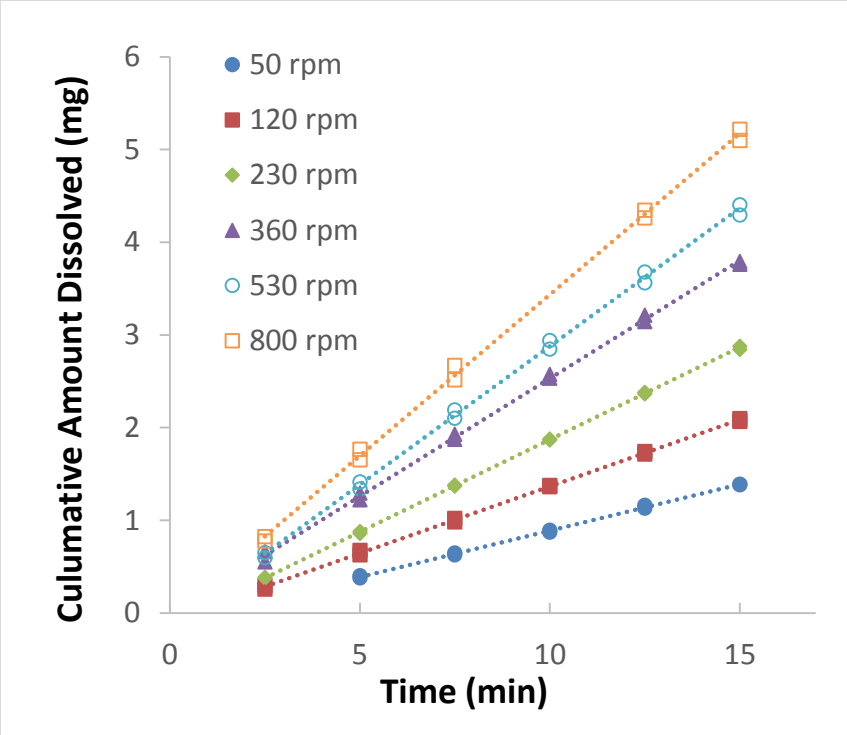

Figure 3-9. Benzoic acid dissolution profiles at various rotational speeds at 10 ℃.

Table 3-6. Benzoic acid dissolution rates at various rotational speeds and temperatures.

RPM	Dissolution rate (mg/min-cm^2)		
	37^{0}C	10^{0}C	3^{0}C
50	0.523	0.135	0.089
120	0.794	0.195	0.138
230	1.129	0.269	0.178
360	1.372	0.344	0.223
530	1.678	0.403	0.263
800	2.095	0.469	0.288

Table 3-7. Salicylic acid dissolution rates at various rotational speeds and temperatures.

RPM	Dissolution rate (mg/min-cm^2)		
	37^{0}C	10^{0}C	3^{0}C
50	0.391	0.096	0.066
120	0.583	0.136	0.096
230	0.879	0.184	0.125
360	1.092	0.225	0.156
530	1.290	0.266	0.179
800	1.552	0.333	0.215

Table 3-8. Cinnamic acid dissolution rates at various rotational speeds and temperatures.

RPM	Dissolution rate (mg/min-cm^2)		
	37^{0}C	10^{0}C	3^{0}C
50	0.078	0.018	0.012
120	0.118	0.026	0.017
230	0.170	0.036	0.023
360	0.220	0.044	0.028
530	0.246	0.052	0.034
800	0.309	0.063	0.039

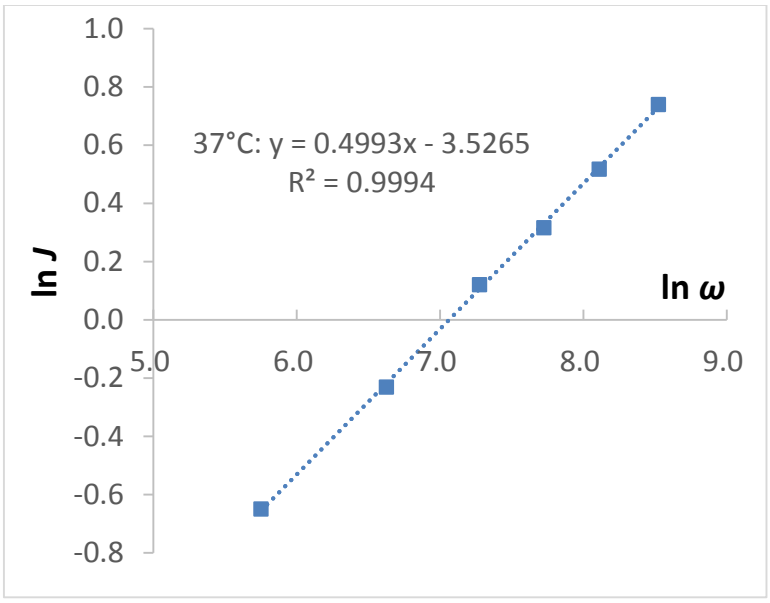

Figure 3-10. Plot of ln$J$ vs. lnω for benzoic acid dissolution at 37°C (J = dissolution rate, ω = rotational speed).

given by the slope (0.4993) and is essentially 0.5. The plots of ln$J$ vs. lnω for salicylic acid and *trans*-cinnamic acid (Figures 3-15 and 3-16) shows that their dissolution at 37 ℃ in the present work was also transport-controlled with slopes 0.508 and 0.501. Setting b = 0.5, Eqn.(2-22) becomes:

$$P_I(\omega) = \frac{N\omega^{0.5}}{\kappa_p + N\omega^{0.5}} = \frac{(N/\kappa_p)\omega^{0.5}}{1+(N/\kappa_p)\omega^{0.5}} \tag{3-3}$$

Therefore, the problem of calculating the degree of interface control for a given rotational speed reduces to the calculation of N/κ_p. One way of calculating this quantity is to invert Eqn.(2-20):

$$J = \frac{R_t}{1 + \frac{\kappa_p}{N\omega^{0.5}}} \Rightarrow \frac{1}{J} = \frac{1}{R_t} + \frac{\kappa_p}{R_t N\omega^{0.5}} \tag{3-4}$$

where, R_t is the total detachment rate. Eqn.(3-4) shows that $1/J$ varies linearly with $\omega^{-0.5}$ with slope $\kappa_p/(R_t N)$ and intercept $1/R_t$. Thus, the intercept-to-slope ratio is equal to N/κ_p. Figures 3-11 - 3-13 show the plots of $1/J$ vs. $\omega^{0.5}$ for the three compounds with slopes, intercepts and intercept/slope ratios given in Table 3-9.

Another method of estimating N/κ_p is from the plot of ln$J$ vs. lnω. Consider a general forced flow system with hydrodynamic constant b. First, writing Eqn.(2-20) in dimensionless form as:

$$\frac{J}{R_t} = \frac{1}{1 + \frac{\kappa_p}{N\omega^b}} = \frac{(N/\kappa_p)\omega^b}{1 + (N/\kappa_p)\omega^b} \tag{3-5}$$

Taking the logarithms of both sides yields:

$$\ln\frac{J}{R_t} = b\ln\frac{N^{1/b}\omega}{\kappa_p^{1/b}} - \ln\left(1 + \frac{N\omega^b}{\kappa_p}\right) \tag{3-6}$$

Under transport control, that is, when $N\omega^b/\kappa_p << 1$, Eqn.(3-6) reduces to:

$$\ln\frac{J}{R_t} \approx b\ln\frac{N^{1/b}\omega}{\kappa_p^{1/b}} \tag{3-7}$$

and the plot of $\ln(J/R_t)$ against $\ln(N^2\omega/\kappa_p^2)$ will be a straight line with the slope equal to b, which is essentially a reiteration of Eqn.(2-24). In the general case of Eqn.(3-6), the plot of

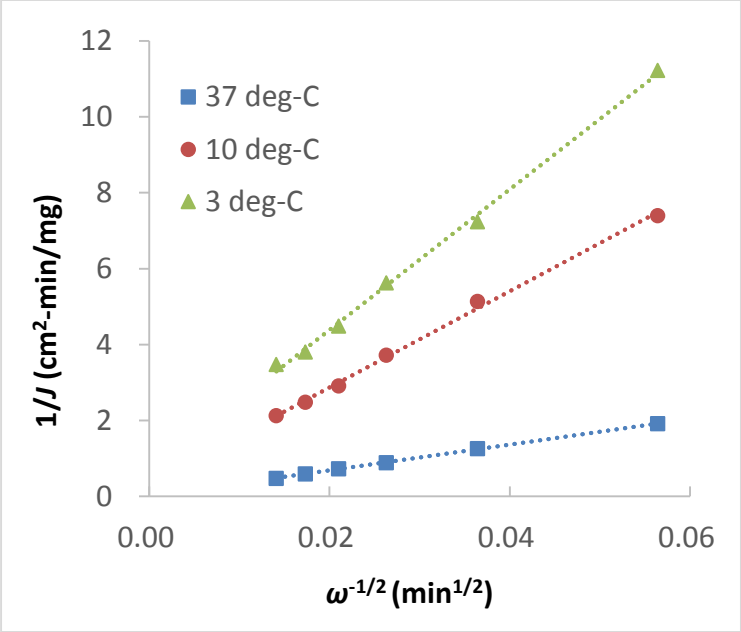

Figure 3-11. Plots of $1/J$ vs. $\omega^{0.5}$ for benzoic acid dissolution at 37, 10 and 3 ℃ (J = dissolution rate, ω = rotational speed).

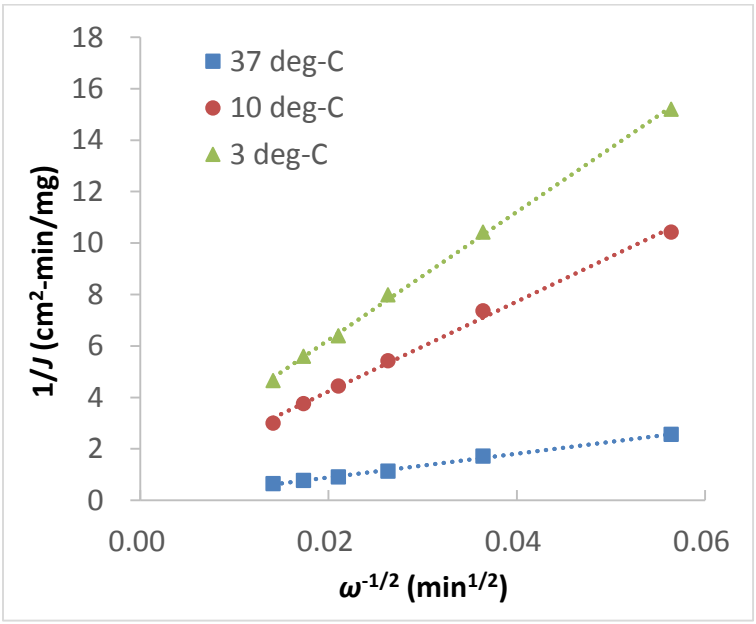

Figure 3-12. Plots of $1/J$ vs. $\omega^{0.5}$ for salicylic acid dissolution at 37, 10 and 3 ℃ (J = dissolution rate, ω = rotational speed).

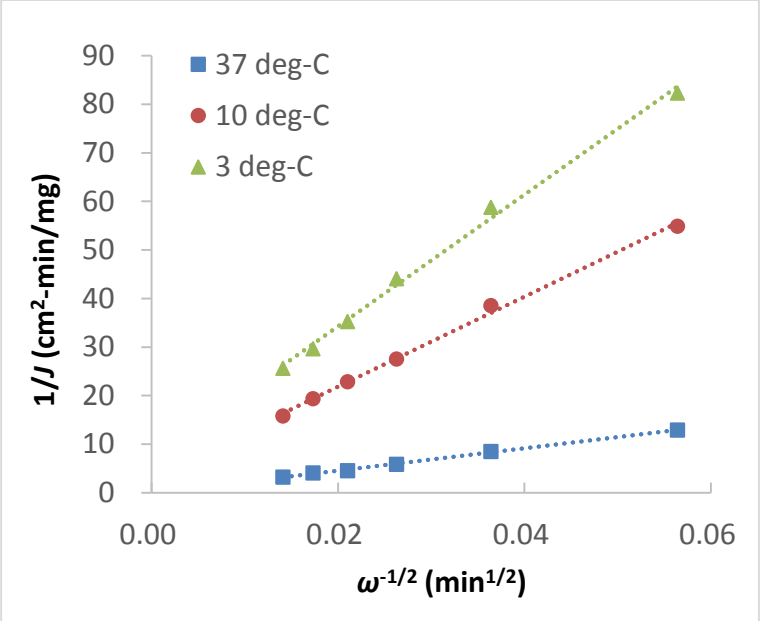

Figure 3-13. Plots of $1/J$ vs. $\omega^{0.5}$ for *trans*-cinnamic acid dissolution at 37, 10 and 3 ℃ (J = dissolution rate, ω = rotational speed).

Table 3-9. Slopes, intercepts, intercept/slope (I/S) ratios for plots of $1/J$ vs. $\omega^{0.5}$ plots for benzoic acid (BA), salicylic acid (SA) and *trans*-cinnamic acid (CA).

	Temperature	Slope (cm^2-$min^{0.5}$/mg)	Intercept (cm^2-min/mg)	I/S = N / κ_p (x10^{-3} $min^{0.5}$)
BA	37 ℃	33.9	0.007	-
	10 ℃	126.7	0.34	2.7
	3 ℃	185.1	0.68	3.7
SA	37 ℃	46.1	-0.03	-
	10 ℃	174.7	0.74	4.2
	3 ℃	248.8	1.26	5.1
CA	37 ℃	230.0	-0.06	-
	10 ℃	926.8	3.32	3.6
	3 ℃	1356.3	7.15	5.3

$\ln(J/R_t)$ vs. $\ln(N^{1/b}\omega/\kappa_p^{1/b})$ will not be linear, since the second term on the right hand side, $-\ln[1+(N\omega^b/\kappa_p)]$, is a nonlinear function of $\ln(N^{1/b}\omega/\kappa_p^{1/b})$ (This may be understood as follows: let $x=\ln(N^{1/b}\omega/\kappa_p^{1/b})$, then $N^{1/b}\omega/\kappa_p^{1/b}=e^x$ and hence $\ln[1+(N\omega^b/\kappa_p)]=\ln(1+e^{bx})$ is a nonlinear function of *x*). However, when $N\omega^b/\kappa_p$ is sufficiently small (yet not small enough to be neglected as in the case of transport control), $-\ln[1+(N\omega^b/\kappa_p)]$ may be treated as a small perturbation to Eqn.(3-7) so that the overall linearity of $\ln(J/R_t)$ vs. $\ln(N^{1/b}\omega/\kappa_p^{1/b})$ is maintained. The effect of this perturbation is a small negative correction (-Δb) to the slope which results from the variation of $-\ln[1+(N\omega^b/\kappa_p)]$ as a function of $\ln(N^{1/b}\omega/\kappa_p^{1/b})$. For a given range of agitation intensity, $\omega_{min}\le\omega\le\omega_{max}$, Δb may be estimated by:

$$\Delta b=\frac{\ln(1+\frac{N\omega_{max}^b}{\kappa_p})-\ln(1+\frac{N\omega_{min}^b}{\kappa_p})}{\ln\frac{N^{1/b}\omega_{max}}{\kappa_p^{1/b}}-\ln\frac{N^{1/b}\omega_{min}}{\kappa_p^{1/b}}}=\frac{\ln\left[\frac{1+(N\omega_{max}^b/\kappa_p)}{1+(N\omega_{min}^b/\kappa_p)}\right]}{\ln(\omega_{max}/\omega_{min})} \qquad (3\text{-}8)$$

Eqn.(3-8) functionally correlates N/κ_p with the deviation of the apparent slope of $\ln(J/R_t)$ vs. $\ln(N^{1/b}\omega/\kappa_p^{1/b})$ from the hydrodynamic constant, *b*.

The plots of ln*J* vs. lnω for the present study are shown in Figures 3-14 - 3-16 and their slopes are listed in Table 3-10. (Changing from $\ln(J/R_t)$ to $\ln J$ and $\ln(N^{1/b}\omega/\kappa_p^{1/b})$ to $\ln\omega$ has no effect on the slope, since they differ by the constants $-\ln R_t$ and $b^{-1}\ln(N/\kappa_p)$, respectively). It can be seen that for each compound, the slope deviates negatively from the hydrodynamic constant (0.5) at low temperatures, which is indicative of small degrees of interface control. Eqn.(3-8) was used in combination with Microsoft Excel® Solver to calculate

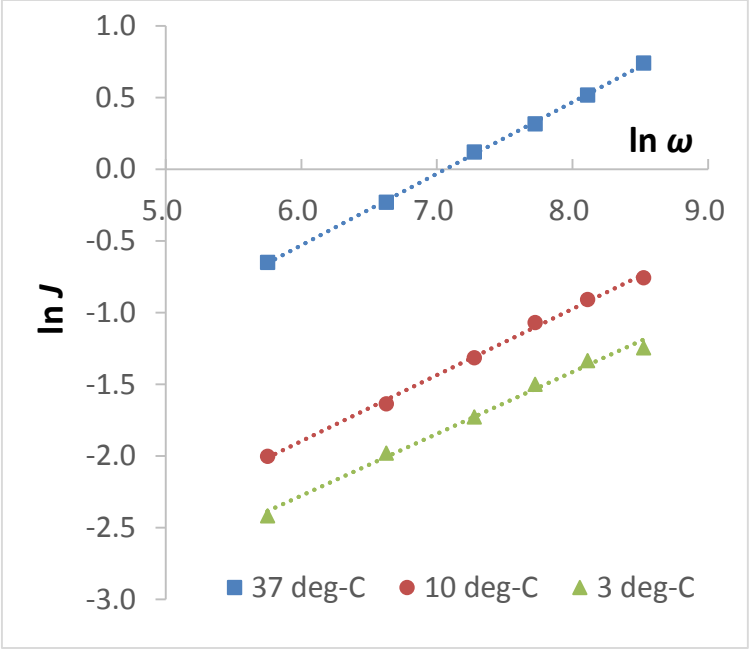

Figure 3-14. Plots of ln$J$ vs. lnω for benzoic acid at 37 ℃, 10 ℃ and 3 ℃ (J = dissolution rate, ω = rotational speed).

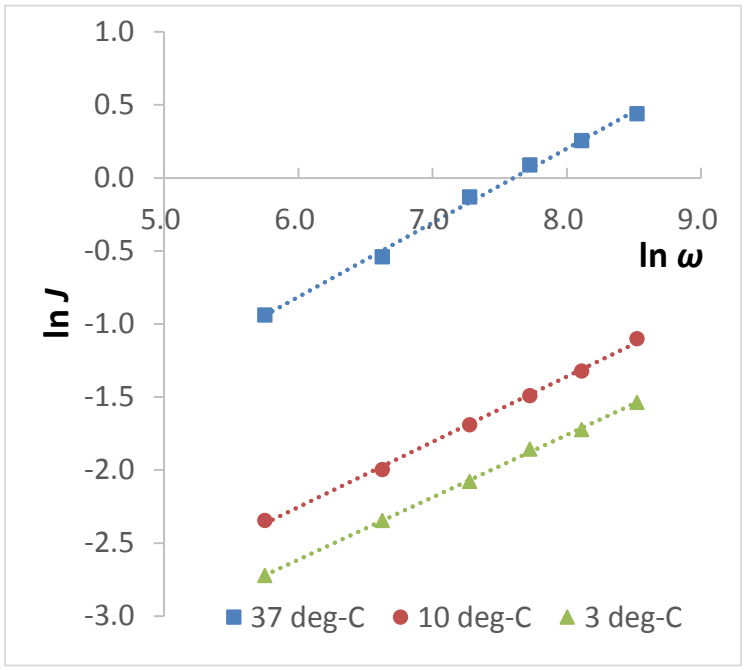

Figure 3-15. Plots of ln$J$ vs. lnω for salicylic acid at 37 ℃, 10 ℃ and 3 ℃ (J = dissolution rate, ω = rotational speed).

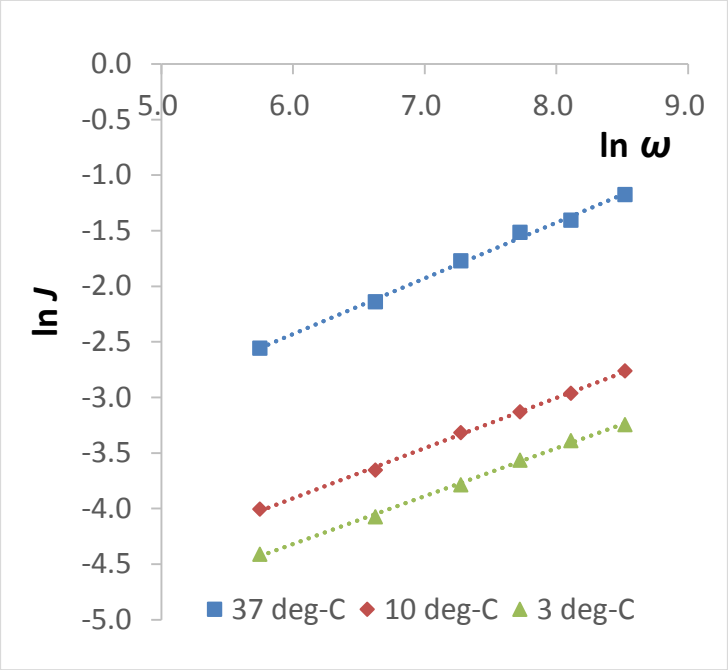

Figure 3-16. Plots of ln$J$ vs. lnω for *trans*-cinnamic acid at 37, 10 and 3 ℃ (J = dissolution rate, ω = rotational speed).

Table 3-10. Slopes of ln$J$ vs. lnω for benzoic acid, salicylic acid and *trans*-cinnamic acid.

	Slope of ln$J$ vs. lnω		
Temperature (^{0}C)	Benzoic acid	Salicylic acid	*trans*-Cinnamic acid
37	0.499	0.508	0.501
10	0.461	0.447	0.451
3	0.432	0.427	0.431

N / κ_p from these deviations.

After determining N / κ_p using one of these two methods, the degree of interface control, $P_i(\omega)$, at each rotational speed can be calculated using Eqn.(3-3). Table 3-11 shows that the results obtained by these methods are in reasonable agreement. It can be seen that as the temperature decreases, $\kappa_p / N(D,\nu)$ becomes smaller, indicating that the collective re-deposition rate constant decreases faster than the transport function. This is the reason why the dissolution of these compounds exhibited increasing degrees of interface control at low temperatures. It should be noted, however, that the present model by itself cannot predict the temperature

Table 3-11. Values of N / κ_p and the degree of interface control (P_I) calculated from the deviations of the slopes of ln$J$ vs. lnω from the hydrodynamic constant (0.5) and from the plots of $1/J$ vs. $\omega^{-0.5}$ for dissolution data at 10℃ and 3℃.

	Benzoic acid		Salicylic acid		Cinnamic acid	
	10℃	3℃	10℃	3℃	10℃	3℃
Δb	0.038	0.067	0.061	0.081	0.050	0.070
N / κ_p $(x10^{-3}\ min^{1/2})^1$	2.2	4.2	3.1	4.6	2.9	4.3
N / κ_p $(x10^{-3}\ min^{1/2})^2$	2.7	3.7	4.2	5.1	3.6	5.3
P_I [1]	3.8-13.5%	6.9-22.9%	5.2-18.0%	7.5-24.6%	4.9-17.1%	7.1-23.4%
P_I [2]	4.6-16.0%	6.1-20.7%	7.0-23.0%	8.3-26.5%	5.9-20.1%	8.5-27.2%

1. Calculated from the apparent slope of ln$J$ vs. lnω.
2. Calculated from the plot of $1/J$ vs. $\omega^{-0.5}$.

dependence of $\kappa_p / N(D,\nu)$ (and hence the temperature dependence of dissolution mechanism) for a given compound without *a priori* knowledge of the re-deposition rate constants ($k_{p,i}$), the distribution of various types of re-deposition sites on its surface ($\sigma_{p,i}$) and the explicit form of $N(D,\nu)$. An interesting future direction would be to simulate the potential energy surfaces for the approach of a solute molecule to various types of re-deposition sites based on intermolecular interaction properties and site structures. This would enable determination of the activation energies for the re-deposition rate constants, which are the most important factors in the temperature dependence of the collective re-deposition rate constant, κ_p.

Summary

In this study, the dissolution behavior of benzoic acid, salicylic acid and *trans*-cinnamic acid has been investigated under different agitation and temperature conditions. The plots of ln$J$ vs. lnω indicate that all three compounds dissolved by transport control at 37 ℃. The degrees of interface control (P_i) at low temperatures (10 ℃ and 3 ℃) were calculated using two methods. In the first method, the plots of 1/J vs. $\omega^{1/2}$ were constructed from the dissolution data and P_i was calculated from the slope and intercept of each plot. In the second method, a mathematical approach was derived to correlate the degree of interface control with the deviation of the slope of ln$J$ vs. lnω from the hydrodynamic constant of 0.5. These methods yielded comparable values for the degree of interface control. It may be concluded that as the temperature decreases, the collective re-deposition rate constant decreases faster than the transport rate constant, thus leading to the emergence of interface control at low temperatures.

A potential future direction for this study is to utilize computational methods (first principles or semi-empirical) to predict the interfacial rate constants as functions of temperature. This may require the establishment of potential energy surfaces for detachment and re-deposition reactions based on intermolecular interactions and detachment/re-deposition site structures. Such potential energy surfaces will enable determination of activation energies, the main factor in the temperature dependence of rate constants.

CHAPTER 4 DISSOLUTION MECHANISMS IN SURFACTANTS

Introduction

Surfactants play important roles in many chemical and biological processes and are widely used in chemical and biochemical engineering and processing, thanks to their unique properties and functions. One of the most important among these functions is their ability to solubilize limited/low solubility substances by incorporating them into micelles, formed by aggregates of surfactant molecules through hydrophobic interactions. This effect may be understood thermodynamically from the view of partition equilibrium between the solvent phase and the micellar 'pseudo-phase".[52] On the other hand, attempts have been made to understand dissolution kinetics in surfactant solutions. Based on the assumption of transport control, Higuchi proposed an extension of the Nernst-Brunner model to describe dissolution rate in a micellar medium:[53,54]

$$J = \frac{D_{\text{free}}}{h} C_{\text{S}}^{[\text{free}]} + \frac{D_{\text{mic}}}{h} C_{\text{S}}^{[\text{mic}]} \tag{4-1}$$

where, D_{free} = diffusivity of free solute form, D_{mic} = diffusivity of micelle-solubilized solute form, $C_{\text{S}}^{[\text{free}]}$ = solubility in solvent phase, $C_{\text{S}}^{[\text{mic}]}$ = solubility increase due to micelle solubilization and h = diffusion layer thickness. Granero et al. used a rotating disk apparatus to investigate the dissolution behavior of fenofibrate in sodium dodecyl sulfate (NaDS) solutions.[55] They assumed that the system was described by the Levich equation, that is, :

$$J = 0.62 C_{\text{S}}^{\text{T}} D_{\text{eff}}^{2/3} \nu^{-1/6} \omega^{1/2} \tag{4-2}$$

where, C_S^T is the total solubility in the presence of a surfactant, and D_{eff} is an effective diffusivity, defined as the weighted average diffusivity of free and micellar solute forms. However, since fenofibrate existed primarily in the micellar pseudo-phase as indicated by the >2000 fold solublity increase, the definition did not really matter; the effective diffusivity was essentially the same as the drug-loaded micelle diffusivity. The results indicated that in the rotational speed range of 50-200 rpm, the dissolution was governed by transport control, as the dissolution rate varied linearly with the square root of rotational speed. (Dissolution at higher rotational speeds was not investigated.) The diffusivity of the micellar form of fenofibrate was estimated from Eqn.(4-2) to be ~8.4 times smaller than that of the free form.

Crison et al. proposed a different definition for effective solute diffusivity in surfactant media by assuming the total dissolution rate was given by the sum of dissolution rates for free and micellar solute forms:[56]

$$J_T = J_{free} + J_{mic} \tag{4-3}$$

Using the Levich equation, i.e., $J_{free} = 0.62 C_S^{[free]} \nu^{-1/6} \omega^{1/2} D_{free}^{2/3}$, $J_{mic} = 0.62 C_S^{[mic]} \nu^{-1/6} \omega^{1/2} D_{mic}^{2/3}$, the effective diffusivity could be defined by:

$$D_{eff}^{2/3} = \frac{D_{free}^{2/3} + \lambda D_{mic}^{2/3}}{1+\lambda} \tag{4-4}$$

where, $\lambda = C_S^{[mic]} / C_S^{[free]}$ is the equilibrium ratio of the amount of micellar form versus that of free form. For compounds that exist predominantly in the micellar phase (such as fenofibrate in NaDS or griseofluvin in NaDS and CTAB), Eqns.(4-2) and (4-3) are indistinguishable, since $C_S^{[free]} \approx 0$ and thus $D_{mic} \approx D_{eff}$. However, they become different if the amounts of solute in the

aqueous phase and the micellar pseudo-phase are comparable, as is the case for griseofluvin in Tween 80 and Cremophor EL. Balakrishnan et al. applied Eqn.(4-3) to the rotating disk dissolution of griseofluvin in several surfactant media.[57] The results showed that Eqn.(4-3) accurately predicted griseofluvin dissolution rates in NaDS and CTAB (relative to an aqueous medium), but could not describe those in Tween 80 and Cremophor EL. This suggests that Eqn.(4-3) might not be applicable for the latter case.

In a more biologically relevant investigation, Prakongpan et al. studied the dissolution behavior of cholesterol monohydrate in surfactant media containing bile acid, lecithin and benzalkonium chloride, also using a rotating disk apparatus.[48] They found that the s of dissolution rate vs. $\omega^{0.5}$ exhibited marked downward curvature which could be described Berthoud's model (Eqn.(1-5)) and concluded that significant interface control was responsible for cholesterol dissolution in these media. The effective permeability coefficient from Berthoud's equation was believed to be associated with the kinetic processes occurring at the crystal-solution interface. This coefficient was further found to be strongly dependent on electrolyte (i.e., phosphate buffer) concentration, which led them to suspect that the interfacial processes might involve the close approach of negatively charged micelles to a negatively charged solid surface, a process that would be facilitated by counterions or by increasing ionic strength.

This chapter presents an experimental investigation of the intrinsic dissolution rate of benzoic acid as a function of rotational speed and sodium dodecyl sulfate (NaDS) concentration (above the critical micelle concentration) and analyses of the results using a modified version of the mixed-kinetic-controlled dissolution model of Chapter 2.

Effective Diffusivity in a Micellar Solution

Consider a solute that exists in both the solvent phase and the micellar pseudo-phase. If rapid pseudo-equilibrium is assumed between the free and micellar solute forms,[58] their concentrations are related by:

$$\frac{c^{[\mathrm{mic}]}}{c^{[\mathrm{sol}]}} = KC_{\mathrm{mic}} \tag{4-5}$$

where K is the equilibrium constant and C_{mic} is the concentration of micelles (each counted as a single particle). This means the fraction of either form is a constant. If $\alpha \equiv KC_{\mathrm{mic}} / (1 + KC_{\mathrm{mic}})$ is the fraction of the micellar form, the effective diffusivity is given by:

$$D_{\mathrm{eff}} = \alpha D_{\mathrm{mic}} + (1-\alpha) D_{\mathrm{free}} \tag{4-6}$$

that is, a weighted average of the diffusivities of free and micellar forms. Since $D_{\mathrm{free}} > D_{\mathrm{mic}}$, the effective diffusivity is a decreasing function of α, and thus of surfactant concentration or C_{mic}. The problem of solute transport in micellar solutions is discussed in detail in Appendix C.

Benzoic Acid Dissolution in Sodium Dodecyl Sulfate (NaDS) Solutions

For this experimental study, benzoic acid was chosen as the compound to be dissolved and sodium dodecyl sulfate was chosen as the surfactant. The reasons for using benzoic acid for intrinsic dissolution testing have been described in Chapter 3. Sodium dodecyl sulfate (Figure 4-1) is one of the most studied surfactant compounds. It is an anionic surfactant with a critical micelle concentration of ~ 8 mM (or 0.23% w/v) in water at 25 ℃[59,60] and an aggregation number

of ~60.[61,62] The micelle shape remains spherical up to a concentration of 20% w/w in NaDS concentration.[63] The degree of counterion (Na^+) association for NaDS micelles is ~ 0.73 (up to 0.08 mM in NaDS concentration).[64]

Materials and Methods

The benzoic acid used in this study is the same as in the previous chapter. Sodium dodecyl sulfate (AR grade) was from Tianjin Fuchen Chemical Reagents Factory and used as received. NaDS solutions were prepared by dissolving the desired amount of NaDS in deionized water. These solutions were used within 24 hours after preparation.

The solubilities of benzoic acid in water and various concentrations of NaDS were determined by adding excess benzoic acid powder to each solution and placing it in a SHA-C shaking water bath (Gongyi Yuhua Instrument Co., Ltd.) for 24 hours at 25 ℃. The resulting suspensions were filtered and diluted 100-400-fold with water and assayed for benzoic acid content.

The viscosities of several NaDS solutions were measured with an Ostwald viscometer. Their densities were measured with a glass pycnometer using pure water as the reference fluid. All measurements were performed at 25 ℃.

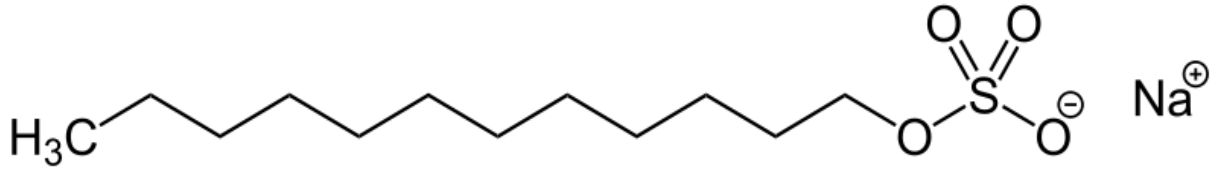

Figure 4-1. Molecular structure of sodium dodecyl sulfate.

The dissolution apparatus, tablet preparation and dissolution test procedures were the same as those described in Chapter 3. The dissolution media were pure water, 0.5%, 2%, 4% and 6% NaDS solutions (200 mL). These NaDS concentrations were all above the critical micelle concentration. For each NaDS concentration, dissolution testing was performed at 5-6 rotational speeds between 50 to 800 rpm at 25 ℃. All experiments were performed in duplicate.

The same UV-Vis spectrophotometer as described in Chapter 3 was used to assay all solution samples. The wavelength at which the absorbance values were recorded was 273 nm, an absorption peak for benzoic acid in water and in NaDS solutions. For solubility determination, a standard plot of benzoic acid in water was used since all samples were diluted at least 100-fold which effectively eliminated potential interferences from NaDS. (NaDS showed no UV absorption at 273 nm.) For the quantitation of dissolution samples, which were performed without dilution, a UV calibration plot was prepared for each NaDS concentration in which the dissolution of benzoic acid was measured because benzoic acid had a different absorptivity in the NaDS micellar phase than in the aqueous phase. These plots can be found in Appendix B.

Results and Discussion

The total solubilities (C_S^T) of benzoic acid in various NaDS concentrations are given in Table 4-1. The difference between C_S^T and the aqueous solubility, $C_S^{[aq]}$, is the concentration of the micellar form. According to Eqn.(4-5), $(C_S^T - C_S^{[aq]}) / C_S^{[aq]} = KC_{mic}$. Figure 4-2 shows the plot of $(C_S^T - C_S^{[aq]}) / C_S^{[aq]}$ against C_{mic}, from which the equilibrium constant, *K*, can be obtained to be 1.35×10^3 mM^{-1}. The density and viscosity data for several NaDS solutions are given in Table 4-2.

Table 4-1. Benzoic acid solubilities in various NaDS solutions at 25 ℃.

NaDS conc.(%w/v)	C_{mic} (mM)[1]	C_S^T (mg/mL)[2]	$(C_S^T - C_S^{[aq]}) / C_S^{[aq]}$	α[3]
0	-	3.33	-	-
0.5	0.16	4.35	0.30	0.23
1	0.45	5.70	0.71	0.42
2	1.02	7.91	1.37	0.58
4	2.18	14.34	3.31	0.77
6	3.33	18.26	4.48	0.82
8	4.49	23.9	6.18	0.86

1. C_{mic} = micelle concentration (with each micelle counted as a single particle).
2. Values in parentheses are standard deviations (n = 2).
3. α = fraction of solute in micelle-solubilized form.

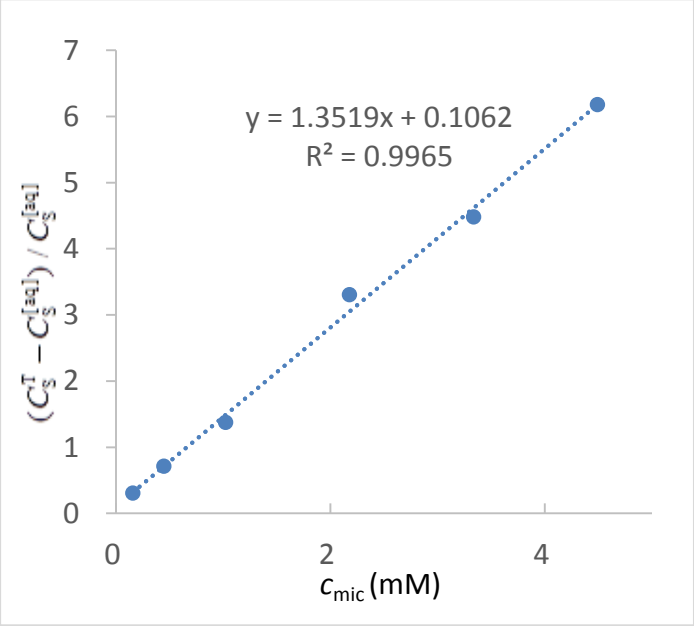

Figure 4-2. Plot of $(C_S^T - C_S^{[aq]}) / C_S^{[aq]}$ against C_{mic} at 25°C (C_S^T = total solubility, $C_S^{[aq]}$ = solubility in aqueous phase, C_{mic} = micelle concentration).

Table 4-2. Density and viscosity values of various NaDS solutions.

NaDS Concentration (%w/v)	Density (g/mL)	Dynamic viscosity (mPa-s)	Kinematic viscosity ($X10^{-2}$ cm^2/s)
0.00	0.997[65]	0.89[65]	0.89
0.5	0.998	1.00	1.00
2	1.000	1.09	1.09
4	1.003	1.23	1.23
6	1.006	1.32	1.31

Figure 4-3 shows the dissolution profiles of benzoic acid at various rotational speeds (ω) in 4% NaDS. All dissolution profiles from this study are linear and can be found in Appendix B. The intrinsic dissolution rates (J), calculated in the same manner as in Chapter 3, are listed in Table 4-3. The hydrodynamic constant, b, for this dissolution apparatus has been determined to be 0.5 in Chapter 3. Figure 4-4 shows the plot of $\ln J$ vs. $\ln\omega$ for benzoic acid dissolution in water has a slope of 0.481, which indicates predominant transport control. Using Eqn.(3-8), the degree of interface control can be calculated to be less than 6%.

Using the nonlinear fitting functions of Origin® 8.5, the plots of J vs. $\omega^{0.5}$ may be fitted with the functional form of Eqn.(2-20) with $b = 0.5$ (Figure 4-5):

$$J = \frac{X}{1 + Y\omega^{-0.5}} \tag{4-7}$$

where, X and Y are ω-independent parameters. Alternatively, we may use the linearized form of

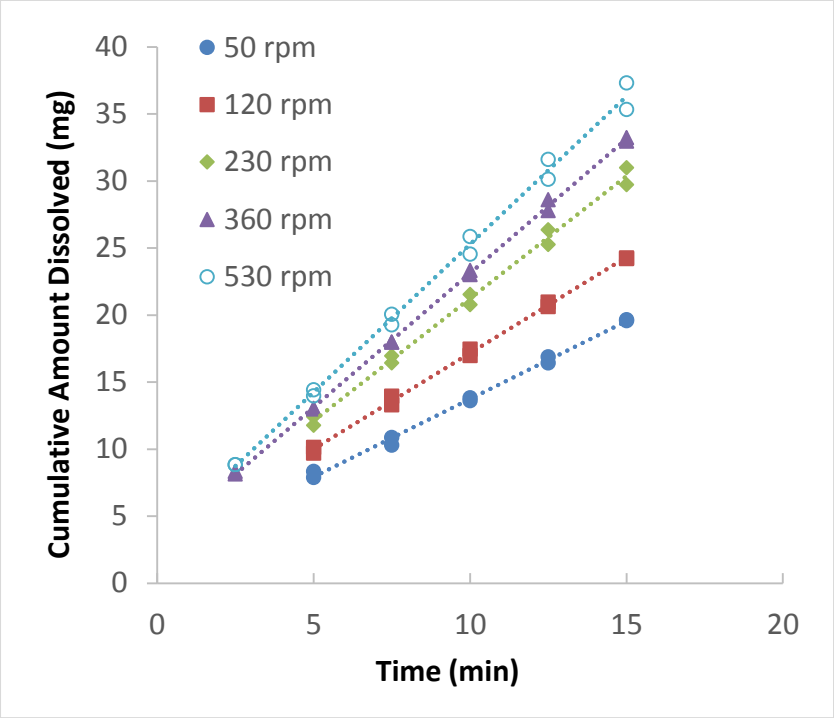

Figure 4-3. Benzoic acid dissolution profiles at various rotational speeds in 4% NaDS at 25 ℃.

Table 4-3. Benzoic acid dissolution rates (J) at various rotational speeds (ω) in various NaDS concentrations at 25 ℃.

ω (RPM)	Dissolution rate (J) in NaDS solutions (mg/min-cm^2)				
	water	0.5%	2%	4%	6%
50	0.257	0.534	1.25	1.57	-
120	0.399	0.673	1.76	1.93	2.18
230	0.535	0.765	2.04	2.47	2.81
360	0.663	0.794	2.27	2.70	3.01
530	0.810	0.877	2.43	2.98	3.23
800	-	-	-	-	3.64

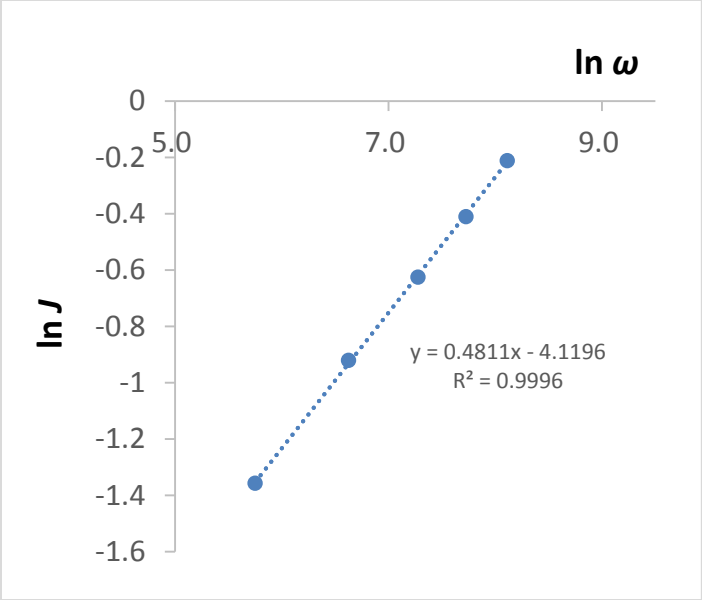

Figure 4-4. Plot of ln$J$ vs. lnω for benzoic acid dissolution in water at 25 ℃ (J = dissolution rate, ω = rotational speed).

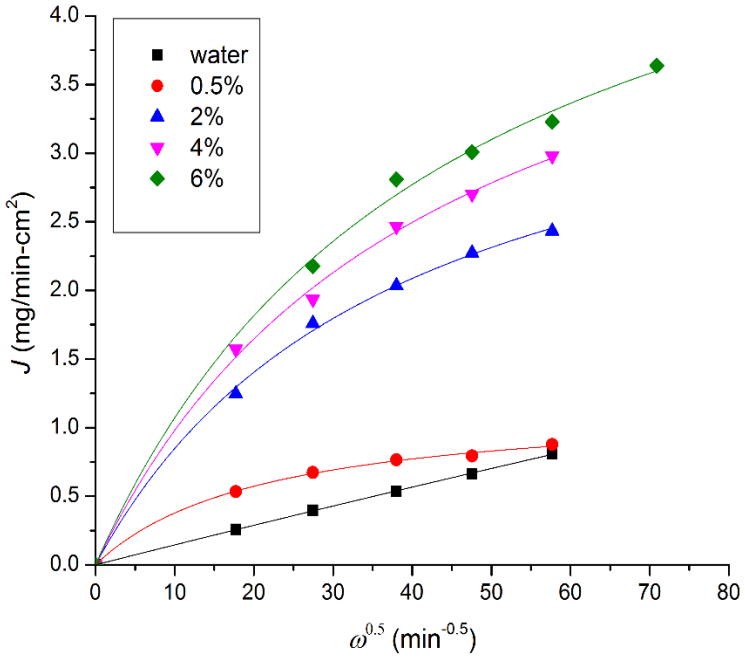

Figure 4-5. Plots of J vs. $\omega^{0.5}$ for benzoic acid dissolution in various NaDS concentrations (25 ℃) fitted with Eqn.(4-8) (J = dissolution rate, ω = rotational speed; the origin is included in all fits).

Eqn.(4-7) (Figure 4-6), similar to what was done in Chapter 3:

$$\frac{1}{J} = \frac{1}{X} + \frac{Y}{X}\omega^{-0.5} \tag{4-9}$$

Table 4-4 shows that the X and Y values obtained from these two fitting methods are similar. Hence, the data can be described to a similar degree of accuracy by the reconstructed plots of J vs. $\omega^{0.5}$ (Figure 4-7) using the X and Y values obtained from linearization. According to Chapter 2, the degree of interface control (P_I) may be defined as $P_I = (1+Y\omega^{-0.5})^{-1}$ ($P_I \to 0$ or 1 when $Y\omega^{-0.5} >> 1$ or $Y\omega^{-0.5} << 1$). Table 4-5 gives P_I calculated over the range of rotational speed in

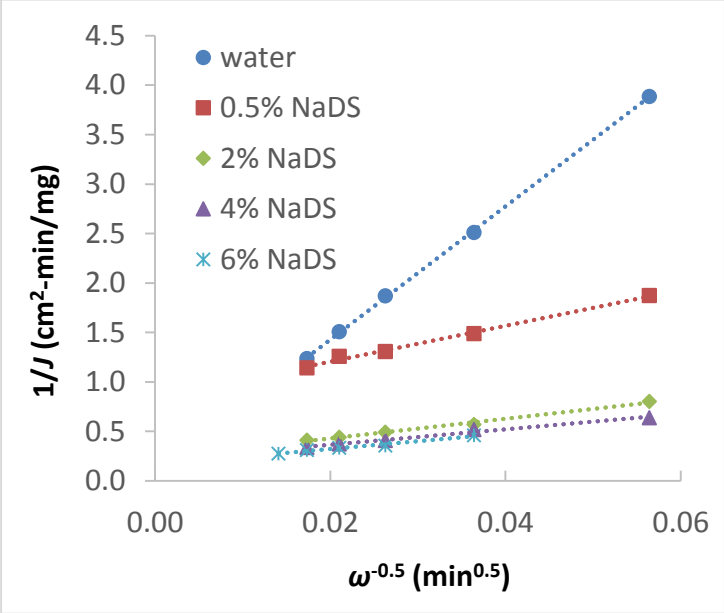

Figure 4-6. Plots of $1/J$ vs. $\omega^{-0.5}$ for benzoic acid dissolution in water and NaDS solutions at 25°C (J = dissolution rate, ω = rotational speed).

Table 4-4. Values of fitting parameter (X, Y) obtained from nonlinear curve fitting (Figure 4-5) and linearization (Figure 4-6).

NaDS Conc. (%w/v)	C_{mic} (mM)	α	Fitting Parameters			
			X (mg/min-cm^2)		Y (min$^{-1/2}$)	
			Nonlinear	Linear	Nonlinear	Linear
0	0	0	16.84	12.36	1150	832
0.5	0.16	0.23	1.18	1.19	21.33	21.54
2	1.02	0.58	4.07	4.38	38.08	43.71
4	2.18	0.77	5.16	4.82	42.70	37.60
6	3.33	0.82	5.87	6.07	44.77	47.86

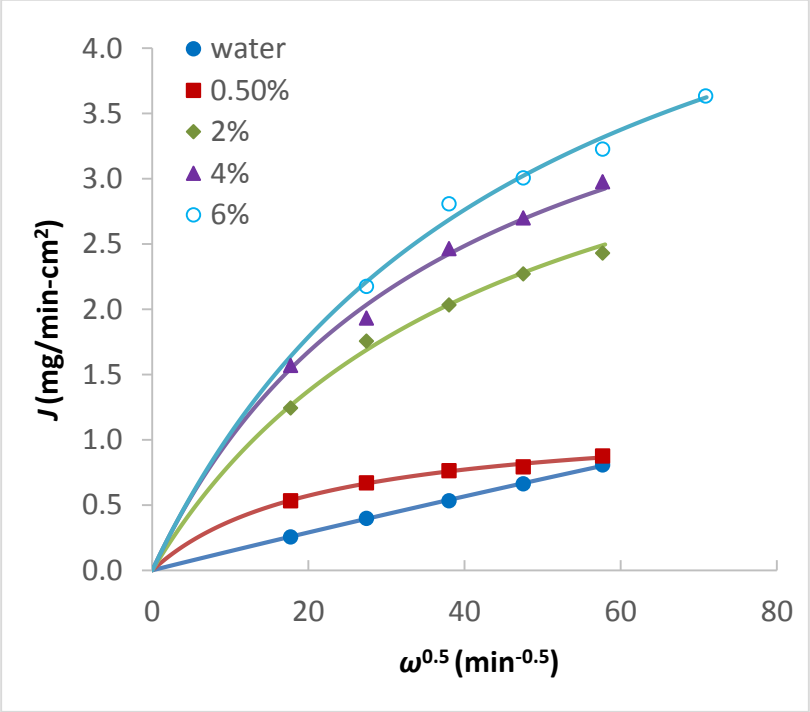

Figure 4-7. Plots of J vs. $\omega^{0.5}$ for benzoic acid dissolution in water and NaDS solutions reconstructed using the fitting parameters obtained from plots of $1/J$ vs. $\omega^{-0.5}$ (J = dissolution rate, ω = rotational speed).

Table 4-5. Degree of interface control calculated from *Y* values for benzoic acid dissolution in NaDS solutions (25°C).

NaDS Conc. (%w/v)	ω range (rpm)	Y ($min^{-1/2}$)		Degree of Interface Control (P_i)	
		Nonlinear	Linear	Nonlinear	Linear
0	50-530	1150	832	1.5-4.8%	2.1-6.5%
0.5	50-530	21.33	21.54	45.4-73.0%	45.1-72.8%
2	50-530	38.08	43.71	31.8-60.2%	28.9-56.9%
4	50-530	42.70	37.60	29.3-57.5%	32.0-60.5%
6	120-800	44.77	47.86	38.0-61.3%	36.5-59.7%

each NaDS concentration. It can be seen that the introduction of NaDS into the dissolution medium caused a dramatic shift in the dissolution mechanism. It is obvious that the main reason for this shift is the significant reduction of parameter *Y*. According to Eqn.(2-20), $Y\,\omega^{-0.5}$ describes the relative magnitude of the re-deposition rate constant versus the transport rate constant. The transport rate constant is smaller in NaDS solutions than in water due to lower diffusivities and higher viscosities.[a] Thus, there must be a huge reduction in the re-deposition rate constant. It may also be noted from Table 4-4 that parameter *X*, which describes the detachment process, is also much lower in NaDS solutions than in water. One possible

[a] As a crude estimate, assume the transport rate constant is given by the Levich theory, i.e., $N(D,v)\omega^b = 0.62D^{2/3}v^{-1/6}\omega^{1/2}$. Using literature diffusivity values (10^{-5} cm^2/s for benzoic acid in water,[44] 10^{-6} cm^2/s for the NaDS micelles[62]), viscosity values from Table 4-2, α from Table 4-1 and Eqn.(4-6) for effective diffusivity, the transport rate constant for benzoic acid in 2% NaDS is about 40% smaller than that in water.

explanation for the significant reductions of these interfacial rate constants is that the wetting of the solid surface by NaDS monomers alters its interaction properties with the solution (e.g., detachment/re-deposition rate constants and site densities). Of course, dissolution experiments in NaDS concentrations below the CMC would be needed to confirm this speculation.

Another interesting result from Table 4-4 is that both *X* and *Y* vary with NaDS concentration or the concentration of NaDS micelles. Since *X* describes the detachment process, it being a function of the micelle concentration seems to indicate that micelles are involved at least in the detaching of solid-state molecules, which, to some degree, agrees with the micelle-interface interaction mechanism proposed by Prakongpan et al.[48] A model describing this mechanism will be proposed in the following section.

Proposed Model for Micellar-Interface Interactions

If the micelle-interface interaction mechanism exists, the dissolution process may be depicted by Figure 4-8. In this model, it is assumed that this mechanism may be regarded as reactions between surfactant micelles and the detachment or re-deposition sites of a solid surface. If the maximum number of molecules that can be solubilized in each micelle is n_{max}, then each micelle may be divided into n_{max} independent reactive regions. A detachment reaction occurs between an empty reactive region and a detachment site, while a re-deposition reaction occurs between an occupied reactive region and a re-deposition site. (The actual reaction process may be pictured as a micellar reactive region undergoing a certain conformational change for the incorporation or release of solute molecules.) Thus, the reactivities of a micelle with occupation number *n* (that is, a micelle that contains a total of *n* solute molecules) with a detachment site and a re-deposition site are proportional to $n_{max} - n$ and *n*, respectively. For instance, an empty micelle ($n = 0$) has no

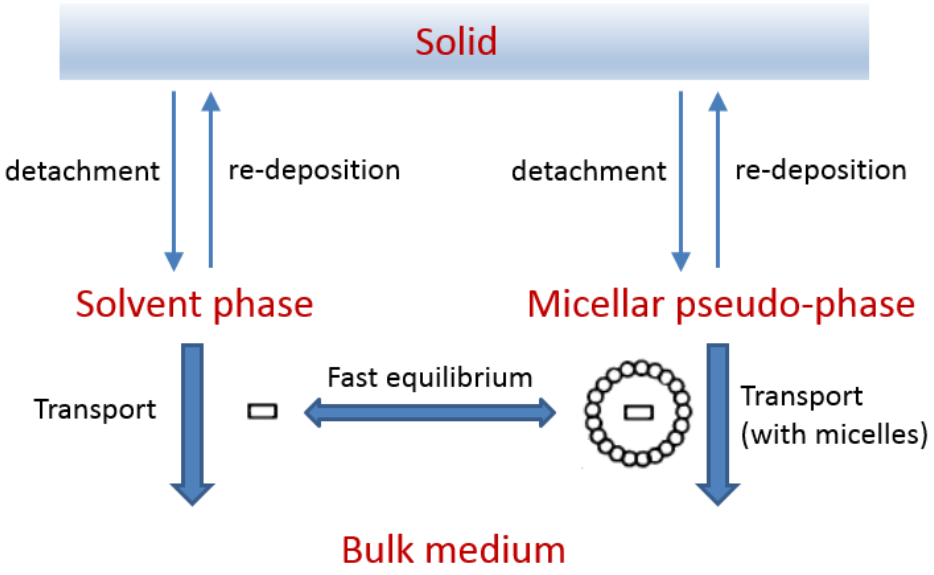

Figure 4-8. Dissolution in a surfactant medium forming micelles.

reactivity for re-deposition and the highest reactivity for detachment, whereas a fully occupied micelle ($n = n_{\max}$) has no reactivity for detachment and the highest reactivity for re-deposition.

The reaction rate between micelles with occupation number n and a given type of detachment site is assumed to be proportional to the concentration (at the solid-liquid boundary) of these micelles and the site density:

$$R_{\mathrm{t},i}^{[\mathrm{mic}]}(n) = (n_{\max} - n) k_{\mathrm{t},i}^{[\mathrm{mic}]} C_{\mathrm{mic}} f_0(n) \sigma_{\mathrm{t},i} \tag{4-10}$$

where, $k_{\mathrm{t},i}^{[\mathrm{mic}]}$ is the reaction rate constant between an *unoccupied* micellar reactive region and a detachment site of the i-th type, C_{mic} is the micelle concentration, $f_0(n)$ is the fraction of micelles with occupation number n (subscript 0 denotes the solid-liquid boundary) and $\sigma_{\mathrm{t},i}$ is the

surface density of this detachment site. The total detachment rate by micelles is thus given by summing Eqn.(4-10) over all occupation numbers and types of detachment sites:

$$R_{\mathrm{t}}^{[\mathrm{mic}]} = \sum_i \sum_{n=0}^{n_{\max}} R_{\mathrm{t},i}^{[\mathrm{mic}]}(n) = \left(\sum_{n=0}^{n_{\max}} (n_{\max} - n) C_{\mathrm{mic}} f_0(n) \right) \cdot \left(\sum_i k_{\mathrm{t},i}^{[\mathrm{mic}]} \sigma_{\mathrm{t},i} \right) \tag{4-11}$$

Since by definition, $\sum_{n=0}^{n_{\max}} f_0(n) = 1$ and $c_0^{[\mathrm{mic}]} = C_{\mathrm{mic}} \sum_{n=0}^{n_{\max}} f_0(n) n$ is the boundary concentration of the micellar solute form, Eqn.(4-11) reduces to:

$$R_{\mathrm{t}}^{[\mathrm{mic}]} = \sum_i \sum_{n=0}^{n_{\max}} (n_{\max} - n) k_{\mathrm{t},i}^{[\mathrm{mic}]} C_{\mathrm{mic}} f_0(n) \sigma_{\mathrm{t},i} = (n_{\max} C_{\mathrm{mic}} - c_0^{[\mathrm{mic}]}) \kappa_{\mathrm{t}}^{[\mathrm{mic}]} \tag{4-12}$$

where, $\kappa_{\mathrm{t}}^{[\mathrm{mic}]} = \sum_i k_{\mathrm{t},i}^{[\mathrm{mic}]} \sigma_{\mathrm{t},i}$. Similarly, the total re-deposition rate from micelles is:

$$R_{\mathrm{p}}^{[\mathrm{mic}]} = \sum_i R_{\mathrm{p},i}^{[\mathrm{mic}]}(n) = \left(\sum_{n=0}^{n_{\max}} C_{\mathrm{mic}} f_0(n) n \right) \cdot \left(\sum_i k_{\mathrm{p},i}^{[\mathrm{mic}]} \sigma_{\mathrm{p},i} \right) = c_0^{[\mathrm{mic}]} \kappa_{\mathrm{p}}^{[\mathrm{mic}]} \tag{4-13}$$

where, $k_{\mathrm{p},i}^{[\mathrm{mic}]}$ is the reaction rate constant between an *occupied* micellar reactive region and a re-deposition site of the *i*-th type, $\sigma_{\mathrm{p},i}$ is the surface density of this re-deposition site and $\kappa_{\mathrm{p}}^{[\mathrm{mic}]} = \sum_i k_{\mathrm{p},i}^{[\mathrm{mic}]} \sigma_{\mathrm{p},i}$.

In Figure 4-8, mass transfers from the solid to the solvent phase and the micellar pseudo-phase occur in parallel. Thus, the total detachment and re-deposition rates are given by:

$$R_{\mathrm{t}} = R_{\mathrm{t}}^{[\mathrm{sol}]} + R_{\mathrm{t}}^{[\mathrm{mic}]} \tag{4-14}$$

$$R_{\mathrm{p}} = R_{\mathrm{p}}^{[\mathrm{sol}]} + R_{\mathrm{p}}^{[\mathrm{mic}]} \tag{4-15}$$

where, $R_{\mathrm{t}}^{[\mathrm{sol}]}$ and $R_{\mathrm{p}}^{[\mathrm{sol}]}$ are detachment and re-deposition rates for the solvent phase and are described by Eqns.(2-2) and (2-4) of Chapter 2 (with superscript "[sol]" added to indicate the solvent phase):

$$R_{\mathrm{t}}^{[\mathrm{sol}]} = \kappa_{\mathrm{t}}^{[\mathrm{sol}]}, \quad \kappa_{\mathrm{t}}^{[\mathrm{sol}]} = \sum_i k_{\mathrm{t},i}^{[\mathrm{sol}]} \sigma_{\mathrm{t},i} \tag{4-16}$$

$$R_{\mathrm{p}}^{[\mathrm{sol}]} = c_0^{[\mathrm{sol}]} \kappa_{\mathrm{p}}^{[\mathrm{sol}]}, \quad \kappa_{\mathrm{p}}^{[\mathrm{sol}]} = \sum_i k_{\mathrm{p},i}^{[\mathrm{sol}]} \sigma_{\mathrm{p},i} \tag{4-17}$$

Eqns.(4-12)-(4-17) gives the interfacial mass transfer flux:

$$J_{\mathrm{I}} = R_{\mathrm{t}} - R_{\mathrm{p}} = \kappa_{\mathrm{t}}^{[\mathrm{sol}]} + (n_{\max} C_{\mathrm{mic}} - c_0^{[\mathrm{mic}]}) \kappa_{\mathrm{t}}^{[\mathrm{mic}]} - c_0^{[\mathrm{mic}]} \kappa_{\mathrm{p}}^{[\mathrm{mic}]} - c_0^{[\mathrm{sol}]} \kappa_{\mathrm{p}}^{[\mathrm{sol}]} \tag{4-18}$$

or, using the pseudo-equilibrium condition (4-5) and the fraction of solute in micellar form, $\alpha \equiv KC_{\mathrm{mic}} / (1 + KC_{\mathrm{mic}})$, to express it in terms of the total solute concentration, $c_0^{[\mathrm{T}]} = c_0^{[\mathrm{sol}]} + c_0^{[\mathrm{mic}]}$:

$$J_{\mathrm{I}} = \kappa_{\mathrm{t}}^{[\mathrm{sol}]} + n_{\max} C_{\mathrm{mic}} \kappa_{\mathrm{t}}^{[\mathrm{mic}]} - c_0^{\mathrm{T}} (\alpha \kappa_{\mathrm{t}}^{[\mathrm{mic}]} + \kappa_{\mathrm{p,eff}}) \tag{4-19}$$

where, $\kappa_{\mathrm{p,eff}} = \alpha \kappa_{\mathrm{p}}^{[\mathrm{mic}]} + (1-\alpha) \kappa_{\mathrm{p}}^{[\mathrm{sol}]}$ is an effective re-deposition rate constant defined in a same manner as the effective diffusivity (Eqn.(4-6)).

In Appendix C, it is shown that the steady-state transport flux is given by:

$$J_{\mathrm{T}} = c_0^{\mathrm{T}} N(D_{\mathrm{eff}}, \nu) \omega^b \tag{4-20}$$

Using the steady-state requirement: $J_{\mathrm{I}} = J_{\mathrm{T}}$, $c_0^{[\mathrm{T}]}$ may be eliminated to give the dissolution rate:

$$J = \frac{\kappa_{\mathrm{t}}^{[\mathrm{sol}]} + n_{\max} C_{\mathrm{mic}} \kappa_{\mathrm{t}}^{[\mathrm{mic}]}}{1 + \dfrac{\alpha \kappa_{\mathrm{t}}^{[\mathrm{mic}]} + \kappa_{\mathrm{p,eff}}}{N(D_{\mathrm{eff}}, \nu) \omega^b}} \tag{4-21}$$

We see that Eqn.(4-21) has the functional form of Eqn.(4-7), with $X = \kappa_t^{[sol]} + n_{max} C_{mic} \kappa_t^{[mic]}$ and $Y = (\alpha \kappa_t^{[mic]} + \kappa_{p,eff}) / N(D_{eff}, \nu)$. Since micelles are assumed to be directly involved in the interfacial processes, both *X* and the numerator of *Y* become functions of C_{mic} (the denominator of parameter *Y* is a function of C_{mic} regardless of this assumption). It appears that *X* must vary linearly with C_{mic}. However, for the present study of benzoic acid dissolution in NaDS solutions, the plot of *X* vs. C_{mic} using the nonlinear fitting results from Table 4-4 is downward curved (Figure 4-9). A possible explanation for this is micellar activity effects. It is known that in a

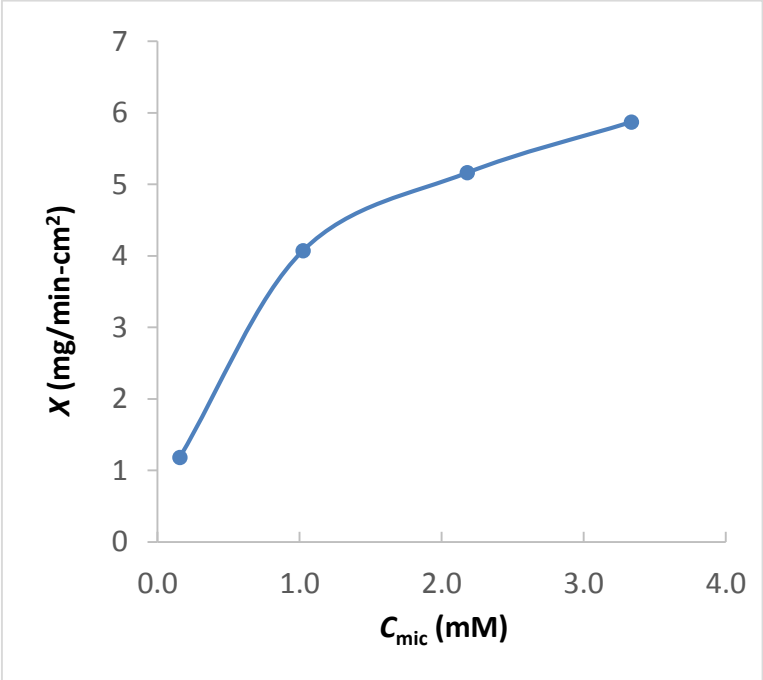

Figure 4-9. Plot of fitting parameter *X* against micelle concentration (C_{mic}) for benzoic acid dissolution in NaDS solutions.

solution of electrolytes, each ion is surrounded by an ion cloud (or atmosphere) because of electrostatic interactions. This cloud screens the electric field produced by the central ion. The effect of this charge screening is a reduced effective ion concentration, given by the limiting Debye-Hückel equation:

$$\ln \frac{c_{\text{eff}}}{c} = \ln \gamma = -Az^2 \sqrt{I} \tag{4-22}$$

where, A is a positive constant, z is the ion charge number and I is the ionic strength of the solution. In the case of colloidal ions which typically have large radii (e.g., ~ 20 Å for an NaDS micelle[62]) and high charge numbers (e.g., -16 for an NaDS micelle, calculated based on the mean aggregation number and degree of counterion association), it has been shown that the activity coefficient is usually much smaller than predicted by the Debye-Hückel theory,[66] which means an even lower effective concentration. Thus, $X = \kappa_{\text{t}}^{[\text{sol}]} + n_{\max} C_{\text{mic}} \kappa_{\text{t}}^{[\text{mic}]}$ would be modified to:

$$X = \kappa_{\text{t}}^{[\text{sol}]} + n_{\max} C_{\text{mic}} \gamma_{\text{mic}} \kappa_{\text{t}}^{[\text{mic}]} \tag{4-23}$$

Since the micellar activity coefficient, γ_{mic}, is a decreasing function of ionic surfactant concentration or C_{mic}, Eqn.(4-23) predicts that the plot of X against C_{mic} will curve downward, as is the case in Figure 4-9.

This model needs to be further tested by conducting a similar dissolution study for benzoic acid or other compounds in a nonionic surfactant system, where there is no ionic activity effects. In this case, if the model is correct, parameter X (if it could be obtained from fitting) should vary linearly with the micelle concentration. If this is not the case, further modifications to the model will be necessary.

Summary

In this chapter, the intrinsic dissolution rate of benzoic acid as a function of agitation intensity was investigated in water and various NaDS concentrations above the CMC at 25°C. The plots of dissolution rate vs. (rotational speed)$^{1/2}$ were fitted with the functional form of the mixed-kinetic-controlled dissolution model of Chapter 2. The results indicate that significant interface control was responsible for benzoic acid dissolution in NaDS solutions. The values of the fitting parameters are both significantly smaller in NaDS solutions than those in water, which is possibly the result of altered solid surface properties due to wetting by NaDS monomers. In NaDS solutions, both parameters vary as function of the micelle concentration, which suggests possible micellar involvement in the interfacial processes. A model for describing this micelle-interface interaction mechanism is proposed in which a micelle is assumed to have a number of reactive regions equal to its maximum solubilizing capacity and its reactivities with detachment and re-deposition sites are proportional to the numbers of unoccupied and occupied reactive regions, respectively. This model leads to a formula for dissolution rate in which the aforementioned parameters are functions of micelle concentration, as well as collective interfacial rate constants. For the present study, the manner in which one of the fitting parameters varies with the micelle concentration seems to indicate the presence of micellar activity effects, where the interfacial rate constants are effectively reduced due to the charge screening of anionic NaDS micelles.

CHAPTER 5 DISSOLUTION IN DYE SOLUTIONS

Introduction

What distinguishes the mixed-kinetic-controlled dissolution model of Chapter 2 from the models by Berthoud and Rickard et al.[20,21] is the assumption that dissolution occurred from various types of detachment and re-deposition sites at a solid surface. These rates are given by summing the products of reaction rate constant and surface density for all types of detachment or re-deposition sites. The studies in Chapter 3 were mainly interested in the effect of the reaction rate constants as a function of temperature. It is therefore of interest to probe the effects of site densities on dissolution rate.

Dyes are extensively used as colorants in drug formulations such as tablets, tablet coating, and suspensions. Therefore, the potential effects of dyes on drug dissolution need to be carefully studied. Piccolo et al. found that low concentrations (5-100 μg/mL) of FD&C Blue #1, a certified water-soluble dye, were able to significantly inhibit the dissolution rates of phenobarbital monohydrate, sulfathiazole and sulfaguanidine,[67] examples of which are shown in Figures 5-1 – 5-3. They attributed this type of inhibition to the dye adsorbing preferentially on dissolution sites, such as kink sites in crystal surface ledges. By assuming that: 1) the fractional dissolution rate reduction is proportional to the fraction of the dissolving surface covered by the dye and that 2) the dye adsorption can be described by a simple Langmuir isotherm, an expression for dissolution rate as a function of dye concentration was proposed:[68]

$$J(C) = J_0(1-\theta\frac{KC}{1+KC}) \tag{5-1}$$

where, $J(C)$ and J_0 are dissolution rates with and without dye, respectively, θ is fraction of surface covered when the surface is saturated with dye, C is dye concentration in bulk solution and K is Langmuir isotherm constant. Using the data in Figure 5-1, θ and K were obtained to be 0.61 and 0.76 mol^{-1}, respectively, for sulfaguanidine single crystal. The authors believed that θ_S being smaller than one was indicative of a "selective adsorption mechanism" rather than complete surface coverage. In other words, 39% of sulfaguanidine surface did not adsorb the dye and was responsible for the limiting dissolution rate, $J(\infty) = J_0(1-\theta)$.

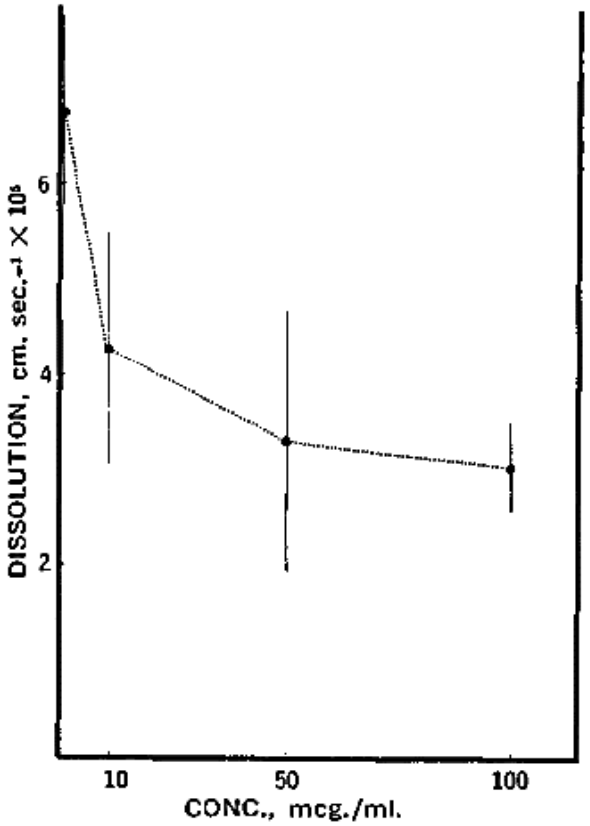

Figure 5-1. Effect of dye concentration on the dissolution rate of sulfaguanidine single crystals in 0.1 N HCl.[67]

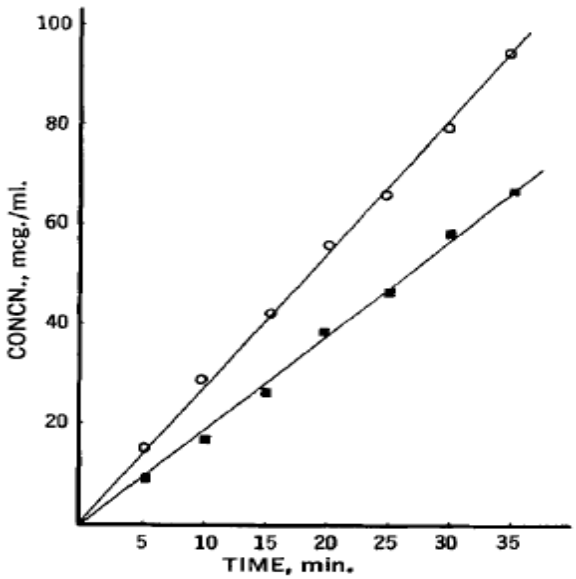

Figure 5-2. Dissolution behaivior of sulfathiazole compressed disks (○: in 0.1 N HCl; ■: in 0.1 N HCl containing 5 μg/mL FD&C Blue #1).[67]

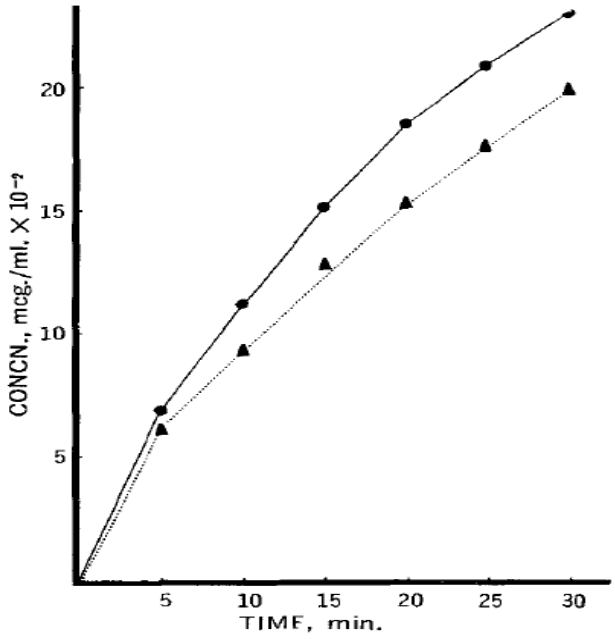

Figure 5-3. Dissolution behaivior of sulfathiazole crystalline powder (●: in 0.1 N HCl; ▲: in 0.1 N HCl containing 50 μg/mL FD&C Blue #1).[67]

This chapter presents an experimental investigation of the intrinsic dissolution behavior of sulfathiazole in various concentrations of FD&C Blue #1 in water and HCl solutions and a qualitative analysis of the results based on the kinetic model of Chapter 2.

Materials and Methods

Materials

Sulfathiazole (Fluka®, Sigma-Aldrich, Co., St. Louis, MO) and FD&C blue #1 (Sigma-Aldrich, Co., St. Louis, MO) were used as received. HCl solutions (0.1 and 0.01 N) were prepared by diluting 37% HCl (Mallinckrodt® Chemicals, Inc., Paris, KY) 120-fold and 1200-fold with distilled water, respectively.

Dissolution Test System

An intrinsic dissolution apparatus (USP Apparatus 6; VK700, Vankel®, Cary, NC) was used for all dissolution studies. Sulfathiazole powder was compressed into a flat-faced tablet (0.8 cm, diameter; 0.502 cm^2, area) using a hydraulic press (Model C; Carver, Inc., Wabash, Indiana) the accessory holder-punch-die set. The compression pressure was 3000 lbs and the dwell time was 30 s. A dissolution run was initiated by lowering the sample holder into 250 mL of dissolution medium in a 900-mL vessel (depth of immersion ~1.7 cm from the liquid surface) at 25 (±0.1) ℃, upon which it was brought to a rotational speed of 100 rpm. The medium was sampled at five time points up to 40-50 minutes without replacement due to the small sample volumes (1 mL) removed, but the total volume change was accounted for in dissolution rate calculations. All experiments were performed in duplicate.

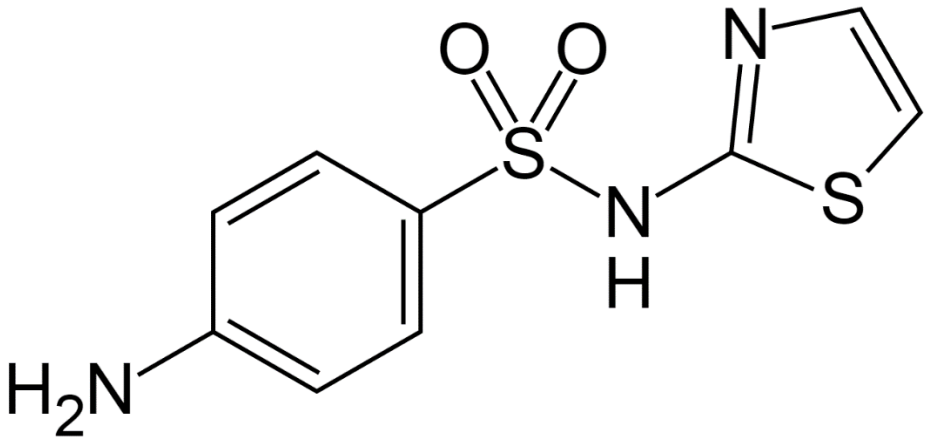

Figure 5-4. Molecular structure of sulfathiazole (MW = 255.32).

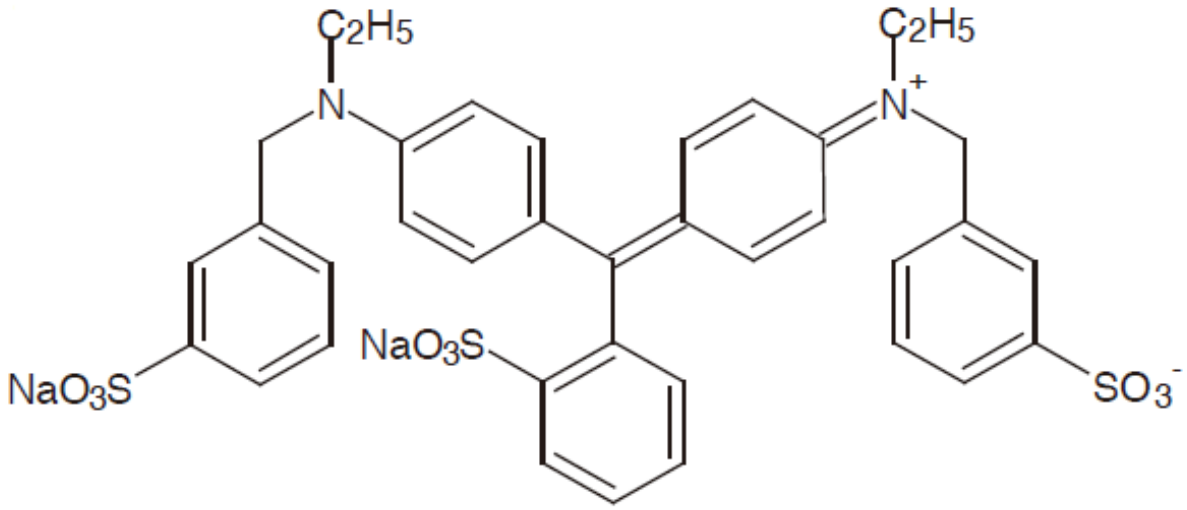

Figure 5-5. Molecular structure of FD&C Blue #1 (MW = 792.85).

Solubility Determination

Sulfathiazole solubilities were determined (in duplicate) in water, 0.01 N and 0.1 N HCl with and without FD&C Blue #1. Saturated sulfathiazole solutions were prepared by adding excess sulfathiazole powder to these media. The suspensions were stirred vigorously at room temperature (25 (±0.5) ℃) for 24 hours, after which they were filtered through 0.22-μm syringe filter units (Millex®, Billerica, MA) and diluted for assay.

HPLC Analysis

The wavelength of maximum UV absorption for sulfathiazole in water was determined to be 258 nm using a Hewlett-Packard 8453 diode array UV-Vis spectrophotometer. All samples were analyzed using an Agilent® 1100 Series HPLC unit. The HPLC conditions are listed in Table 5-1.

Figures 5-6 and 5-7 show the chromatograms of sulfathiazole and FD&C Blue #1 in water and 0.01 N HCl solutions, respectively. The retention time for sulfathiazole was ~6 min. Standard calibration plots for sufathiazole in water, 0.01 N and 0.1 N HCl can be found in Appendix D. The calibration ranges in each medium were chosen so that dissolution samples could be assayed without dilution.

Table 5-1. HPLC conditions for sulfathiazole sample analysis.

Column	Phenomenex® C18, 250 x 4.60 mm, 5 μ
Mobile phase	80% water + 20% acetonitrile
Flow rate	1 mL/min
Injection volume	50 uL
UV detection wavelength	257 nm

1. 99.9%, Optima®, Fisher Scientific, Inc., Fair Lawn, NJ.

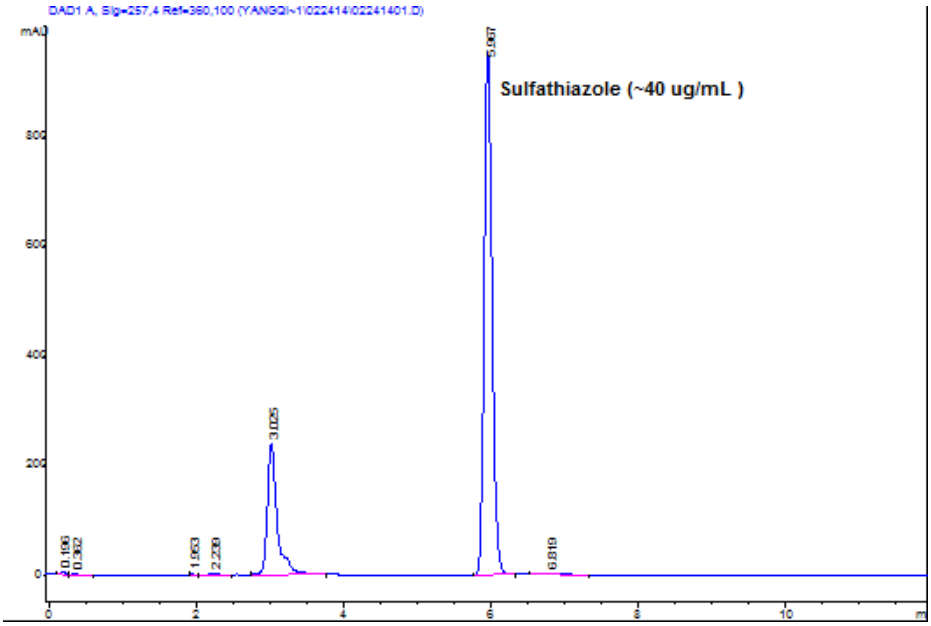

Figure 5-6. Chromatogram of sulfathiazole (~40 µg/mL) in a FD&C Blue #1 solution (~100 µg/mL) in water.

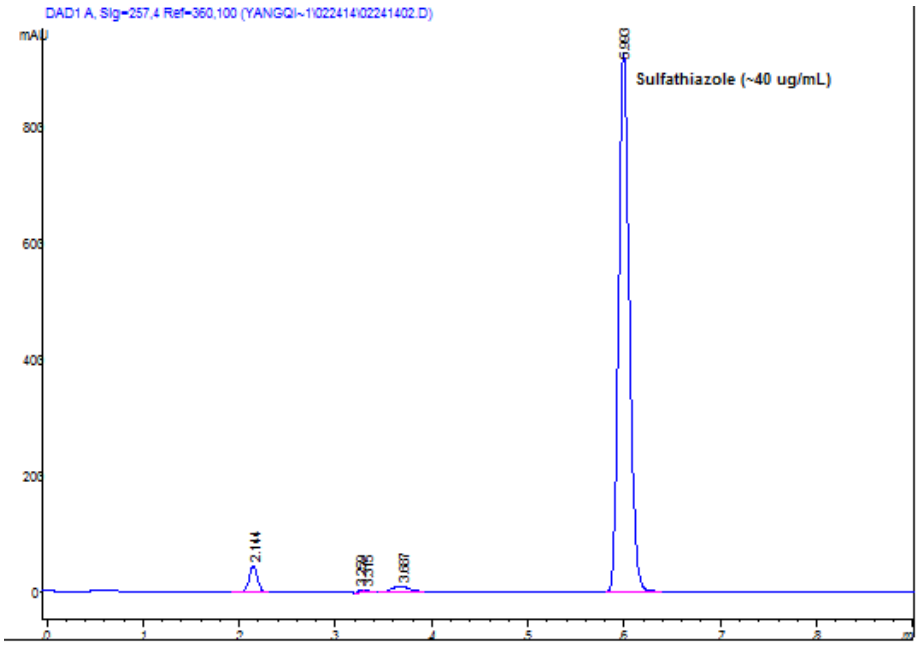

Figure 5-7. Chromatogram of sulfathiazole (~40 µg/mL) in FD&C Blue #1 (~100 ug/mL) and 0.1 N HCl.

Results and Discussion

Although the molecular structure of FD&C Blue #1, a triphenyl methane dye, is commonly depicted as in Figure 5-5, a carbonium ion structure (Figure 5-8) is considered a better representation by those who study the basic spectroscopy and other fundamental properties of this class of dyes.[69] The dye appeared blue in water, slightly green in 0.01 N HCl, and green in 0.1 N HCl. This is due to the protonation of one of the aniline groups (the highly acidic sulfonate groups are not expected to be protonated). Such color changes associated with amino group protonation have been documented for Coomassie Blue G,[70] a dye of a similar molecular structure. Using spectral methods, the pK_a's associated with the aniline groups of Coomassie Blue G were calculated to be between 1 and 2. The observed color changes in 0.01 N and 0.1 N HCl suggest that the aniline groups in FD&C Blue #1 should have similar pK_a's.

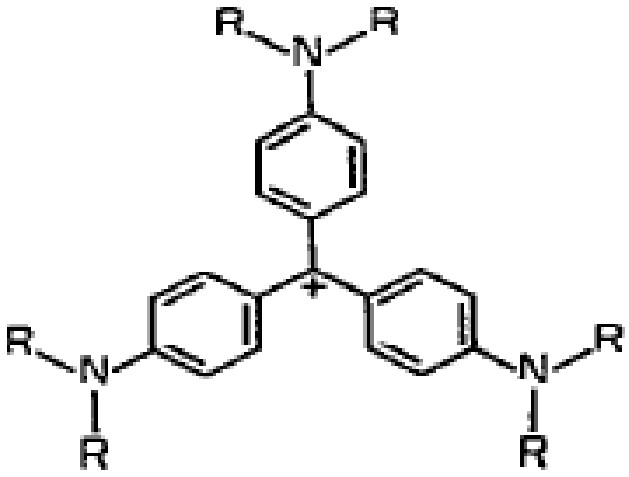

Figure 5-8. Carbonium ion structure of a triphenylmethane dye.[69]

Sulfathiazole solubilities in water, 0.01 N and 0.1 N HCl with and without added FD&C Blue #1 are given in Table 5-2. The molecule (Figure 5-4) has a basic aniline group (pK_a = 2.2) and an acidic sulfonamide group (pK_a = 7.2).[71] Due to their low acidity or basicity, sulfathiazole is predominantly unionized (SH) in water. In acidic solutions, a certain portion of it will become protonated (SH_2^+) depending on the acidity. This is the main reason for the solubility increase in HCl solutions. With the addition of 100 μg/mL (~0.13 mM) dye, sulfathiazole solubility increased by 0.04 mg/mL (~0.16 mM) and 0.26 mg/mL (~1 mM) in 0.01 N and 0.1 N HCl, respectively. If these increases are due solely to sulfathiazole-dye complexation, the mean sulfathiazole-to-dye stoichiometric ratios would be 1.2 : 1 and 7.7 : 1 in 0.01 N and 0.1 N HCl, respectively. More definitive experiments, which are not part of the present work, would be necessary to verify these ratios.

Figures 5-9 - 5-11 show the intrinsic dissolution profiles of sulfathiazole in water, 0.01 N HCl and 0.1 N HCl solutions with and without added FD&C Blue #1; the dissolution rates, calculated in the same manner as in Chapter 3, are given in Table 5-2. It can be seen that in the absence of the dye, the dissolution rate increased almost proportionately with the solubility, which may also be attributed to the ionization, $SH + H^+ \rightarrow SH_2^+$. Figure 5-12 shows the variation of sulfathiazole dissolution rate (normalized with respect to the value in the absence of the dye) in each medium with dye concentration. In 0.1 N HCl, the dye exhibited significant inhibitory effects, reducing the dissolution rate by up to 34%. In 0.01 N HCl, the inhibitory effects were much smaller (< 9%). In water, the dye effects were almost non-existent. One factor that might have contributed to the reductions in dissolution rate was sulfathiazole-dye complexation, which can slow down the transport of sulfathiazole by reducing its effective diffusivity. However, this effect is expected to be minor since less than 5% sulfathiazole complexed with the dye as indicated by the

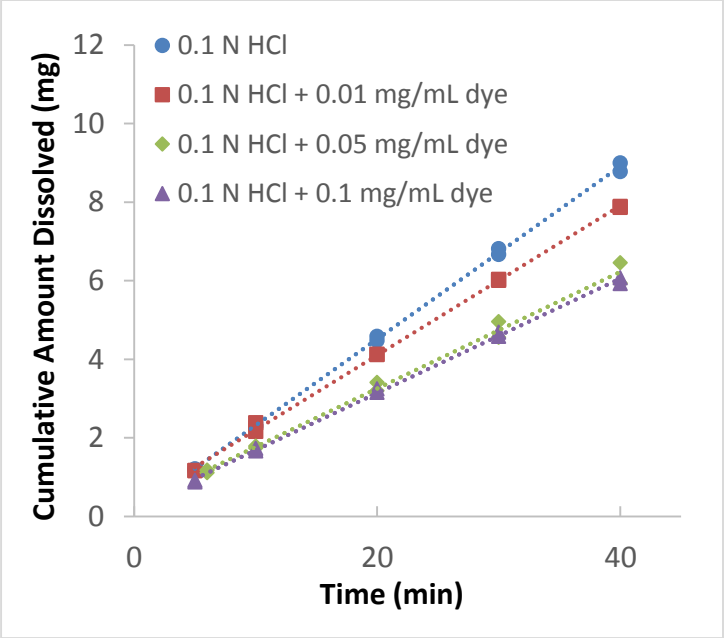

Figure 5-9. Sulfathiazole dissolution profiles in water with added FD&C Blue #1 (0, 0.01 mg/mL and 0.1 mg/mL) at 100 rpm and 25 ℃.

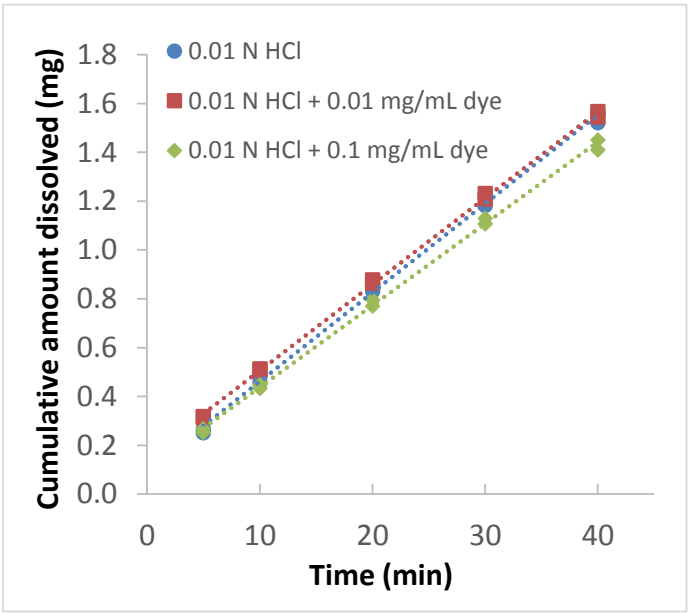

Figure 5-10. Sulfathiazole dissolution profiles in 0.01 N HCl with added FD&C Blue #1 (0, 0.01 mg/mL, 0.1 mg/mL) at 100 rpm and 25 ℃.

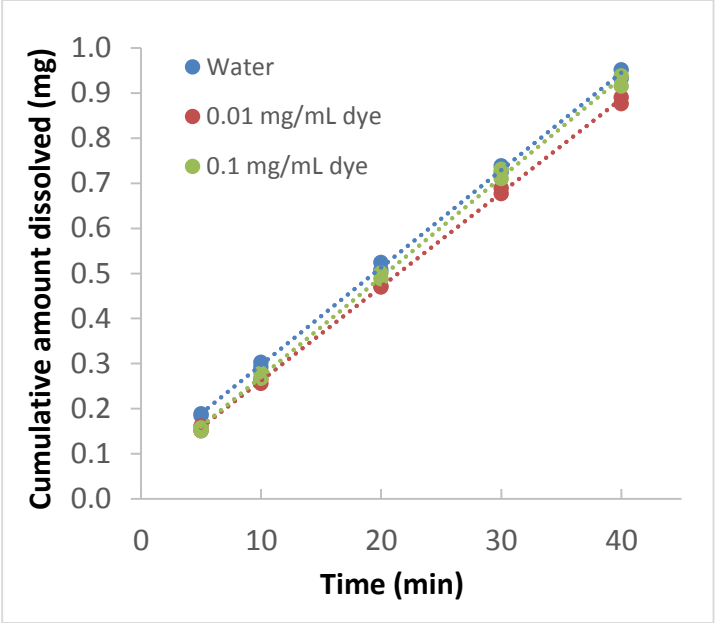

Figure 5-11. Sulfathiazole dissolution profiles in 0.1 N HCl with added FD&C Blue #1 (0, 0.01 mg/mL, 0.05 mg/mL and 0.1 mg/mL) at 100 rpm and 25 ℃.

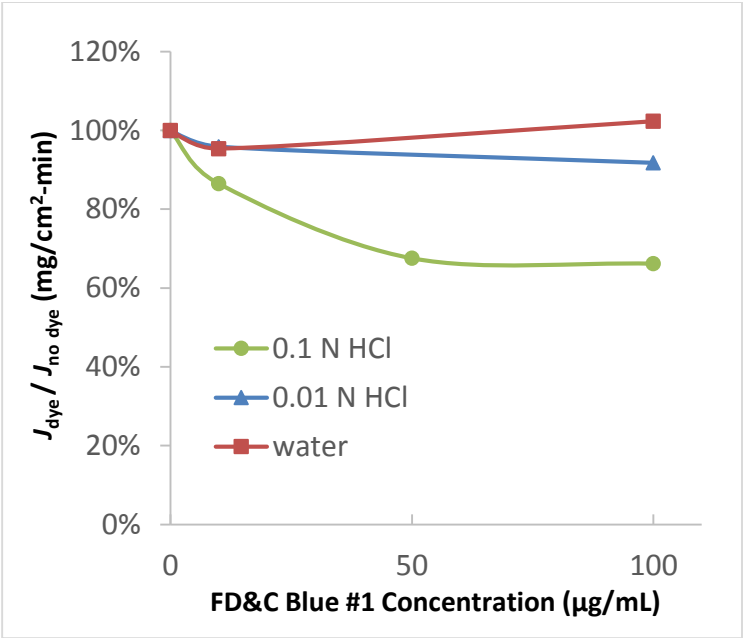

Figure 5-12. Effect of FD&C Blue #1 on sulfathiazole dissolution rate (*J*) in water, 0.01 N and 0.1 N HCl.

Table 5-2. Sulfathiazole dissolution rates (100 rpm) and solubilities in water and HCl solutions with and without added FD&C Blue #1 at 25 ℃.

Medium		Sulfathiazole Dissolution rate (J) (mg/min-cm^2)	Solubility (C_S) (mg/mL)[1]
HCl (N)	FD&C Blue #1 (μg/mL)		
0.1	-	0.438	5.02 ± 0.04
	10	0.379	-
	50	0.296	-
	100	0.290	5.28 ± 0.04
0.01	-	0.073	0.88
	10	0.070	-
	100	0.067	0.92 ± 0.01
-	-	0.043	0.54
	10	0.041	-
	100	0.044	0.55

1. ± values represent the plus/minus ranges of two measurements (values smaller than 0.01 are not listed)

solubility changes in Table 5-2. Thus, the most likely cause for the dissolution rate reductions was dye adsorption. (In this study, dye adsorption was indicated by all dissolving surfaces in dye solutions were dyed blue, the color being darker in higher dye concentrations.) However, Piccolo's equation (5-1)cannot explain why the inhibitory effect of FD&C Blue #1 was significantly smaller in 0.01 N HCl and absent in water.

According to the kinetic model of Chapter 2, the detachment rate (R_t) and the collective re-

deposition rate constant (κ_{p}) are given by:

$$R_{\mathrm{t}} = \sum_i k_{\mathrm{t},i}\sigma_{\mathrm{t},i},\ \kappa_{\mathrm{p}} = \sum_i k_{\mathrm{p},i}\sigma_{\mathrm{p},i}$$

Each term in the sums is proportional to the surface density of a particular type of detachment ($\sigma_{\mathrm{t},i}$) or re-deposition sites ($\sigma_{\mathrm{p},i}$). If a detachment or re-deposition site is also an adsorption site for a dye, its surface density will be reduced by dye adsorption. We divide these sites into adsorptive and non-adsorptive types, so that

$$R_{\mathrm{t},0} = \sum_{\text{adsorptive}} k_{\mathrm{t},i}\sigma_{\mathrm{t},i} + \sum_{\text{non-adsorptive}} k_{\mathrm{t},j}\sigma_{\mathrm{t},j} \tag{5-2}$$

$$\kappa_{\mathrm{p},0} = \sum_{\text{adsorptive}} k_{\mathrm{p},i}\sigma_{\mathrm{p},i} + \sum_{\text{non-adsorptive}} k_{\mathrm{p},j}\sigma_{\mathrm{p},j} \tag{5-3}$$

where, adsorptive and non-adsorptive sites are labeled by *i* and *j*, respectively, and subscript 0 is added to indicate the absence of the dye. In a dye solution, a certain fraction ($f_{\mathrm{t},i}$ or $f_{\mathrm{p},i}$) of each type of adsorptive detachment or re-deposition site will be covered by the dye (assuming adsorption equilibrium), reducing R_{t} and κ_{p} to:

$$R_{\mathrm{t}} = \sum_{\text{adsorptive}} k_{\mathrm{t},i}(1-f_{\mathrm{t},i})\sigma_{\mathrm{t},i} + \sum_{\text{non-adsorptive}} k_{\mathrm{t},j}\sigma_{\mathrm{t},j} \tag{5-4}$$

$$\kappa_{\mathrm{p}} = \sum_{\text{adsorptive}} k_{\mathrm{p},i}(1-f_{\mathrm{p},i})\sigma_{\mathrm{p},i} + \sum_{\text{non-adsorptive}} k_{\mathrm{p},j}\sigma_{\mathrm{p},j} \tag{5-5}$$

These fractions are certain functions of the dye concentration (in bulk solution): $f_{\mathrm{t},i} = f_{\mathrm{t},i}(C_{\mathrm{dye}})$, $f_{\mathrm{p},i} = f_{\mathrm{p},i}(C_{\mathrm{dye}})$. For example, if the adsorption on each type of site is described by a Langmuir isotherm, they are give by:

$$f_{\mathrm{t},i}(C_{\mathrm{dye}}) = \frac{K_{\mathrm{t},i} C_{\mathrm{dye}}}{1 + K_{\mathrm{t},i} C_{\mathrm{dye}}},\ f_{\mathrm{p},i}(C_{\mathrm{dye}}) = \frac{K_{\mathrm{p},i} C_{\mathrm{dye}}}{1 + K_{\mathrm{p},i} C_{\mathrm{dye}}} \tag{5-6}$$

where, $K_{\mathrm{t},i}$ and $K_{\mathrm{p},i}$ are Langmuir isotherm constants. If all detachment sites have the same $K_{\mathrm{t},i}$, i.e., $K_{\mathrm{t},i} = K_{\mathrm{t}}$, the detachment rate (5-4) reduces to:

$$R_{\mathrm{t}} = \frac{1}{1 + K_{\mathrm{t}} C_{\mathrm{dye}}} \sum_{\text{adsorptive}} k_{\mathrm{t},i} \sigma_{\mathrm{t},i} + \sum_{\text{non-adsorptive}} k_{\mathrm{t},j} \sigma_{\mathrm{t},j} \tag{5-7}$$

If we define the fraction of detachment due to adsorptive sites as:

$$\theta_{\mathrm{t}} \equiv \frac{\sum_{\text{adsorptive}} k_{\mathrm{t},i} \sigma_{\mathrm{t},i}}{\sum_{\text{adsorptive}} k_{\mathrm{t},i} \sigma_{\mathrm{t},i} + \sum_{\text{non-adsorptive}} k_{\mathrm{t},j} \sigma_{\mathrm{t},j}} = \frac{\sum_{\text{adsorptive}} k_{\mathrm{t},i} \sigma_{\mathrm{t},i}}{R_{\mathrm{t},0}} \tag{5-8}$$

Substituting this into Eqn.(5-7) gives:

$$R_{\mathrm{t}} = R_{\mathrm{t},0}\left(1 - \theta_{\mathrm{t}} \frac{K_{\mathrm{t}} C_{\mathrm{dye}}}{1 + K_{\mathrm{t}} C_{\mathrm{dye}}}\right) \tag{5-9}$$

Similarly, the collective re-deposition rate constant (5-5) becomes:

$$\kappa_{\mathrm{p}} = \kappa_{\mathrm{p},0}\left(1 - \theta_{\mathrm{p}} \frac{K_{\mathrm{p}} C_{\mathrm{dye}}}{1 + K_{\mathrm{p}} C_{\mathrm{dye}}}\right) \tag{5-10}$$

with the fraction of re-deposition due to adsorptive sites, θ_{p}, is defined by:

$$\theta_{\mathrm{p}} \equiv \frac{\sum_{\text{adsorptive}} k_{\mathrm{p},i} \sigma_{\mathrm{p},i}}{\sum_{\text{adsorptive}} k_{\mathrm{p},i} \sigma_{\mathrm{p},i} + \sum_{\text{non-adsorptive}} k_{\mathrm{p},j} \sigma_{\mathrm{p},j}} = \frac{\sum_{\text{adsorptive}} k_{\mathrm{p},i} \sigma_{\mathrm{p},i}}{\kappa_{\mathrm{p},0}} \tag{5-11}$$

Eqns.(5-9) and (5-10) are similar to Eqn.(5-1). Thus, Piccolo's theory may be separately applicable to detachment and re-deposition processes if the simplifying assumptions (Langmuir-type adsorption, same Langmuir isotherm constant for all detachment or re-deposition sites) are valid. However, since the dissolution rate is given by (Eqn.(2-20)):

$$J = \frac{R_{\mathrm{t}}}{1 + \dfrac{\kappa_{\mathrm{p}}}{N(\nu, D)\omega^{b}}}$$

the effects of dye adsorption on dissolution rate cannot be described by a simple function such as Eqn.(5-1).

Due to the qualitative nature of this analysis, an explicit function for $f_{\mathrm{t},i}(C_{\mathrm{dye}})$ or $f_{\mathrm{p},i}(C_{\mathrm{dye}})$ is not necessary. Substituting Eqns.(5-4) and (5-5) into Eqn.(2-20) gives the dissolution rate:

$$J = \frac{\sum_{\text{adsorptive}} k_{\mathrm{t},i}(1 - f_{\mathrm{t},i})\sigma_{\mathrm{t},i} + \sum_{\text{non-adsorptive}} k_{\mathrm{t},j}\sigma_{\mathrm{t},j}}{1 + \dfrac{\sum_{\text{adsorptive}} k_{\mathrm{p},i}(1 - f_{\mathrm{p},i})\sigma_{\mathrm{p},i} + \sum_{\text{non-adsorptive}} k_{\mathrm{p},j}\sigma_{\mathrm{p},j}}{N(\nu, D)\omega^{b}}} \tag{5-12}$$

This is an decreasing function of $f_{\mathrm{t},i}$ and an increasing function of $f_{\mathrm{p},i}$. Hence, the dissolution rate will be decreased by adsorption on detachment sites and increased by adsorption on re-deposition sites. The reductions in sulfathiazole dissolution rate in HCl solutions indicate that the adsorption was such that the decrease in R_{t} outweighed the decrease in κ_{p}. One possible explanation for this is depicted in Figure 5-13. In an acidic solution, sulfathiazole solid surface is positively charged due to surface protonation, that is, the adsorption of hydrogen ions to "exposed" aniline groups. An "exposed" aniline group is one that is not hydrogen-bonded with other functionalities of neighboring sulfathiazole molecules. Such groups are expected to be

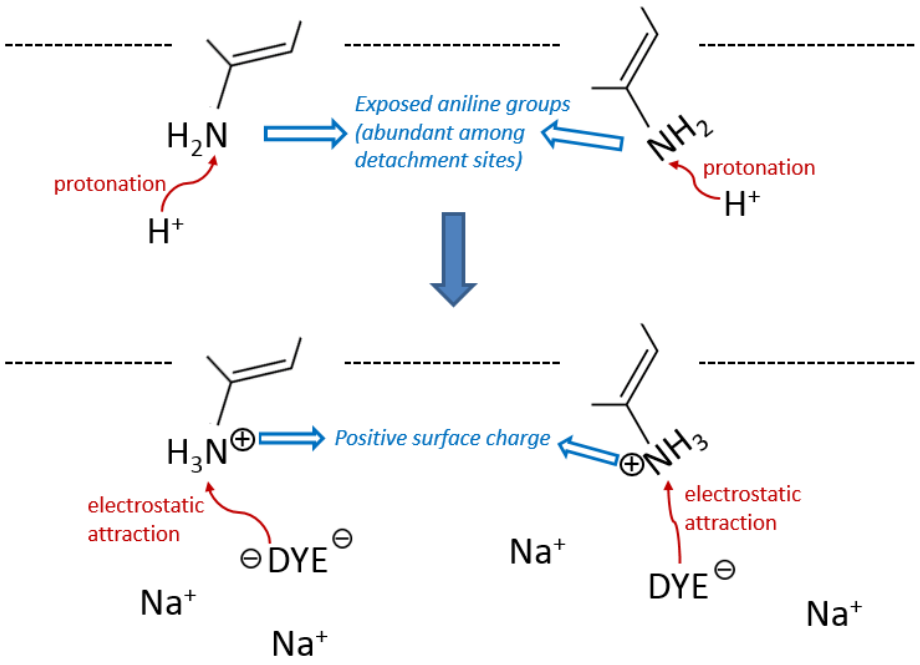

Figure 5-13. Possible effects of surface protonation on dye adsorption on sulfathiazole solid surface (the dye may have charge -2 or -1 depending on whether it is protonated).

more abundant among detachment sites, which are formed by molecules with low coordination numbers. Thus, detachment sites will adsorb more hydrogen ions and carry a larger portion of the positive surface charge. This makes them the preferred adsorption sites for the anionic FD&C Blue #1, which is the reason why the decrease in R_t outweighed the decrease in κ_p in HCl solutions. It is obvious that this adsorption preference depends directly on the hydrogen ion concentration, which determines the extent of surface protonation. This is the reason for the much smaller inhibition in 0.01 N HCl and the lack of inhibition in water.

It can be seen in Figure 5-12 that in 0.1 N HCl, the dye inhibitory effect started to plateau in a

similar fashion to Figure 5-1 at concentrations above 50 μg/mL. At these concentrations, all adsorptive dissolution sites were covered by the dye ($f_{t,i} \to 1$, $f_{p,i} \to 1$), and Eqn.(5-12) reduces to:

$$J = \frac{\sum_{\text{non-adsorptive}} k_{t,j}\sigma_{t,j}}{1 + \frac{\sum_{\text{non-adsorptive}} k_{p,j}\sigma_{p,j}}{N(\nu, D)\omega^b}} = \frac{(1-\theta_t)R_{t,0}}{1 + \frac{(1-\theta_p)\kappa_{p,0}}{N(\nu, D)\omega^b}} \tag{5-13}$$

According to Figure 5-12, non-adsorptive sites accounted for ~66% of sulfathiazole dissolution in 0.1 N HCl.

Future work for this study includes measuring the adsorption isotherms for FD&C Blue #1 on sulfathiazole solid (powder or compressed tablets) in water and HCl solutions. This will provide more definitive evidence of dye adsorption and determine the amount of adsorbed dye as a function of dye concentration and solution pH, although it will not reveal adsorption preferences for detachment / re-deposition sites. The studies of the effects of other dyes (ionic and non-ionic) on the dissolution behavior of sulfathiazole and other compounds would also be worth pursuing for a better understanding of such phenomena.

Summary

This study shows that low concentrations (10-100 μg/mL) of FD&C Blue #1, a water-soluble dye, reduced the intrinsic dissolution rate of sulfathiazole by up to 34% in 0.1 N HCl. At the same time, the same levels of FD&C Blue #1 only slightly inhibited sulfathiazole dissolution in 0.01 N HCl and exhibited no effect in water. Solubility results indicate that less than 5% sulfathiazole complexed with the dye, which rules out complexation as a major contributor to the

dissolution rate reductions and leaves dye adsorption as a probable cause. The dissolution model of Chapter 2 indicates that dissolution rate may be decreased by adsorption on detachment sites and increased by adsorption on re-deposition sites. It is postulated that in acidic media, sulfathiazole solid surface becomes positively charged due to the protonation of exposed aniline groups. Detachment sites have more exposed aniline groups to adsorb more hydrogen ions, which makes them carry a larger portion of the positive surface charge and become the preferred adsorption sites for the anionic FD&C Blue #1. Thus, the effects of adsorption on detachment sites outweighed those on re-deposition sites, resulting in the dissolution rate reductions observed in HCl solutions. This surface protonation-induced adsorption preference for detachment sites diminishes as the hydrogen ion concentration decreases, which is the reason for the much smaller inhibition in 0.01 N HCl and the lack of inhibition in water.

APPENDIX A UV QUANTITATION AND DISSOLUTION PROFILES FOR BENZOIC ACID, SALICYLIC ACID AND CINNAMIC ACID

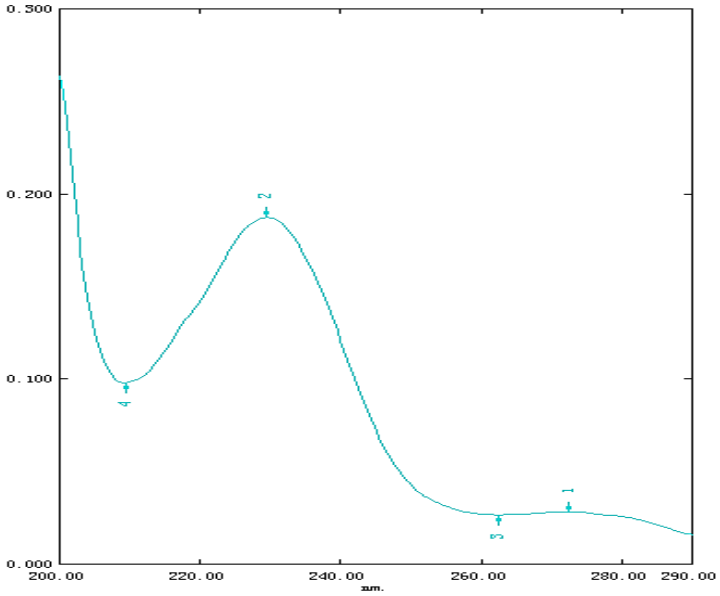

Figure A-1. UV spectrum for benzoic acid in 0.011 N HCl.

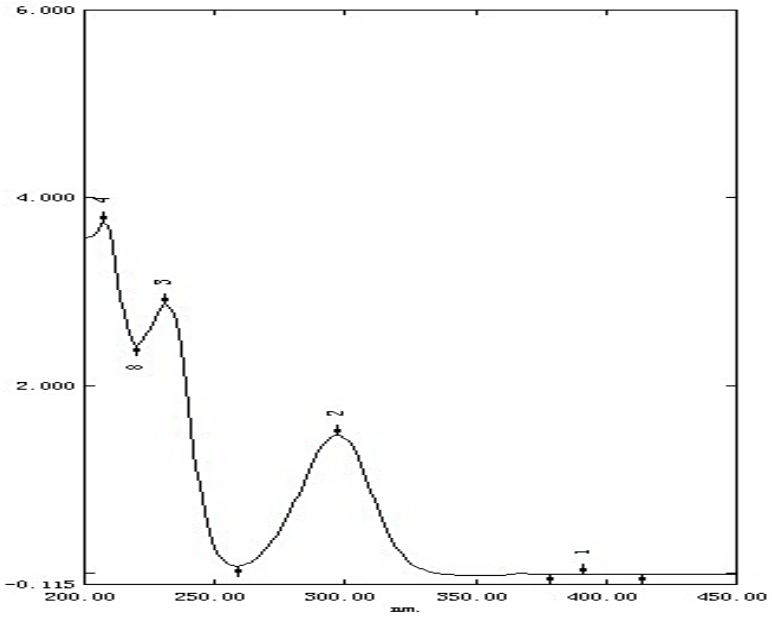

Figure A-2. UV spectrum of salicylic acid in water.

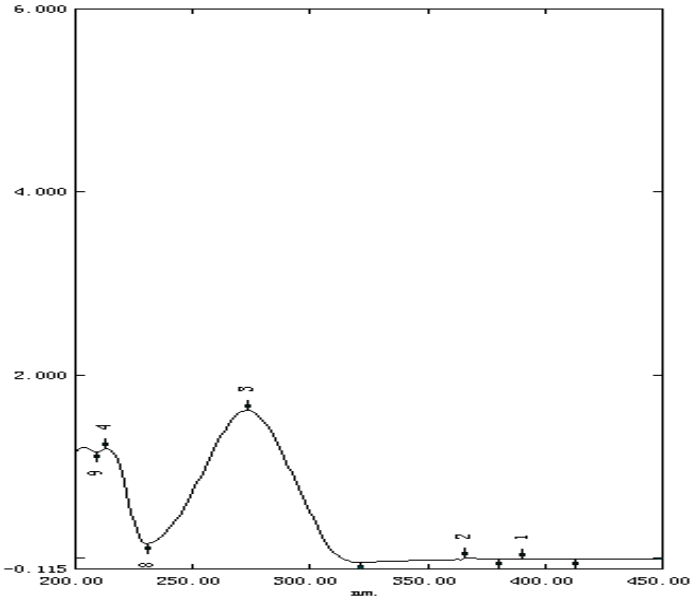

Figure A-3. UV Spectrum of cinnamic acid in water.

Table A-1. Wavelengths for UV assay, maximum dilution factors and dissolution test durations for benzoic acid, salicylic acid and cinnamic acid.

	UV wavelength (nm)	Maximum dilution factor	Dissolution test duration (min)
Benzoic acid	229.5	10	15-20
Salicylic acid	297	5	15-40
Cinnamic acid	273	5	15-40

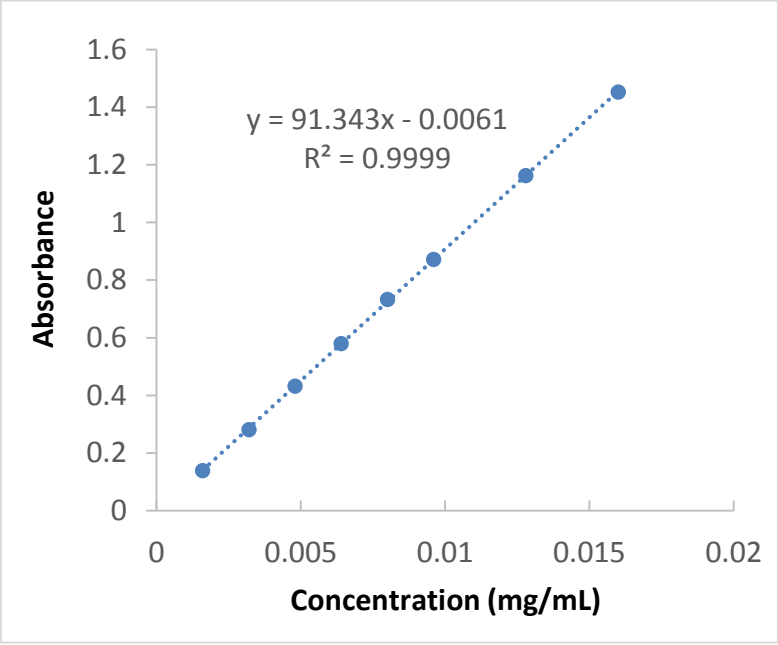

Figure A-4. UV standard plot for benzoic acid in 0.011 N HCl (229.5 nm).

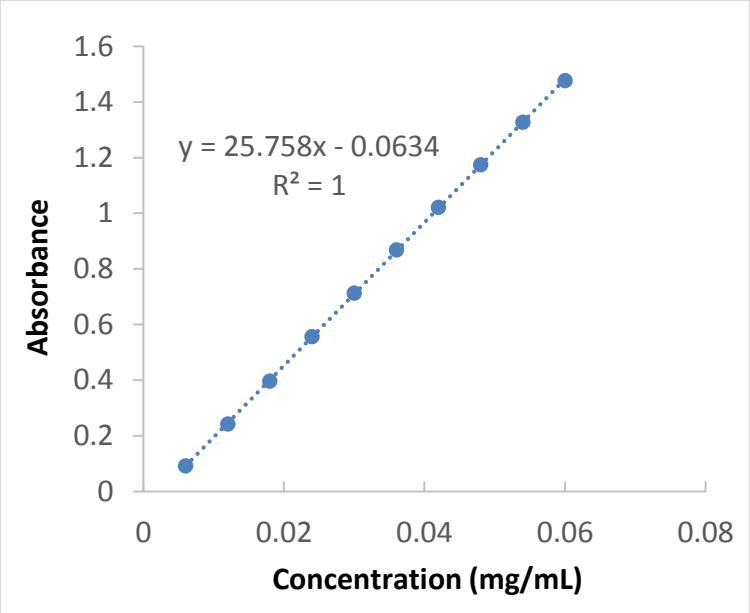

Figure A-5. UV standard plot for salicylic acid in water (297 nm).

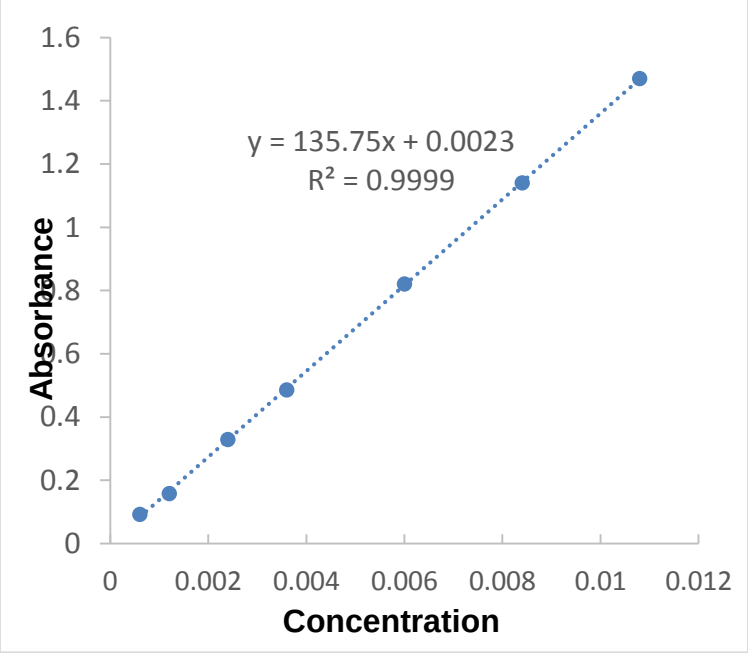

Figure A-6. UV standard plot for cinnamic acid in water (273 nm).

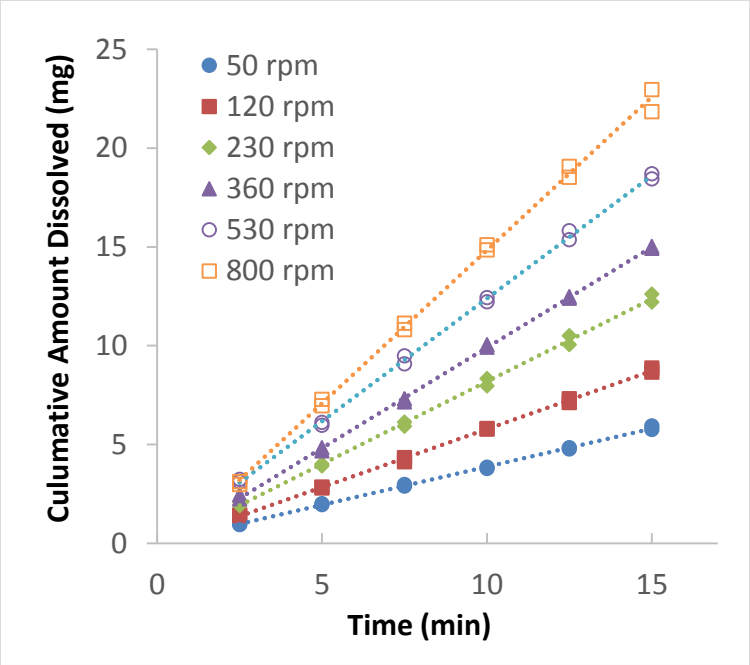

Figure A-7. Benzoic acid dissolution profiles at various rotational speeds at 37 ℃.

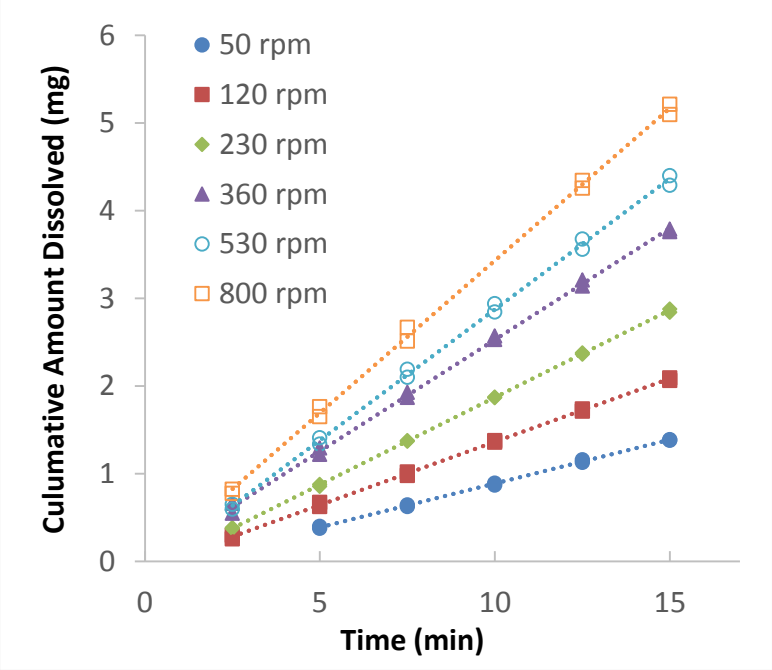

Figure A-8. Benzoic acid dissolution profiles at various rotational speeds at 10 ℃.

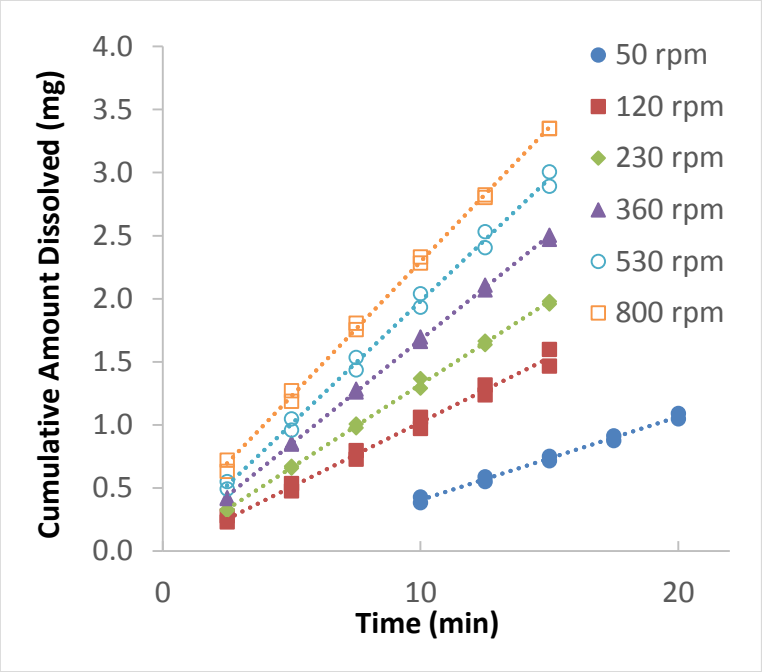

Figure A-9. Benzoic acid dissolution profiles at various rotational speeds at 3 ℃.

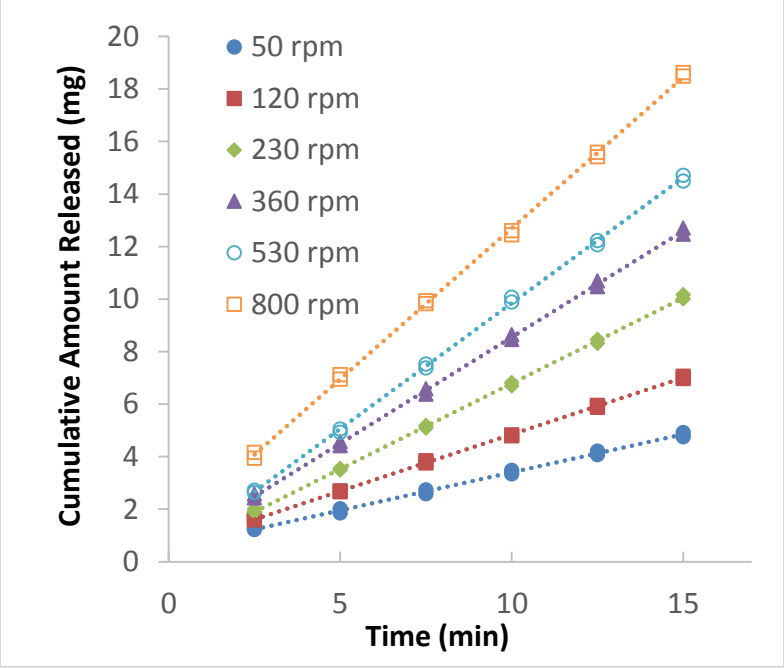

Figure A-10. Salicylic acid dissolution profiles at various rotational speeds at 37 ℃.

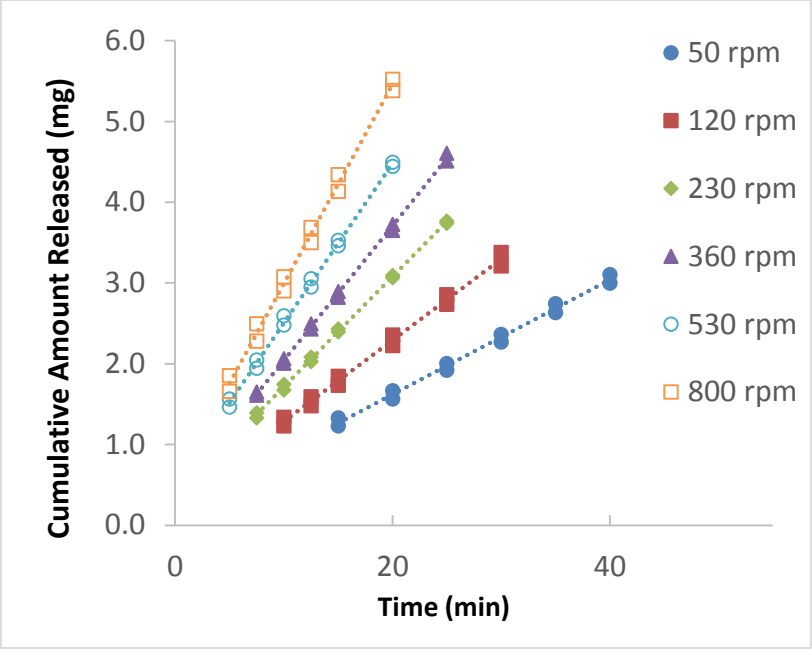

Figure A-11. Salicylic acid dissolution profiles at various rotational speeds at 10 ℃.

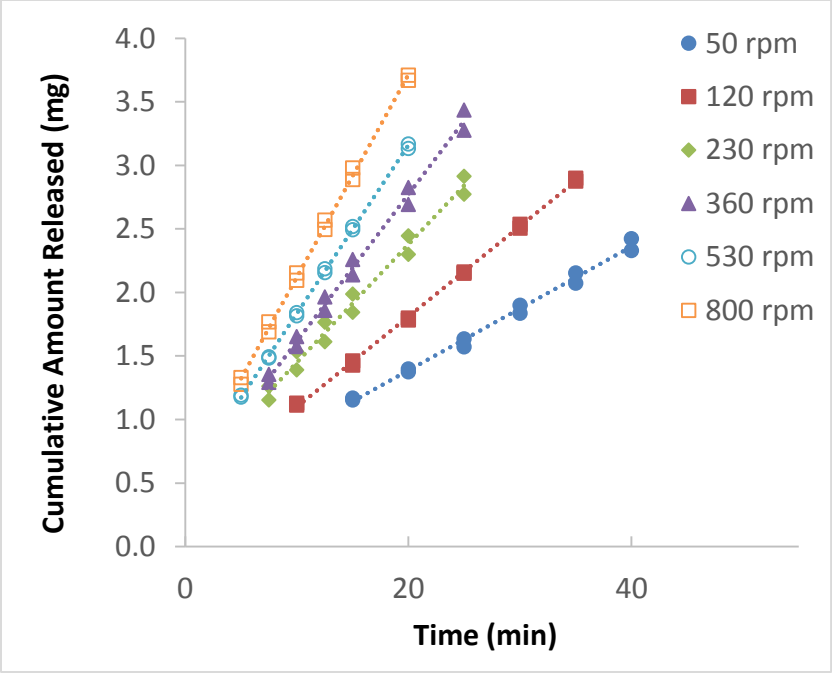

Figure A-12. Salicylic acid dissolution profiles at various rotational speeds at 3 ℃.

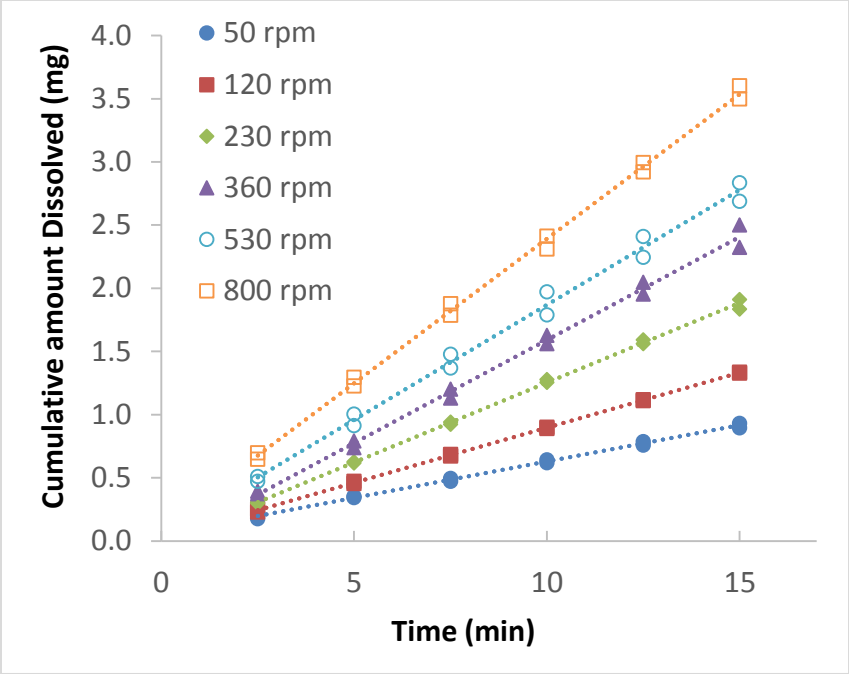

Figure A-13. Cinnamic acid dissolution profiles at various rotational speeds at 37 ℃.

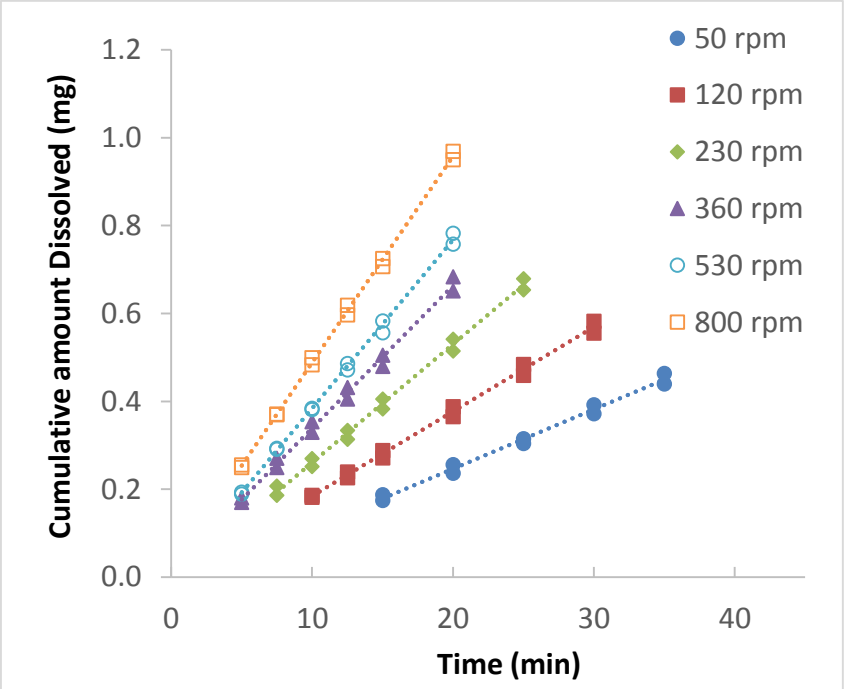

Figure A-14. Cinnamic acid dissolution profiles at various rotational speeds at 10 ℃.

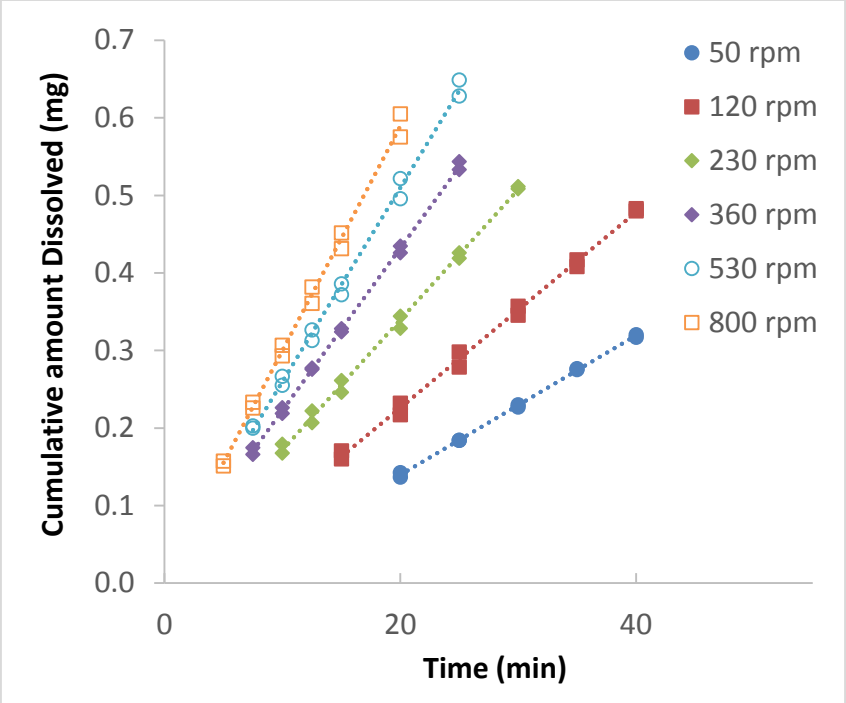

Figure A-15. Cinnamic acid dissolution profiles at various rotational speeds at 3 ℃.

APPENDIX B UV QUANTITATION AND DISSOLUTION PROFILES FOR BENZOIC ACID IN SODIUM DODECYL SULFATE SYSTEMS

All absorbance readings shown in this appendix were at 273 nm.

NaDS = Sodium dodecyl sulfate

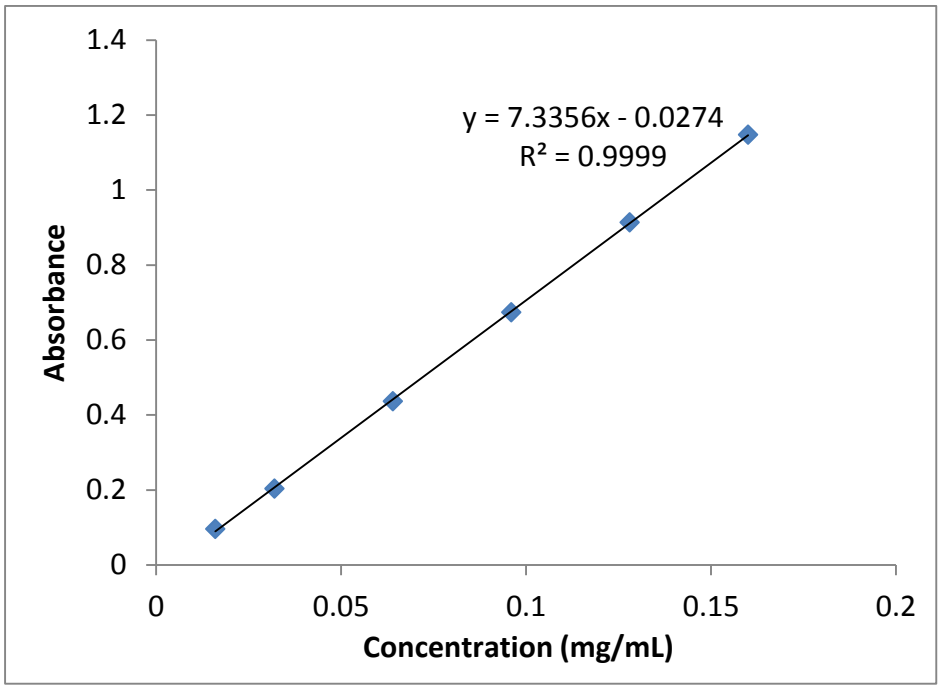

Figure B-1. UV standard plot for benzoic acid in water.

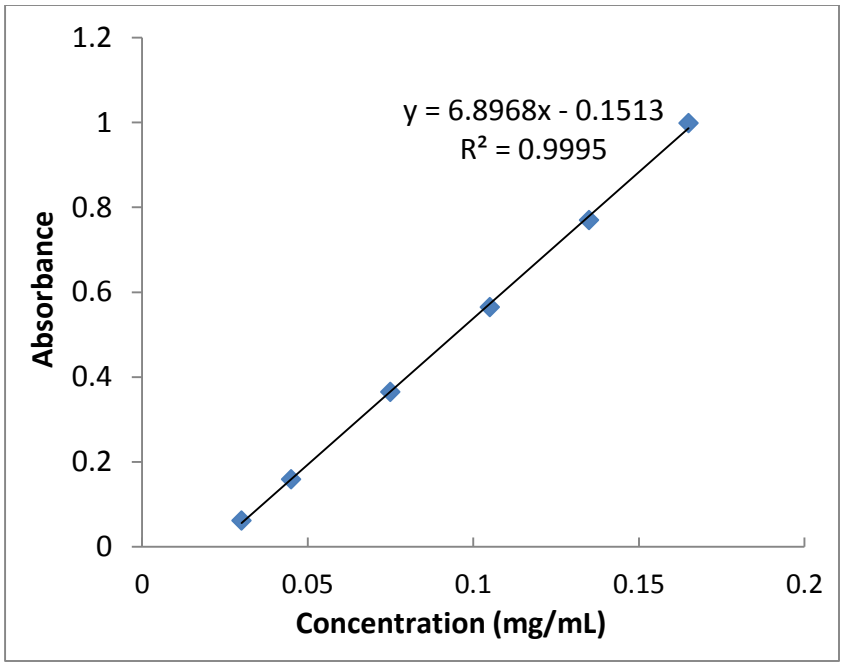

Figure B-2. UV standard plot for benzoic acid in 0.5% (w/v) NaDS.

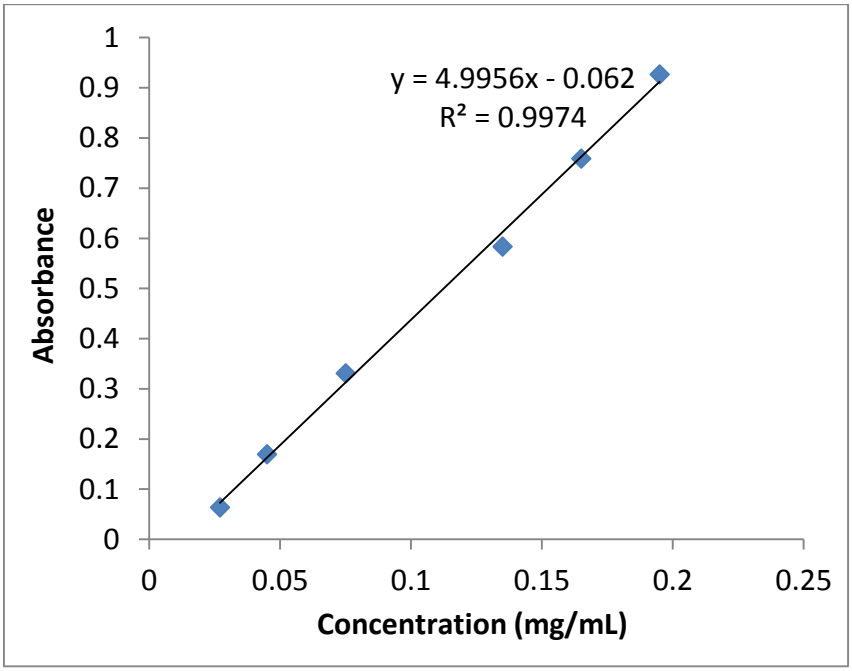

Figure B-3. UV standard plot for benzoic acid in 2% (w/v) NaDS.

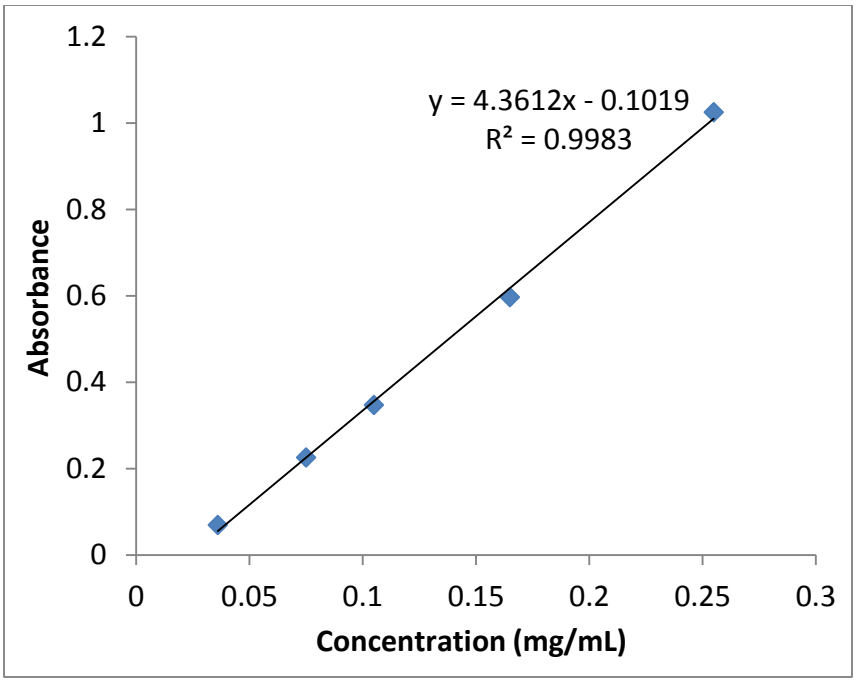

Figure B-4. UV standard plot for benzoic acid in 4% (w/v) NaDS.

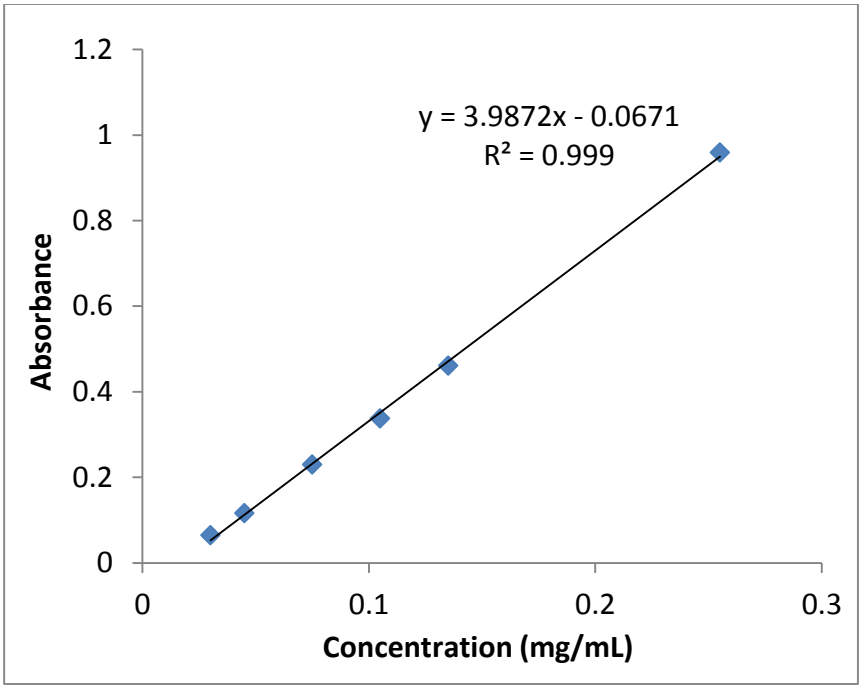

Figure B-5. UV standard plot for benzoic acid in 6% (w/v) NaDS.

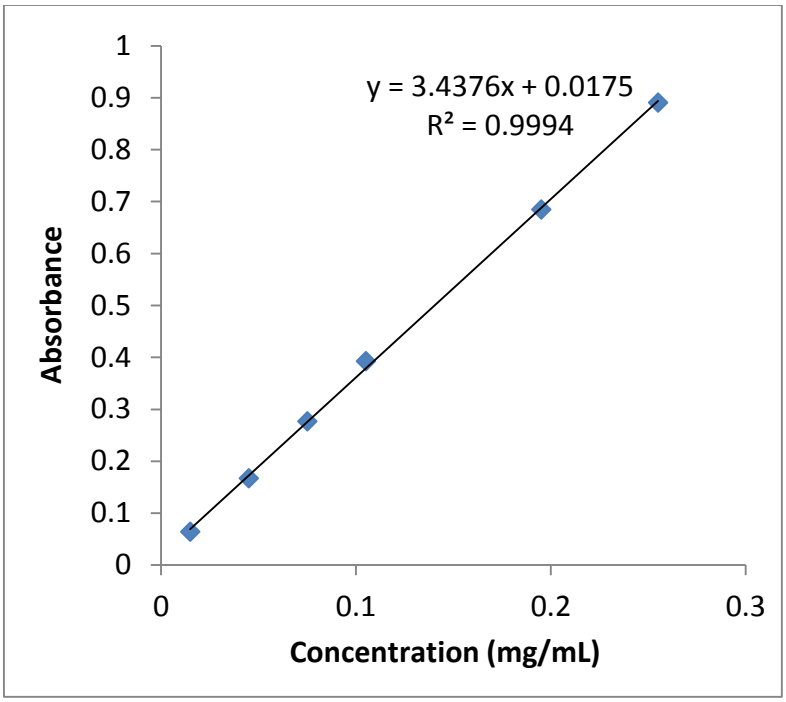

Figure B-6. UV standard plot for benzoic acid in 8% (w/v) NaDS.

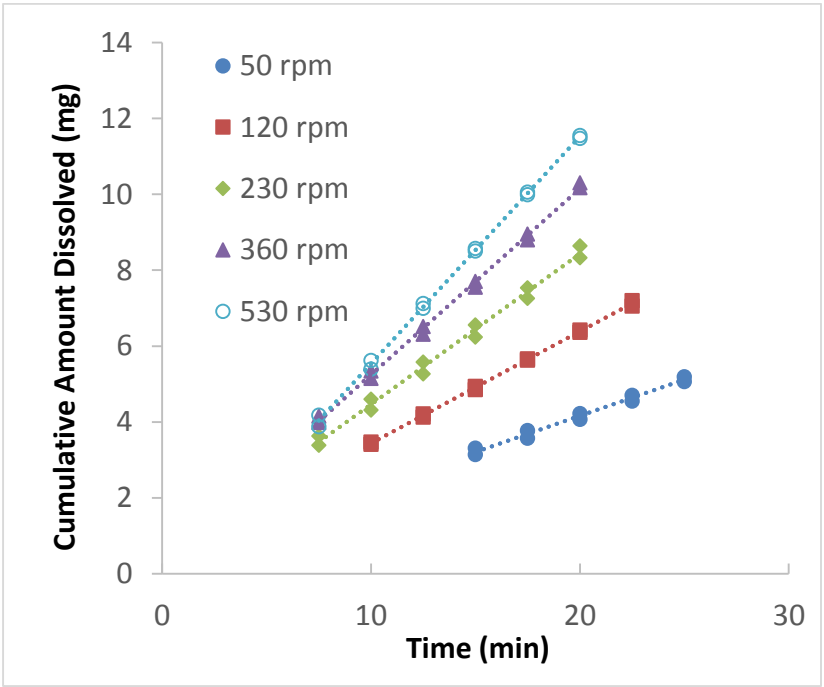

Figure B-7. Benzoic acid dissolution profiles in water at 25 ℃.

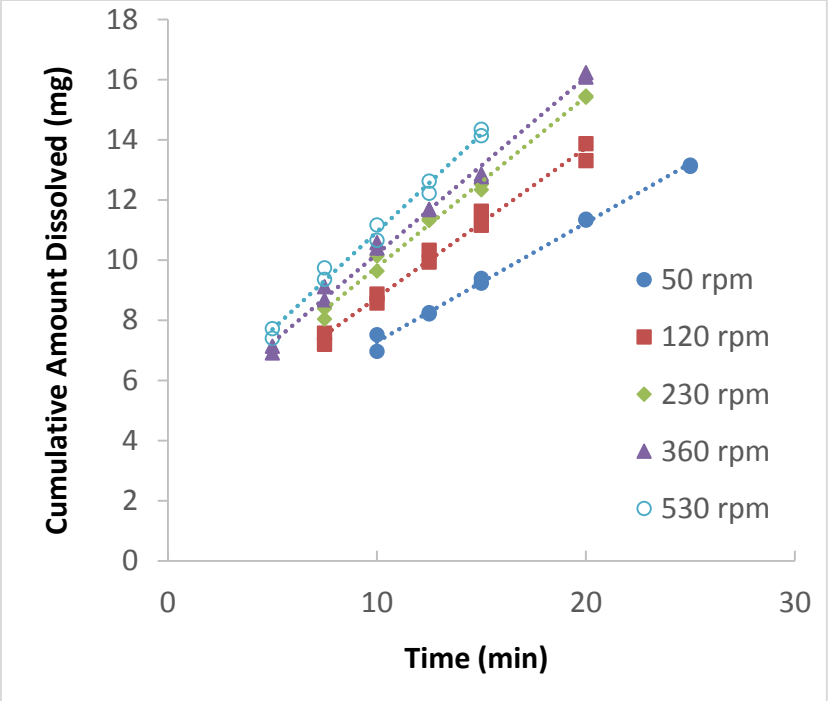

Figure B-8. Benzoic acid dissolution profiles in 0.5% NaDS at 25 ℃.

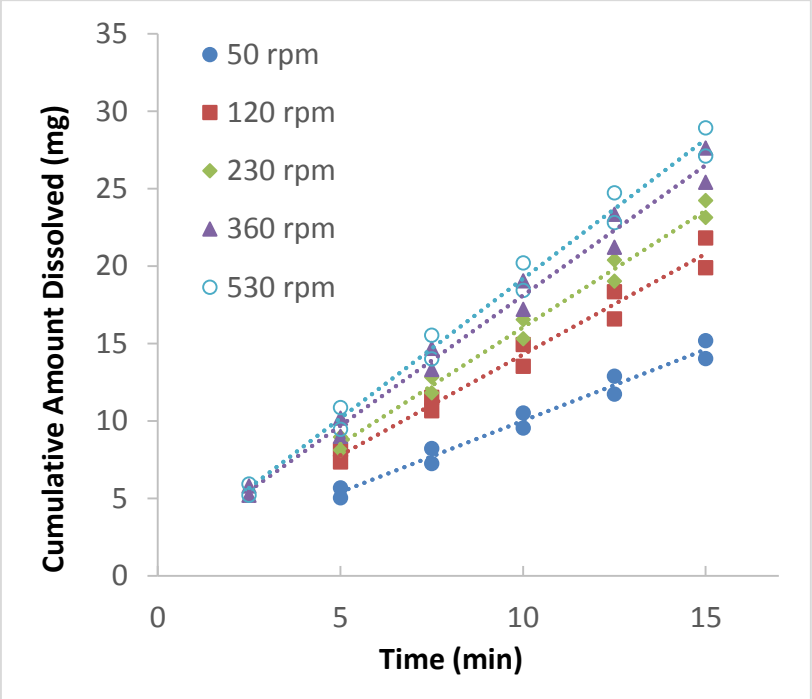

Figure B-9. Benzoic acid dissolution profiles in 2% NaDS at 25 ℃.

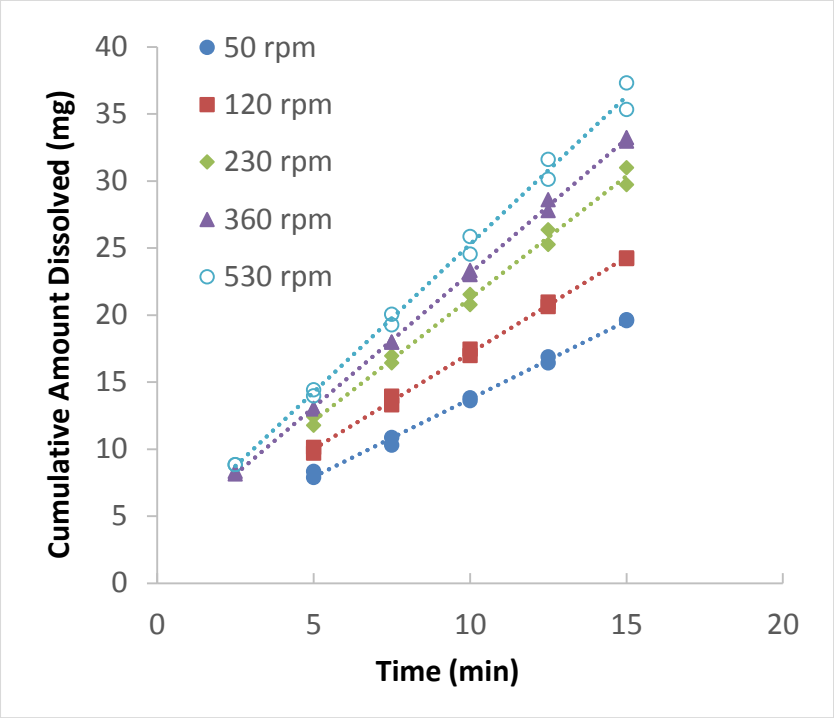

Figure B-10. Benzoic acid dissolution profiles in 4% NaDS at 25 ℃.

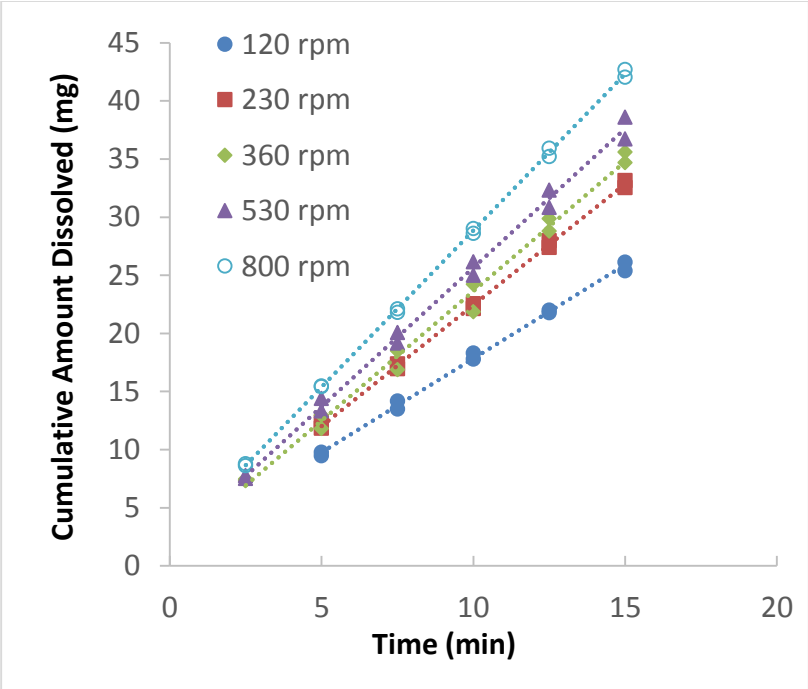

Figure B-11. Benzoic acid dissolution profiles in 6% NaDS at 25 ℃.

APPENDIX C MATHEMATICAL TREATMENT OF SOLUTE TRANSPORT IN MICELLAR SOLUTIONS

The complete mathematical description of solute transport in a surfactant solution is as follows: at equilibrium, solute molecules are statistically distributed among micelles, and the system may be described by the following equilibria (A = solute species; M = empty micelle; MA_i = micelle with *i* solubilized molecules):

$$\begin{aligned} M + A &\underset{k_{1-}}{\overset{k_{1+}}{\rightleftharpoons}} MA \\ MA + A &\underset{k_{2-}}{\overset{k_{2+}}{\rightleftharpoons}} MA_2 \\ &\vdots \\ MA_{N-1} + A &\underset{k_{N-}}{\overset{k_{N+}}{\rightleftharpoons}} MA_N \end{aligned}$$

where, k_{i+} and k_{i-} are entrance and exit rate constants for the corresponding process, respectively. (These rate constants often have large values. For example, typical values for exit and entrance rate constants for arenes with sodium dodecyl sulfate (NaDS) micelles are 10^3-10^6 s^{-1} and 5-8 x 10^7 M^{-1} s^{-1}, respectively.[58]) Almgren et al. proposed a simplified treatment in which solubilized molecules are assumed to neither interact specifically with each other nor perturb micelle properties, so that:[58]

$$\begin{aligned} k_{i+} &= k_+ \\ k_{i-} &= ik_- \end{aligned} \qquad \text{(C-1)}$$

i.e., all entrance rate constants are identical, while the exit rate constant is proportional to the number of solubilized molecules in the micelle. If the equilibrium constant is defined by:

$$K = \frac{k_+}{k_-} \tag{C-2}$$

(*K* is also referred to as the "micellar partition coefficient"), the equilibrium conditions are:

$$\frac{c_{\mathrm{MA}}}{c_{\mathrm{M}}} = \frac{2c_{\mathrm{MA}_2}}{c_{\mathrm{MA}}} = \cdots = \frac{Nc_{\mathrm{MA}_N}}{c_{\mathrm{MA}_{N-1}}} = Kc^{[\mathrm{free}]} \tag{C-3}$$

Since $\sum_{i=1}^{N} ic_{\mathrm{MA}_i} = c^{[\mathrm{mic}]}$ is the concentration of A in the micellar phase and $c_{\mathrm{M}} + c_{\mathrm{MA}} + \cdots c_{\mathrm{MA}_{N\text{-}1}}$ $= C_{\mathrm{mic}}$ is the total concentration of micelles (the fact that c_{MA_N} is missing is unimportant because it is at the tail end of the distribution), the equilibrium conditions may be combined to give:

$$\frac{c^{[\mathrm{mic}]}}{c^{[\mathrm{free}]}} = KC_{\mathrm{mic}} \tag{C-4}$$

i.e., the concentration ratio of the micellar form to the free form is a constant.

The differential equations governing the steady-state distributions of $c^{[\mathrm{free}]}$ and $c^{[\mathrm{mic}]}$ in a forced flow system are (assuming no change in micellar diffusivity due to solubilization so that micelles containing different numbers of solute molecules may be treated the same):

$$D_{\mathrm{free}} \frac{d^2c^{[\mathrm{free}]}}{dz^2} - v_z \frac{dc^{[\mathrm{free}]}}{dz} - \phi = 0 \tag{C-5}$$

$$D_{\mathrm{mic}} \frac{d^2c^{[\mathrm{mic}]}}{dz^2} - v_z \frac{dc^{[\mathrm{mic}]}}{dz} + \phi = 0 \tag{C-6}$$

where, ϕ is the net amount of solute entering the micellar phase per unit time, given by:

$$\phi = k_+ c^{[\mathrm{free}]} C_{\mathrm{mic}} - k_- c^{[\mathrm{mic}]} \tag{C-7}$$

If $c^{[\text{free}]}(z)$ and $c^{[\text{mic}]}(z)$ satisfy the equilibrium condition (C-4) for all *z*, ϕ would be zero everywhere and Eqn.(C-6) could be replaced by:

$$D_{\text{mic}} \frac{d^2 c^{[\text{free}]}}{dz^2} - v_z \frac{dc^{[\text{free}]}}{dz} = 0 \qquad \text{(C-8)}$$

Comparing this with Eqn.(C-5) (with $\phi = 0$) yields:

$$(D_{\text{mic}} - D_{\text{free}}) \frac{d^2 c^{[\text{free}]}}{dz^2} = 0$$

Since $D_{\text{mic}} \neq D_{\text{free}}$, $d^2 c^{[\text{free}]} / dz^2$ must be zero. It follows immediately from Eqn.(C-8) that $dc^{[\text{free}]} / dz$ must also be zero; in other words, there would be no concentration gradient, which is clearly impossible for a dissolution process. Therefore, it may be concluded that it is not possible to achieve true equilibrium between free and micellar forms in a dissolution process. Nevertheless, a "pseudo-equilibrium" approximation may be applicable if the rate constants k_+ and k_- have large values. According to Eqn.(C-7), if at any point *z*, $c^{[\text{mic}]}(z) / c^{[\text{sol}]}(z)$ is appreciably different from KC_{mic}, the large values of k_+ and k_- would make ϕ so large that $c^{[\text{mic}]}(z) / c^{[\text{sol}]}(z)$ would be rapidly brought to a value close (but not equal) to KC_{mic}. In other words, $c^{[\text{mic}]}(z) / c^{[\text{sol}]}(z) \approx KC_{\text{mic}}$ must be satisfied to a high degree of accuracy in order for ϕ at steady-state to be comparable in magnitude to the diffusive and convective terms in Eqns.(C-5) and (C-6). It is worth noting that the pseudo-equilibrium assumption does not permit equating the total transport flux to the sum of fluxes for free and micellar forms (as was done in Eqn.(4-3)). Such a summation would only be legal if ϕ is negligible compared to the diffusive and convective terms, that is, the exchange of solute between the two phases is so slow that the

transport of free and micellar forms are practically independent, which is the exact opposite of the pseudo-equilibrium condition.

Eqns.(C-5) and (C-6) can be added to eliminate ϕ:

$$D_{\text{free}} \frac{d^2 c^{[\text{free}]}}{dz^2} + D_{\text{mic}} \frac{d^2 c^{[\text{mic}]}}{dz^2} - v_z \frac{dc^{\text{T}}}{dz} = 0 \tag{C-9}$$

where, $c^{\text{T}} = c^{[\text{free}]} + c^{[\text{mic}]}$ is the total solute concentration. Using the pseudo-equilibrium approximation and substituting in Eqn.(C-4) yields:

$$\frac{D_{\text{free}} + Kc_{\text{mic}} D_{\text{mic}}}{1 + Kc_{\text{mic}}} \frac{d^2 c^{\text{T}}}{dz^2} - v_z \frac{dc^{\text{T}}}{dz} = 0 \tag{C-10}$$

Thus, the total concentration distribution is governed by the same differential equation as in the absence of surfactants with a modified diffusivity:

$$D_{\text{eff}} = \frac{D_{\text{free}} + Kc_{\text{mic}} D_{\text{mic}}}{1 + Kc_{\text{mic}}} = (1-\alpha) D_{\text{free}} + \alpha D_{\text{mic}} \tag{C-11}$$

where, $\alpha = KC_{\text{mic}} / (1 + KC_{\text{mic}})$ is the fraction of the micellar form. It follows that the total transport flux from the disk surface is given by the same functional form as Eqn.(2-17):

$$J_{\text{T}} = c_0^{\text{T}} N(D_{\text{eff}}, \nu) \omega^b \tag{C-12}$$

where, $c_0^{\text{T}} = c_0^{[\text{sol}]} + c_0^{[\text{mic}]}$ is the total solute concentration at the solid-liquid boundary and ν is the kinematic viscosity of the surfactant solution.

APPENDIX D HPLC CALIBRATION OF SULFATHIAZOLE IN WATER AND HCl SOLUTIONS

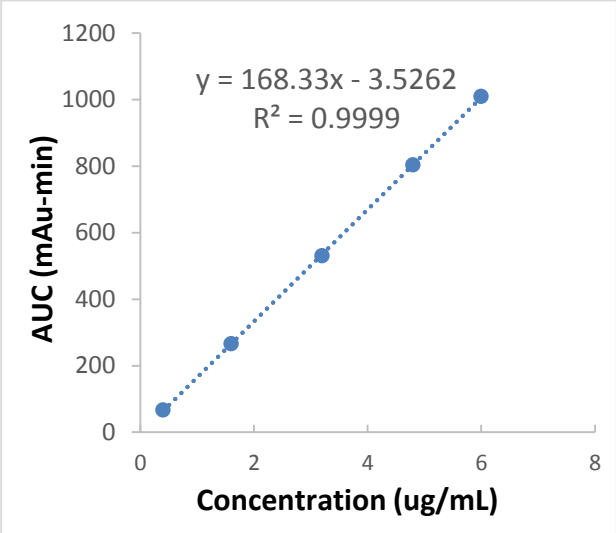

Figure D-1. HPLC standard plot for sulfathiazole in water.

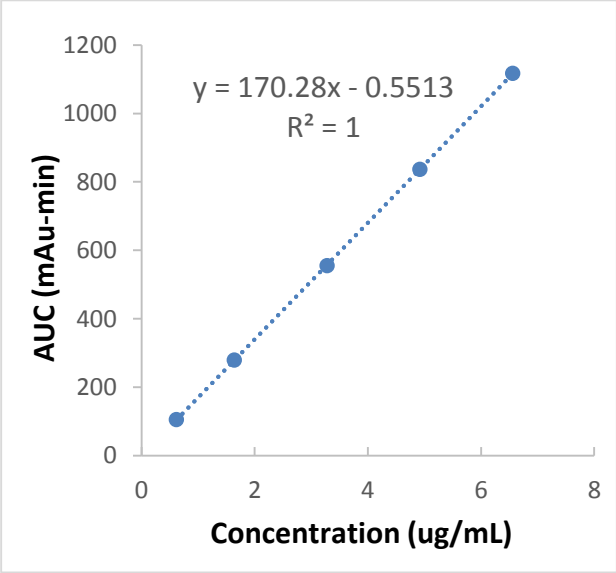

Figure D-2. HPLC standard plot for sulfathiazole in 0.01 N HCl.

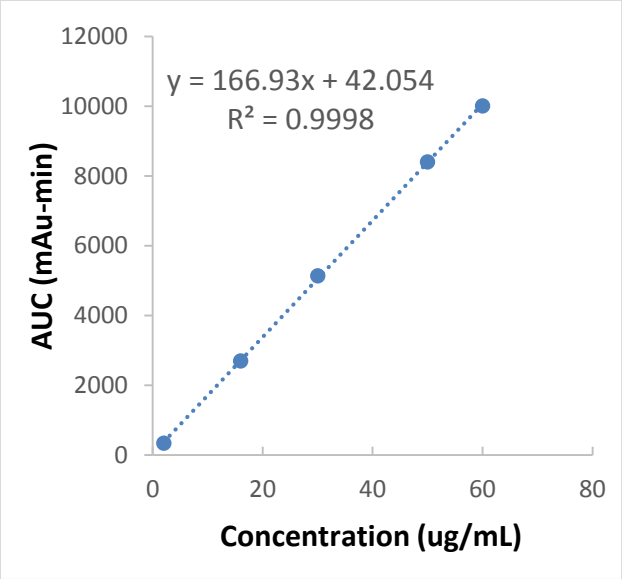

Figure D-3. HPLC standard plot for sulfathiazole in 0.1 N HCl.

REFERENCES

1. Sperandio, G. J., Evanson, R. V., Dekay, H. G. 1948. The disintegration of compressed tablets. J. Am. Pharm. Assoc. 37:71-76.
2. Parrott, E. L., Wurster, D. E., Higuchi, T. 1955. Investigation of drug release from solids. 1. Some factors influencing the dissolution rate. J. Am. Pharm. Assoc. 44:269-273.
3. Nelson, E. 1957. Solution rates of theophylline salts and effects from oral administration. J. Am. Pharm. Assoc. 46:607-614.
4. Morozowich, W., Wagner, J. G., Jones, P. M., Hamlin, W. E., Purmalis, A., Northam, J. I., Chulski, T. J. 1962. Relationship between *in vitro* dissolution rates, solubilities, and LT_{50}'s in mice of some salts of benzphetamine and etryptamine. Am. Pharm. Assoc. 51:993-996.
5. Levy, G. 1961. Comparison of dissolution and absorption rates of different commercial aspirin tablets. J. Pharm. Sci. 50:388-392.
6. Wagner, J. G. 1971. Biopharmaceutics and relevant pharmacokinetics. Hamilton, IL: Drug Intelligence Publications, pp. 65-66.
7. Abdou, H. M. 1989. Evolution of dissolution testing: Dissolution, bioavailability and bioequivalence. Easton, PA: Mack Publishing Co. pp. 5-10.
8. Dressman, J. B., Amidon, G. L., Reppas, C., Shah, V. P. 1998. Dissolution testing as a prognostic tool for oral drug absorption: Immediate release dosage forms. Pharm. Res. 15: 11-22.
9. United States Pharmacopeial Convention, Inc. 1999. The United States Pharmacopeia. 24 ed. (USP 24) Rockville, MD. pp. 1944-1951.
10. Nelson, K. G., Shah, A. C. 1975. Convective diffusion model for a transport-controlled dissolution rate process. J. Pharm. Sci. 64:610-614.
11. Shah, A. C., Nelson, K. G. 1975. Evaluation of a convective diffusion drug dissolution rate model. J. Pharm. Sci. 64:1518-1520.
12. Noyes, A. S., Whitney, W. R. 1897. The rate of solution of solid substances in their own solution. J. Am. Chem. Soc. 19:930-934.
13. Dokoumetzidis, A., Macheras, B. 2006. A century of dissolution research: From Noyes and Whitney to the biopharmaceutics classification system. Int. J. Pharm. 321:1-11.
14. Wurster, D. E., Taylor, P. W. 1965. Dissolution rates. J. Pharm. Sci. 54:169-175.
15. Wang, J. Z. 2002. Modeling and experimental evaluation of spherical particle dissolution. Ph.D. thesis, University of Iowa.
16. Higuchi, T. 1961. Rate of release of medicaments from ointment bases containing drugs in suspension. J. Pharm. Sci. 50:847-845.
17. Zdanovskii, A. B. 1946. The role of the interface solution in the kinetics of the solution of salts. Zhur. Fiz. Khim. 20:869-880.
18. Miyamoto S. 1933. A theory of the rate of solution of solid into liquid. Trans. Faraday Soc. 29:789-794.
19. Dokoumetzidis, A. Papadopoulou, V., Valsami, G., Macheras, P. 2008. Development of a reaction-limited model of dissolution: Application to official dissolution tests experiments. Int. J. Pharm. 355:114-125.

20. Berthoud, A. J. 1912. Theorie de la formation des faces d'un crystal. J. Chim. Phys. 10: 624-635.
21. Rickard, D. T., Sjöberg, E. L. 1983. Mixed kinetic control of calcite dissolution rates. Am. J. Sci. 283:815-830.
22. Sjöberg, E. L., Rickard, D. T. 1984. Temperature dependence of calcite dissolution kinetics between 1 and 62 ℃ at pH 2.7 to 8.4 in aqueous solutions. Geochim. Cosmochim. Acta. 48:485-493.
23. Touitou, E., Donbrow, M. 1981. Deviation of dissolution behavior of benzoic acid from theoretical predictions with lowering of temperature: Limitations as a model dissolution substance. Int. J. Pharm. 9:97-106.
24. Banakar, U. V. 1992. Pharmaceutical dissolution testing. New York, NY: Marcel Dekker, Inc. pp. 63.
25. Landau, L. D., Lifshitz, E. M. 1987. Fluid mechanics, 2nd Ed. Elmsford, New York: Permagon Press, pp. 75-76.
26. Albery, W. J., Hitchman, M. L. 1971. Ring-disc electrodes. Ely House, London: Oxford University Press, pp. 8-16.
27. Levich VG. 1962. Physicochemical hydrodynamics. Englewood Cliffs, NJ: Prentice-Hall, pp. 39-72.
28. Riddiford, A. C. 1966, in "Advances in electrochemistry and electrochemical engineering", Vol.4, Edited by Delahay, P. New York, NY: Interscience, pp. 47-86.
29. Gregory, D. P., Riddiford, A. C. 1956. Transport to the surface of a rotating disc. J. Chem. Soc. 3756-3764.
30. Smets, N., Van Damme, S., De Wilde, D., Weyns, G., Deconinck, J. 2008. Time averaged concentration calculations in pulse electrochemical machining. J. Appl. Electrochem. 38: 1577-1582.
31. Gregory, N., Stuart, J. T., Walker, W. S. 1955. Phil. Trans. Roy. Soc. London. 248:155-199.
32. Smith, N. H. 1947. N.A.C.A. Tech. Note, No. 1227.
33. Tiller, W. A. 1991. The science of crystallization: Microscopic interfacial phenomena. New York, NY: Cambridge University Press. pp. 37-42.
34. Constable, F. H. 1925. The mechanism of catalytic decomposition. Proc. R. Soc. London. 108:355-378.
35. Laidler, K. J. 1987. Chemical kinetics, 3rd ed. New York, NY: Harper & Row, pp. 243-244.
36. Myerson, A. S. 2001. Handbook of industrial crystallization, 2nd Ed. Boston, MA: Butterworth-Heinemann, pp. 71-72.
37. Compton, R. G., Harding, M. S., Pluck, M. R., Atherton, J. H., Brennan, C. M. 1993. Mechanism of solid / liquid interfacial reactions. The dissolution of benzoic acid in aqueous solution. J. Phys. Chem. 97:10416-10420.
38. Mooney, K. G., Mintun, M. A., Himmelstein, K. J., Stella, V. J. 1981. Dissolution kinetics of carboxylic acids I: Effect of pH under unbuffered conditions. J. Pharm. Sci. 70:13-22.
39. Bircumshaw, F. F., Riddiford, A. C. 1952. Transport control in heterogeneous reactions. Q. Rev. Chem. Soc. 6:157-185.
40. Swarbrick, J. 1970. Current concepts in the pharmaceutical sciences, biopharmaceutics. Philadelphia, PA: Lea & Febiger, pp. 271.
41. Wong, W. H. 1982. Dissolution mechanisms of calcium oxalate monohydrate and artificial renal calculi in reactive media. Ph. D. thesis, University of Iowa, pp. 24-25.

42. Banerjee, D., Gupta, B. K. 1980. The estimation of compound hydrophobicities and their relevance to partition coefficients. Can. J. Pharm. Sci. 15:61-63.
43. Humphreys, K. J., Rhodes, C. T. 1968. Effect of temperature upon solubilization by a series of nonionic surfactants. J. Pharm. Sci. 57:79-83.
44. Delgado, J. M. P. Q. 2006. Molecular diffusion coefficients of organic compounds in water at different temperatures. J. Phase Equilib. Diff. 28:427-432.
45. Kaunisto, E., Marucci, M., Axelsson, A. 2011. Dissolution kinetics or pure mass transfer? A mechanistic study of dissolution. AIChE J. 57:2610-2617.
46. Korsen, L., Drost-Hansen, W., Millero, F. J. 1969. Viscosity of water at various temperatures. J. Phys. Chem. 73:34-39.
47. Kestin, J., Sokolov, M., Wakeham, W. A. 1978. Viscosity of liquid water in the range -8 ℃ to 150 ℃. 7:941-948.
48. Prakongpan, S., Higuchi, W. I., Kwan, K. H., Molokia, K. M. 1976. Dissolution rate studies of cholesterol monohydrate in bile acid-lecithin solutions using the rotating disk method. J. Pharm. Sci. 65:685-689.
49. Lide, D.R., Haynes, W. M. 2009. CRC handbook of chemistry and physics. 90th ed., Boca Raton, Florida: CRC Press, pp.8-(47-48).
50. Feldman, S., Gibaldi, M. 1967. Effect of solubility on urea-Role of water structure. J. Pharm. Sci. 56:370-375.
51. Eisenberg, M., Chang, P., Tobias, C. W., Wilke, C. R. 1955. Physical properties of organic acids. AIChE J. 1:558.
52. Hoiland, H., Blokhus, A. M. 2009. in "Hand book of surface and colloid chemistry", 3rd. ed. Edited by Birdi, K. S. Boca Raton, Florida: CRC Press, pp.379-384.
53. Higuchi, W. I. 1964. Effects of interacting colloids on transport rates. J. Pharm. Sci. 5:532-535.
54. Higuchi, W. I. 1967. Diffusional models useful in biopharmaceutics: Drug release rate processes. J. Pharm. Sci. 56:315-324.
55. Granero, G. E., Ramachandran, C., Amidon, G. L. 2005. Dissolution and solubility behavior of fenofibrate in sodium lauryl sulfate solutions. Drug Dev. Ind. Pharm. 31:917-922.
56. Crison, J. R., Shah, V. P., Skelly, J. P., Amidon, G. L. 1996. Drug dissolution into micellar solutions: Development of a convective diffusion model and comparison to the film equilibrium model with application to surfactant-facilitated dissolution of carbamezapine. J. Pharm. Sci. 85:1005-1011.
57. Balakrishnan, A., Rege, B. D., Amidon, G. L., Polli, J. E. 2004. Surfactant-mediated dissolution: Contributions of solubility enhancement and relatively low micelle diffusivity. J. Pharm. Sci. 93:2064-2075.
58. Almgren, M., Grieser, F., Thomas, J. K. 1979. Dynamic and static aspects of solubilization of neutral arenes in ionic micellar solutions. J. Am. Chem. Soc. 101:279-291.
59. Dominguez, A., Fernández, A., González, N., Iglesias, E., Montenegro, L. 1997. Determination of critical micelle concentration of some surfactants by three techniques. J. Chem. Edu. 74:1227-1231.
60. Cifuentes, A., Bernal, J. L., Diez-Masa, J. C. 1997. Determination of critical micelle concentration values using capillary electrophoresis instrumentation. Anal. Chem. 69:4271-4274.

61. Turro, N. J., Yekta, A. 1978. Luminescent probes for detergent solutions: A simple procedure for determination of mean aggregation number of micelles. J. Am. Chem. Soc. 100:5951-5952.
62. Evans, D. F., Mukherjee, S. Mitchell, D. J., Ninham, B. W. 1982. Surfactant diffusion: New results and interpretations. J. Colloid Interface Sci. 93:184-204.
63. Reise-Husson, F., Luzzati, V. 1964. The structure of the micellar solutions of some amphiphilic compounds in pure water as determined by absolute small-angle X-ray scattering techniques. J. Phys. Chem. 68:3504-3511.
64. Sasaki, T., Hattori, M., Sasaki, J., Nukina, K. 1974. Studies of aqueous sodium dodecyl sulfate solutions by activity measurements. Bull. Chem. Soc. Jpn. 48:1397-1403.
65. Lide, D.R., Haynes, W. M. 2009. CRC handbook of chemistry and physics. 90th ed., Boca Raton, Florida: CRC Press, pp. 6-1.
66. Hartley, G. S. 1935. The application of the Debye-Hückel theory to colloidal electrolytes. Trans. Faraday Soc. 31:31-50.
67. Piccolo, J., Tawashi, R. 1970. Inhibited dissolution of drug crystals by a certified water-soluble dye. J. Pharm. Sci. 59:56-59.
68. Piccolo, J., Tawashi, R. 1971. Inhibited dissolution of drug crystals by certified water-soluble dyes II. J. Pharm. Sci. 60:59-63.
69. Clark, F. T., Drickamer, H. G. 1985. High-pressure studies of rotational isomerism of triphenylmethane dye molecules. Chem. Phys. Lett. 115:173-175.
70. Chial, H. J., Thompson, H. B., Splittgerber, A. G. 1993. A spectral study of the charged forms of Coomassie Blue G. Anal. Chem. 209:258-266.
71. Boreen, A. L., Arnold, W. A., McNeill, K. 2004. Photochemical fate of sulfa drugs in the aquatic environment: Sulfa drugs containing five-membered heterocyclic groups. Environ. Sci. Technol. 38:3933-3940.